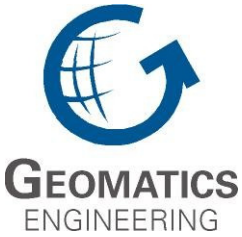

UCGE Reports
Number 20262

Department of Geomatics Engineering

Enhanced Cellular Network Positioning using Space-Time Diversity

(URL: http://www.geomatics.ucalgary.ca/research/publications/GradTheses.html)

by

Ahmad Reza Abdolhosseini Moghaddam

December 2007

UNIVERSITY OF CALGARY

Enhanced Cellular Network Positioning using Space-Time Diversity

by

Ahmad Reza Abdolhosseini Moghaddam

A THESIS

SUBMITTED TO THE FACULTY OF GRADUATE STUDIES

IN PARTIAL FULFILMENT OF THE REQUIREMENTS FOR THE

DEGREE OF MASTER OF SCIENCE

DEPARTMENT OF GEOMATICS ENGINEERING

CALGARY, ALBERTA

DECEMBER, 2007

Abstract

The accuracy of radio positioning based on terrestrial wireless cellular network signals is limited by multipath effects. This limitation results from non-line-of-sight (NLOS) multipath signal components interfering with the desired line-of-sight (LOS) component and therefore distorting the estimate of the propagation time of the radio signals. Consequently, multipath mitigation techniques are essential for attaining acceptable positioning accuracy in a cellular network. Two such multipath mitigation methods are proposed, developed, and tested in this thesis. These methods are based on exploiting the multipath diversity across both spatial and temporal dimensions. The first scheme uses coherent combining of the time domain complex channel impulse responses (CIR) corresponding to observations taken over a spatial extent. This scheme is applicable to receivers based on a stationary array of antenna elements or a single antenna receiver that is spatially translated as observations are made. In the second scheme, a generalization to Multiple-Signal-Classification (MUSIC) is derived using spatial-temporal diversities. Experimental results and analyses with the space-time MUSIC estimation algorithm are presented. These results demonstrate that in addition to providing more accurate estimates of the arrival time of the received signals, both proposed methods provide enhanced robustness by effectively mitigating losses due to localized spatial fades.

Ancillary aspects of practical and theoretical challenges involved in the estimation of IS-95 CDMA signal arrival times are also addressed. These include CDMA receiver implementation and characterization, theoretically optimal Neyman-Pearson detector implementation for non-coherent detection of the signal, schemes for base station detection, and base station identification based on ambiguity analysis.

Acknowledgments

- I owe my existence, my achievements, my original inspirations for finding a prideful life style and literally every rewarding move that needed to be fostered, to my parents.
- Special thanks to my supervisor, Dr. Gérard Lachapelle, for his gracious financial and technical supports during my MSc program. He provided me with an opportunity to experience a period of my life full of lessons. This era could help me enormously to know better myself, my strength points, weak points, features and capabilities. This awareness will help me massively to carry on my life more wisely.
- Another special thanks to my co-supervisor, Dr. John Nielsen. To me, he was more than a technical supervisor, but an inspirational, clever and compassionate friend. His positive aura, open-minded and liberal attitude were invaluable things, I did need during my work.
- Thanks to my easy-going friend Ali Broumandan. His supportive and plausible attitude, since the start of our friendship over the last year is particularly appreciated.
- Many thanks to my colleagues in PLAN group and associates at Geomatics Engineering of University of Calgary who have answered my questions, shared their time with me or merely put up with me with positive waves. In particular, I would like to acknowledge two wonderful friends who paved the way toward this

research, Alfredo Lopez for his sincere commitments and Surendran K. Shanmugam for his generous helps. This research could be much more challenging without their endeavours and knowledge.

- Mark Petovello and Rob Watson. Thank you for kindly and thoroughly answering all of my questions.
- I also would like to acknowledge from Tao Lin, a helpful, hard work and self-motivated colleague.

Dedication

To my beloved parents and three brothers, Mohammad, Reza and Nima who are my most precious entities, God privileged me and in memory of my deceased brother, Hamid

Table of Contents

Abstract iii

Acknowledgments iv

List of Tables xi

List of Figures and Illustrations xii

Abbreviations and Acronyms xvi

Chapter One: Introduction 1

1.1 Cellular Network Positioning 1

1.2 Cellular Network Positioning Challenges 2

1.2.1 Detectability Challenge 3

1.2.2 Multipath Challenge 4

1.3 Meeting the Multipath Challenge 6

1.4 Research Overview 8

1.4.1 Motivation 8

1.4.2 Objective and Intended Contributions 9

1.4.3 Thesis Outline 10

Chapter Two: Cellular Network Positioning Techniques 12

2.1 RSS Method 12

Statistical Model of RSS 13

2.2 Fingerprint Method 15

2.3 Cell ID Method 17

2.4 TOA Method 19
2.5 TDOA Method 23
2.6 AOA Method 25
2.7 Performance Comparison in Different Radiolocation Systems and Approaches ... 28

Chapter Three: Signal Structure and PLAN Prototype Receiver Architecture 30
3.1 IS-95 CDMA Forward Link Pilot 30
3.2 Pilot Signal Generator 32
3.3 Despreading Process 35
3.4 PLAN Prototype Receiver Architecture 39
3.4.1 Receiver Challenges 42
3.4.1.1 Phase Imbalance 43
3.4.1.2 Frequency Stability 48

Chapter Four: Cellular Network Positioning Implementation and Test 52
4.1 Positioning Method Selection 52
4.2 Steps Toward TDOA Position Fix 53
4.2.1 Base Stations Detection and Identification 54
4.2.2 Optimum Noncoherent Processing for BTS Detection 55
4.2.2.1 Analytical Derivation 56
4.2.2.2 Analytical Approximation 59
4.2.3 BTS Identification using GPS Time Reference 62
4.2.4 BTS Identification without using GPS Time Reference 63

4.3 Fixing Position 67
4.3.1 Least Square Position Fix 68
4.3.2 Maximum Likelihood (ML) Position Fix 71
4.4 Results and Analyses 72
4.4.1.1 BTS–Sector Masking 76
4.4.1.2 Reference Selection 79

Chapter Five: Positioning Enhancement using Space-Time Observations 80
5.1 Multipath Induced Bias 81
5.2 Space – Time Paradigm 82
5.2.1 Coherent Combining of the Spatial Observation 86
5.2.2 Obstacles toward Coherent Combining of the Space-Time Observations 87
5.2.2.1 Residual Frequency 87
5.2.2.2 Clock Drift 90
5.2.2.3 Variable Inter-Channel Delays 92
5.2.2.4 Inter-Channel Coupling and Leakage 93
5.3 Analyses and Results 94

Chapter Six: Space-Time Paradigm in MUSIC 103
6.1 MUSIC Technique 105
6.2 Practical Implementation Challenges 110
6.2.1 Covariance Matrix 110
6.2.2 Segment Size 113

6.2.3 Number of Multipath Components 114
6.2.4 Estimation Bias 115
6.3 Field Measurement Results 119
6.3.1 Positioning Results using Conventional Correlation Technique 123
6.3.2 Positioning Results using MUSIC Technique 129
6.4 Space-Time MUSIC 134
6.4.1 Space-Time MUSIC Derivation 135
6.4.2 Spatial Diversity Realization 140
6.4.3 Temporal Diversity Realization 141
6.4.4 Frequency Diversity Realization 142
6.4.5 Field Measurement Results 143
6.5 Performance Comparison 150

Chapter Seven: Conclusions and Recommendations for Future Work 173

References 178

List of Tables

Table 1.1: E-911 Accuracy 1

Table 2.1: Typical parameters of NCPS system 17

Table 3:1 Percentage of Composite RF Power Assigned to Different IS-95 Channel 32

Table 3: 2 GAGE card specification 41

Table 4.1: Northing - Easting errors 77

Table 5.1: Allan Deviation for Front End Master Clock (TCXO) 91

Table 5.2: Easting-Northing Error Statistics 101

Table 6.1: Easting-Northing Error Statistics 148

Table 6.2: Positioning Error with Only One Sector Usage 168

Table 6.3: Position Errors (Mean) 171

Table 6.4: Position Error (Standard Deviations) 172

List of Figures and Illustrations

Figure 2.1: Fingerprint radiolocation a) off line phase, b) operational phase..... 16

Figure 2.2: Cell ID Radiolocation..... 17

Figure 2.3: Telus BTSs in Calgary 18

Figure 2.4: Illustration of TOA based method on three BTS's..... 20

Figure 2.5: Illustration of AOA based method with three BTSs 25

Figure 2.6: Positioning error in AOA 26

Figure 2.7: Overview of some wireless positioning system 28

Figure 3.1: Quadrature spreading stage for the forward channel..... 33

Figure 3.2: Despreading process of IS-95 CDMA signal 35

Figure 3.3: Despread IS-95 signal 36

Figure 3.4: FFT-based Correlation Method..... 39

Figure 3.5: PLAN prototype 5 channel CDMA receiver..... 40

Figure 3.6: Overall architecture of the CDMA PCS receiver..... 42

Figure 3.7: Test set up for investigating misbalance among different channels..... 43

Figure 3.8: Phase imbalance 43

Figure 3.9: Complex despreading process 44

Figure 3.10: Phase imbalance correlation loss..... 45

Figure 3.11: Measured power in different channels 46

Figure 3.12: Long term behavior in measured power..... 47

Figure 3.13: Short term stability of quartz and rubidium oscillator 49

Figure 3.14: Coarse frequency offset..... 50

Figure 3.15: Frequency offset histogram 51

Figure 4.1: BTS detection 55

Figure 4.2: Decision Making Process 56

Figure 4.3: ROC curves for Matched filter processing and non linear processing 61

Figure 4.4: 64 Chip demarcations for successive BTS's 63

Figure 4.5: LS algorithm (Yu et al 2003) 70

Figure 4.6: ML Position Fix 71

Figure 4.7:Likelihood fingerprint 72

Figure 4.8: Field data collection set up 73

Figure 4.9: Scatter plot 74

Figure 4.10: Parking lot result 75

Figure 4.11: BTS-Sector masking results 77

Figure 4.12: Indoor result 78

Figure 4.13: Reference alteration (measurement point surrounded by a circle) 79

Figure 5.1: Specular-correlative multipath 81

Figure 5.2: Large bias due to strong indoor multipath 82

Figure 5.3: BTS1-CIR profiles from different antenna elements (space diversity) 83

Figure 5.4: Indoor environment during data collection 84

Figure 5.5: BTS1-CIR Profiles in different spots (time diversity) 85

Figure 5.6: Complex CIR (Epoch 1) 88

Figure 5.7: Complex CIR (Epoch2) 88

Figure 5.8: Inter-channel leakage 94

Figure 5.9: CIR in different epochs (pedestrian walk) 96

Figure 5. 10: Enriched-combined CIR in different epochs 96
Figure 5.11: TOA (top) and enhanced-combined TOA (bottom) 97
Figure 5.12: TOA (top) and enhanced-combined TOA (bottom) for BTS2 98
Figure 5.13: Scatter plot using original CIRs 99
Figure 5.14: Scatter plot using enhanced-combined CIRs 100
Figure 6.1: Power delay profile of two path signal 110
Figure 6.2: Covariance matrix estimation using forward method 111
Figure 6.3: Functional block diagram for MUSIC delay profile 119
Figure 6.4: Delay profiles obtained by MUSIC and conventional despreading process 122
Figure 6.5: Scatter plot – Pseudoranges obtained by conventional correlation method. 123
Figure 6.6: BTS availability 125
Figure 6.7: Easting and Northing errors (conventional) 126
Figure 6.8: Estimated ranges for different BTSs (conventional) 127
Figure 6.9: Easting-northing error distribution (conventional) 128
Figure 6.10: Scatter plot – Pseudoranges obtained by MUSIC pseudo spectrum 130
Figure 6.11: Easting and Northing errors (MUSIC) 130
Figure 6.12: Estimated ranges for different BTSs (MUSIC) 131
Figure 6.13: False detection of LOS component 132
Figure 6.14: Easting and northing error distribution (MUSIC) 133
Figure 6.15: Correlation coefficient of FCM 136
Figure 6.16: Delay profiles by different methods 144
Figure 6.17: Scatter plot – Pseudoranges obtained by space-time MUSIC pseudospectrum 145

Figure 6.18: Easting-northing errors (space-time MUSIC) 146

Figure 6.19: Estimated ranges for different BTSs (space-time MUSIC)..... 147

Figure 6.20: Easting-northing error distribution (space-time MUSIC) 149

Figure 6.21: Measurement configuration..... 151

Figure 6. 22: Data collection set up 152

Figure 6.23: BTS availability – Antenna 1 (static) 153

Figure 6.24: BTS availability – Antenna 2 (static) 154

Figure 6.25: BTS availability – Antenna 3 (static) 154

Figure 6.26: BTS availability – Antenna 4 (static) 155

Figure 6.27: BTS availability – Antenna 1 (low dynamic)..... 155

Figure 6.28: Easting-northing error distribution (conventional despreading) 158

Figure 6.29: Easting-northing error distribution (conventional MUSIC)..... 159

Figure 6.30: Easting-northing error distribution (space-time MUSIC) 160

Figure 6.31: Easting-northing error for different epochs (conventional despreading) ... 162

Figure 6.32: Easting-northing error for different epochs (conventional MUSIC)..... 162

Figure 6.33: Easting-northing error for different epochs (space-time MUSIC) 163

Figure 6.34: TDOA residual errors corresponding to different BTSs 167

Figure 6.35: TDOA residual error histogram for different BTSs 169

Abbreviations and Acronyms

AGC	Automatic Gain Control
AOA	Angle of Arrival
AWGN	Additive White Gaussian Noise
BER	Bit Error Rate
BS	Base Station
BTS	Base Transceiver Station = (BS)
CCIT	Calgary Centre for Innovative Technology
CFAR	Constant False Alarm Ratio
CIR	Channel Impulse Response
CLT	Central Limit Theorem
CRLB	Cramer Rao Lower Bound
DECT	Digital Enhanced Cordless Telecommunications
DFT	Discrete Fourier Transform
DLL	Delay Locked Loop
DSSS	Direct Sequence Spread Spectrum
FBCM	Forward Backward Correlation Matrix
FCC	Federal Communications Commission
FCM	Forward Correlation Matrix
FT	Fourier Transform
GDOP	Geometric Dilution of Precision
GLRT	Generalized Likelihood Ratio Test
GPS	Global Positioning System
I	In Phase
IDFT	Inverse Discrete Fourier Transform

IID	Identically Independent Distribution
IS-95	Interim Standard 95
LAI	Location Area Identifier
LFSR	Linear Feedback Shift Register
LOS	Line of Sight
LRT	Likelihood Ratio Test
LS	Least Square
MDL	Minimum Descriptive Length
ML	Maximum Likelihood
MS	Mobile Station
MUSIC	MUltiple SIgnal Classification
NCO	Numerically Controlled Oscillator
NCPS	Neural Cellular Positioning System
NLOS	Non Line of Sight
NP	Neyman Pearson
PCB	Printed Circuit Board
PCS	Personal Communication Service
PLAN	Positioning Navigation And Location
PN	Pseudo Noise
PPM	Part per Million
PUF	Power Up Function
Q	Quadrature Phase
ROC	Receiver Operating Characteristic
RSS	Received Signal Strength
SMR	Signal to Multipath Ratio
STD	Standard Deviation
TCXO	Temperature Compensated Crystal Oscillator
TDOA	Time Difference of Arrival

TOA	Time of Arrival
TSE	Taylor Series Expansion
UHF	Ultra High Frequency
UMTS	Universal Mobile Telecommunications System
UofC	University of Calgary
UTC	Universal Time Coordinated
WLAN	Wireless LAN

Chapter One: Introduction

1.1 Cellular Network Positioning

The Global Positioning System (GPS) has been recognized as an efficient positioning technology for offering worldwide availability, reliability, low cost, portability for users, adequate precise location, and a maturity dating back to the1980s. Nevertheless, other positioning technologies using infrastructures independent of GPS are available to offer complementary, supplementary, and alternative solutions for personal positioning and navigation.

Wireless cellular network positioning systems, algorithms, and applications have recently received attention partially as a result of the mandated Federal Communications Commission (FCC) E-911 regulation, which demands deployment of a network-centric or mobile-centric positioning architecture to achieve a predefined accuracy throughout the network coverage area (Adusei, et al., 2002). The E-911 regulation rules that all cellular and personal-communication-services (PCS) service providers must offer mobile location information with the accuracy of Table 1.1 (Liao & Chen, 2006).

Table 1.1: E-911 Accuracy

Confidence Level	Mobile-Centric Accuracy	Network-Centric Accuracy
67%	50 m	100 m
95%	150 m	300 m

The confidence levels of 67% and 95% are horizontal distributions used by the cellular industry, and are defined as the radii of two circles centered at the antenna position containing 67 and 95 percent of the horizontal positions in a scatter plot. The cellular network positioning capability has resulted in a plethora of location sensitive applications and services in addition to security and emergency call services, such as roadside assistance, asset tracking, fleet management, area based billing, network resource management, and personal and civilian/military navigation aids (Woo et al 2000).

Various emerging applications require the positioning of users in typical ultra-high-frequency (UHF) wireless channels. Due to the multipath behaviour of the received signal, positioning techniques suffer degraded performance or fail to comply with E-911 requirements. Research into advanced techniques for overcoming multipath effects in cellular network positioning is required if it is to be deployed as a reliable and accurate solution in the positioning problem either as a prime location system or as a backup to GPS.

1.2 Cellular Network Positioning Challenges

The network-centric and mobile-centric architectures are two paradigms for cellular network positioning. In the network-centric architecture, base transceiver stations (BTS) perform positioning by hearing the mobile station (MS). The reverse is true for mobile-centric architecture. In both architectures, there are several approaches for implementing a radio location system including those based on time-of-arrival (TOA), angle-of-arrival (AOA), time-difference-of-arrival (TDOA), and signal-strength (Caffery, 1998). The

overall performance of the aforementioned location techniques depends on a number of factors including the transmitter, propagation medium, receiver, and architecture (network-centric or mobile-centric) itself. Essentially, the propagation medium along with its temporal-spatial characteristics determines the preference for a specific approach in positioning. For instance, in urban areas, TOA-based techniques outperform the AOA-based methods, and vice-versa for rural environments (Tarighat, et al., 2003). It should be emphasized that the TOA method is not directly realizable because it requires perfect timing at either the transmitter or the receiver. Instead, the TDOA method is favourable whenever the receiver cannot provide the absolute timing of the network. The two biggest challenges for precise mobile location estimation are detectability and the non-line-of-sight (NLOS) problem (Le, 2003).

1.2.1 Detectability Challenge

Detectability is defined as the ability of a receiver to extract signals corresponding to multiple transmitters (Ma 2003). The more transmitters, the more information, and hence the better the accuracy in general. Paradoxically, there exists an apparent conflict between wireless cellular communications providers and wireless cellular location providers. Whereas multiple access wireless data communications systems have great tendencies toward minimizing the power of all inactive transmitters to mitigate interference and to increase the system capacity, cellular network positioning systems should detect as many transmitters as possible to improve location accuracy. The detectability problem is more of a concern in a network-centric architecture in cellular

network positioning in which the BTSs carry the processing burden of positioning. While the MS tries to minimize its power consumption via some power control mechanisms, the weakened transmitted power of the MS may not be received by three or more nearby BTSs which need to have the transmitted signal for multilateration location algorithms (Le 2003). Although mobile-centric architecture still suffers from near-far problems, perhaps, the lower accuracy criteria in the E-911 specification for network-centric solutions show the extra challenges for the network-centric architecture due to the power control inclusion in the MS. System developers have been challenged to overcome this limitation (i.e., detectability). For example, the power-up-function (PUF) was recommended for the current wireless system to allow the MS to increase its power for a limited time interval in the reverse channel (Landa & Munoz, 2000). In this scenario, the time-aligned-idle-period-downlink (TA-IPDL) would be used in the universal-mobile-telecommunications-system (UMTS) which is the European counterpart to the US system (Ludden, et al., 2000).

1.2.2 Multipath Challenge

Virtually, all positioning techniques and architectures fundamentally rely on line-of-sight (LOS) propagation between transmitters and users to ensure accurate ranges, and therefore positions. The propagation path is unimportant in systems designed for digital data communications as long as the desired bit-error-rate (BER) is satisfied. In contrast to this, radio location systems suffer compromised accuracy with any deviation from the LOS path. Interestingly, in wireless digital data communications, different paths of the

propagation channel are used in an opportunistic approach, dubbed a rake receiver, to enhance the system performance and capacity (Proakis, 2001).

Most wireless channels fall somewhere in between the two extremes of pure LOS and pure NLOS. A mixture of both LOS and NLOS manifests itself as a delay spread channel impulse response. In this dissertation, both pure NLOS propagation and a mixture of LOS-NLOS propagation are referred to as multipath, collectively.

In positioning systems, pure NLOS propagation increases the length of propagation path between transmitter and receiver, and is therefore a source of ranging error. According to measurements conducted by M. I. Silventoinen (1996), the mean and standard deviation of range errors in a typical cellular network channel are on the order of 500m and 400 m, respectively. In the best cases for a GPS receiver operating outdoors, minor reflections with low power may be insignificant when strong LOS signals coming from high elevation are available, whereas in terrestrial based systems, reflections are usually comparable with LOS in most cases. Some positioning impacts due to multipath propagation are shown in Chapter 3 for field data. The results will highlight the significance of multipath effect inherent to terrestrial wireless propagation.

Indoors, there are often no LOS signals available for both GPS and cellular network positioning systems due to obstruction by various materials and a high likelihood of pure NLOS propagation. The propagation medium between transmitters and receiver in the indoor case may range from an open window to thick obstructive media along with a multitude of surrounding objects causing reflections and scattering.

Modeling of the wireless channel, both outdoor and indoor, is essential to improve the accuracy and performance of positioning systems. Some comprehensive sources for wireless propagation modeling can be found in Caffery (2000), Blaunstein & Anderson (2002), Liberti & Rappaport (1999), and Parsons (2000), for example, among numerous other sources and references. Nevertheless, characterization of multipath effects is difficult if not impossible due to their complexity and variation particularly in indoor environments.

1.3 Meeting the Multipath Challenge

Given the positioning systems encountering the specified multipath circumstance, an understanding of multipath characteristics and their impact on positioning is critical for overall performance improvement. Deterministic approaches for the modeling of multipath are useful for some ad-hoc applications; however these may not be effective for all circumstances. In contrast, stochastic models provide a more generalized framework for analyzing and characterizing multipath, in addition to allowing algorithm design and development for different multipath-affected circumstances.

Some NLOS mitigation techniques can be found in Le et al (2003), Cong & Zhuang (2001), Wylie & Holtz (1996), Chen (1999), Woo, et al., (2000), Borras, et al., (1998), and Wang & Green (2000), among other references. Most of the aforementioned references assume that the pure NLOS range measurements have a larger variance than LOS measurements, especially when the MS is moving, and then conduct a process for mitigating the NLOS effect. For example, exploiting measurement variance, Le, et al.,

(2003) manipulates two Kalman filter processes, biased and unbiased, to smoothe the NLOS impact on positioning.

Braasch (2001) compares the performance of some well known discriminator-based and correlation-based multipath mitigation techniques (i.e., narrow correlator, strobe and edge correlator, and enhanced strobe correlator) which are applicable to the LOS-NLOS mixture case. The approaches discussed in Braasch (2001) are mostly useful for wide-band GPS signals. Although the cellular network signals are spread over a large bandwidth, the transmitters cut down the side lobes of the spread signal for spectral efficiency. Hence, the side lobes having high frequency content cannot be exploited in wide band oriented scenarios such as the narrow correlator.

Subspace methods (primarily multiple-signal-classification (MUSIC)) have also been proposed for resolving and then mitigating the multipath effect (Selva 1999). This class of multipath mitigation techniques is very useful in separating multipath components from LOS (leading component in general) as the signal of interest. Klukas (1997) demonstrated some experimental results using MUSIC for positioning in a network centric architecture operating under the Advanced Mobile Phone Service (AMPS). Lu (2007) utilized MUSIC to estimate the LOS AOA in order to mitigate the effect of multipath using a beam-former which attenuates the signal coming from NLOS directions. In Chapter 6, MUSIC and a novel approach will be discussed and shown to be applicable to the IS-95 CDMA wireless cellular network architecture.

1.4 Research Overview

1.4.1 Motivation

Due to the narrower spectral content of cellular network signals as compared to GPS, wide band approaches (e.g., narrow correlator, strobe correlator) exploiting autocorrelation properties of a wide band signal cannot be directly used to mitigate the multipath effect. Additionally, due to lower elevations of the cellular transmitters, it is very common in terrestrial wireless channels that the multipath interference conveys a short delay profile with power levels almost comparable to LOS, even in outdoor circumstances. These characteristics intensify the challenge of multipath as a bottleneck, beyond the detectability issue, in achievable accuracy and performance of cellular network positioning. Hence, developing multipath mitigation techniques suitable for cellular network positioning is the overarching motivation for this research.

In Chapters 5 and 6, two techniques are proposed to mitigate the multipath effect using general stochastic properties of the multipath itself. Proposed techniques necessitate spatial-temporal diversities of the incoming signal which are achievable via multichannel architecture in the front end. A multichannel IS-95 CDMA prototype front-end designed, implemented, tested, and verified in the Positioning-Location-And-Navigation (PLAN) group of the University of Calgary, provides an infrastructure for the testing and validation of advanced positioning techniques. The PLAN front end is utilized to assess the feasibility of advanced multipath mitigation techniques proposed in this thesis by providing spatial-temporal field measurements of the IS-95 CDMA signal. It should be mentioned that the PLAN front end was released during the course of study of this thesis.

Hence, Chapter 3 is dedicated to analyzing the front end characteristics which directly impact the proposed mitigation techniques.

1.4.2 Objective and Intended Contributions

Based on the aforementioned motivations, the objective of this research is to improve wireless cellular network positioning accuracy using spatial-temporal observations in a mobile-centric architecture, in a TDOA-based approach, for a typical outdoor multipath wireless channel. Major tasks include empirical measurement of channel effects, PLAN prototype hardware characterization, position fix based on empirical measurements in the cellular network, theoretical manipulation of novel multipath mitigation techniques, algorithm implementation, verification, and test with field data. The major contributions are listed below chronologically:

1- Development of a test bed for collecting field IS-95 CDMA signals and characterizing PLAN multi-channel receiver impairments including thermal noise, phase imbalance, frequency stability, and inter-channel coupling (Chapters 3 and 5)

2- Cellular network position fix and analyses with field measurements (Chapters 4, 5, and 6)

3- BTS identification algorithm (Chapter 4)

4- Optimum non-coherent detector of a signal buried in noise (Chapter 4)

5- A multipath mitigation technique using coherent combining of space-time observations along with analyses and experimental results (Chapter 5)

6- Derivation of space-time super resolution technique (MUSIC) along with corresponding analyses and experimental results (Chapter 6)

Some empirical campaigns have been done for the final objective listed above. In addition, some system developments, both hardware and software, have been done during the course of study to build up the infrastructures needed for collecting field data and analyses. These efforts will not be addressed in this thesis, unless they represent theoretical content or directly impact the analyses addressed in the experimental portions.

1.4.3 Thesis Outline

This thesis consists of six chapters. Chapter 1 has briefly introduced the cellular network positioning challenges and the overall objective of the research. Chapter 2 discusses cellular network positioning approaches, applications, and limitations. Chapter 3 presents additional background material on the IS-95 signal structure, PLAN prototype front end, and practical challenges of its multichannel architecture. Based on the described infrastructure and background in Chapter 3, some field static positioning results and analyses are presented in Chapter 4. Chapter 5 focuses on analyses, implementations and tests of a technique for mitigating multipath effect using space-time observations provided by the PLAN front end in a pseudo-static mode. It also demonstrates some positioning results and enhancements based on the proposed technique. Chapter 6 attempts to give a comprehensive study of the MUSIC algorithm and also to generalize MUSIC into the space-time domain in order to enhance the resolvability of the MUSIC. It also demonstrates some positioning results and enhancements based on the space-time

MUSIC algorithm proposed in this chapter. Conclusions and recommendations for future work are presented in Chapter 7.

Chapter Two: Cellular Network Positioning Techniques

Current wireless positioning systems and techniques consist of some compromises among cost, accuracy, availability, reliability, and flexibility. There are some intrinsic challenges in the systems, approaches and infrastructures which affect the overall performance of each technique. Hence, there is not a conclusive answer to such a question as, "What is the most suitable technique for cellular network positioning?" Nevertheless, *a priori* knowledge about the intended application for the positioning system, intended operational environment, system complexity, and invasiveness toward the previously established infrastructure narrow down the possible alternatives to one preference.

In this chapter, well known ground-based radiolocation techniques applicable to the wireless cellular network positioning problem and some fundamental aspects of each individual technique in the context of cellular network positioning are addressed. The techniques have already been studied thoroughly in many books, articles and theses; hence, it is beyond the scope of this chapter to provide a complete overview of the techniques.

2.1 RSS Method

Received-signal-strength (RSS) is defined as the power measured by a power detector circuit implemented in the receiver. The RSS of RF signals can be obtained during normal signal transmission without demanding additional bandwidth. RSS measurement is relatively inexpensive and can be simply implemented in the receiver; however, it is

unreliable because of its unpredictable and not well modeled (i.e., large variance) sources of error. The RSS method is based on the fact that the average power of a received signal decays as a function of the distance between transmitter and receiver. Hence, a unique relationship between signal power and range can be established. The MS position can be estimated based on the range measurements indirectly obtained from power estimation followed by the traditional trilateration method.

In free space, signal power decays proportionally as d^{-2}, where d is the distance between transmitter and receiver. In a wireless channel, shadowing and multipath are two major error sources in RSS measurement which deteriorate with the quadratic property of free space attenuation. Reflection and refraction of the radio wave from objects are associated into multipath and shadowing phenomena, respectively. Due to the multi-component nature of the multipath, its effect can be constructive or destructive in RSS measurement but shadowing always causes the destructive (i.e., attenuative) effect on the signal. The shadowing effect can be modeled stochastically and some RSS techniques take advantage of the *a priori* stochastic models to enhance the performance of the RSS method.

Statistical Model of RSS

Stochastically, the received mean power in wireless radio channel decays proportional to d^{-n}, where n is typically between two and four. Based on a wide variety of measurements, Hashemi (1993) attests that the difference between a measured received power and its stochastic mean can be modeled as a log-normal distribution (i.e., Guassian if expressed in decibels). Thus, the received power, in terms of dBm, at the receiver is distributed as:

$$f(p) \sim N(p; \overline{P}(d), \sigma_{dB}^2) \tag{2.1}$$

where *N* denotes normal distribution and

$$\overline{P}(d) = P_0 - 10n \log \frac{d}{d_0} \tag{2.2}$$

where P_0 is the received power at a short reference distance, d_0.

It is worthwhile to mention that the standard deviation of received power, σ_{dB} , is expressed in units of dB (not dBm), and is relatively constant with distance. σ_{dB} is typically a constant between 4 and 12 (Patwari, et al., 2005). A range independent constant standard deviation in dB means that any deviation from the actual value leads to a multiplicative factor which has a different impact on the measurement error depending on the actual range. For example, given a multiplicative factor of 1.5 at an actual range of 100 m, the measurement error is 50 m while at an actual range of 10 m, the measurement error becomes 5 m. Hence, RSS-based range estimates have variance proportional to actual range. Therefore, if the distance from MS to BTS increases, the accuracy of the estimation deteriorates. Due to the aforementioned model of measurement, RSS errors are referred to as multiplicative, contrary to the additive behaviour of the errors in the other techniques (e.g., TOA, TDOA).

Besides propagation effects (i.e., multipath fading and shadowing), azimuth-dependent radiation patterns in transmitter antennas and power control mechanisms (for controlling the cell size) are the other error sources in the RSS technique. Measured RSS is also a function of the calibration of both the transmitter and receiver. Generally, the RSS

technique cannot meet the FCC E-911 requirement for positioning accuracy. Nevertheless, its main advantage is its simplicity.

2.2 Fingerprint Method

In an indoor environment or an urban area, multipath fading and shadowing have a dominant effect; hence, the RSS method does not provide sufficient accuracy. For improving accuracy while maintaining the simplicity of the positioning system, advanced propagation models are required. Alternately, the actual field distribution in the area of interest must be extracted from training measurements. In this technique, the RSS in the cellular network is known *a priori* as a function of position. This is technically referred to as the fingerprint method. Due to the highly non-linear input-output mapping between received power and distance, some non-linear technique for pattern matching and learning is required (neural networks are used (Vosseik, et al., 2003)) to identify the closest recorded template to the measured one. Pattern matching, in computer science, is generally used to test whether things have a desired structure, to find relevant structure, to retrieve aligning parts, and to substitute the matching part with something else. In fingerprint radiolocation, the actual distribution of the electromagnetic field is obtained from measurements of the received power at known positions. The distribution is then stored on the central server (off-line phase), and serves as input for the position calculation engine in the operational phase. Figure 2.1 shows the fingerprint-based positioning architecture.

This system is useful under the criteria of minimal installation-integration into standard communication systems, infrastructure, and also maintenance cost.

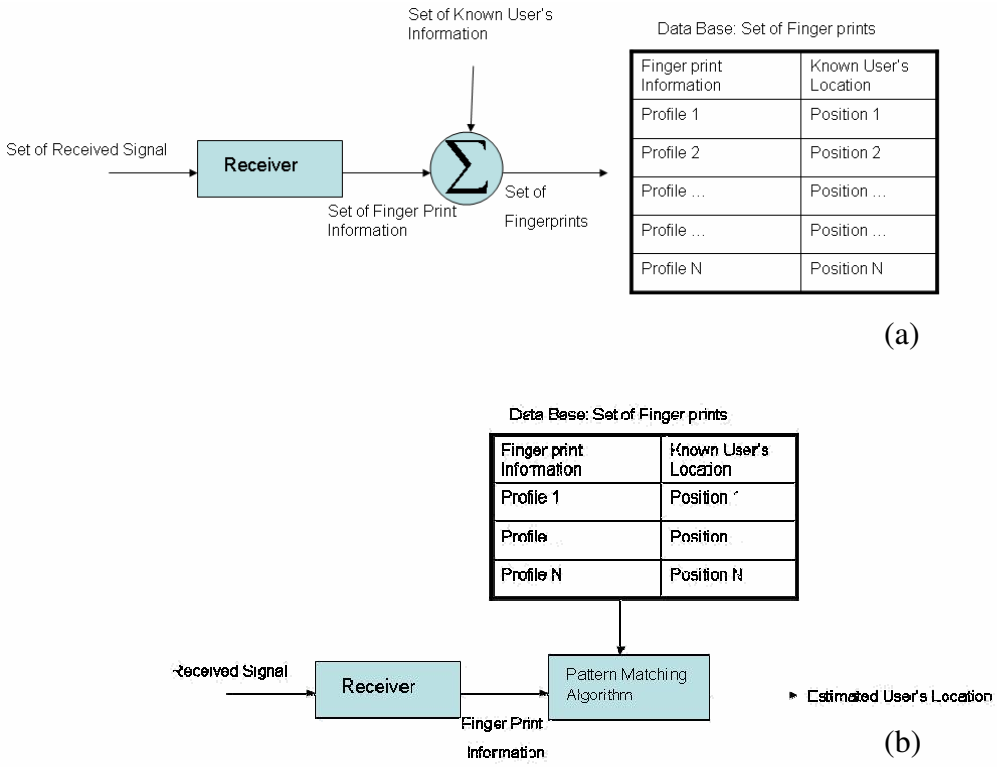

Figure 2.1: Fingerprint radiolocation a) off line phase, b) operational phase

Typical system accuracy and parameters for an indoor scenario are summarized in Table 2.1 (Vossiel, et al., 2003) for a system developed by SIMENS called the neural cellular positioning system (NCPS), deployed on digital-enhanced-cordless-telecommunications (DECT) and wireless-LAN (WLAN) 802.11. While the infrastructure is different than the cellular network positioning, the concept and accuracy are extendable to the cellular network case.

Table 2.1: Typical parameters of NCPS system

Accuracy	5-15 [m]
Coverage	100% inside cellular network LOS and NLOS
Acquisition speed	2-5 second
Infrastructure	DECT or WLAN 802.11

2.3 Cell ID Method

Cell ID positioning is another simple economic method and it does not require any upgrade of handsets or network equipment. Due to the dynamics of the MS within a cell, accuracy depends on the cell size. Accuracy may range from tens of metres to some kilometres (Trevisani & Vitaletti, 2004). Figure 2.2 shows a simplified view of the cellular network topology and MS.

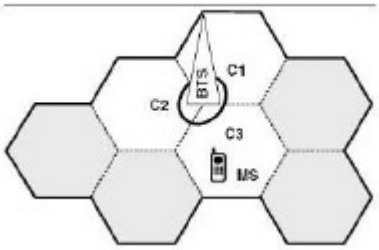

Figure 2.2: Cell ID Radiolocation

The MS continuously selects a cell, and exchanges data and signaling traffic with the host BTS. Cells are grouped into clusters, each of them identified by a location-area-identifier (LAI). For avoiding excessive traffic load, as long as the MS is in idle mode, the network knows only the LAI. The network becomes aware of the cell-ID only when the MS starts

sending/receiving data and then each BTS broadcasts both the LAI and the cell-ID. Hence, the MS position within the resolution of the cell is obtainable on the MS side and within the resolution of the LAI. The cell is obtainable on the BTS side. In TDMA-based cellular network positioning, there is a potential to improve the accuracy by measuring the change in slot timings of the frames (Trevisani & Vitaletti, 2004); however, this method does not have enough potential to be enhanced.

The positioning in the cell-ID approach is not accurate enough for most of the interesting applications. Essentially, if the cell radius is larger, the accuracy degrades. Similar to the other techniques, the cell-ID approach suffers from multipath because the assignment of the MS to an active host cell is based on signal strength. Hence, an obstacle can easily block the nearest BTS relative to the MS and invoke the more remote BTS as host. It is worthwhile to mention that the cell geographical area is not necessarily an idealized symmetric hexagonal shape; it can be very irregular with unconnected parts and can be very large in specific directions. Figure 2.3 shows the topology of some BTSs belonging to the Telus company (cell phone service provider) in Calgary.

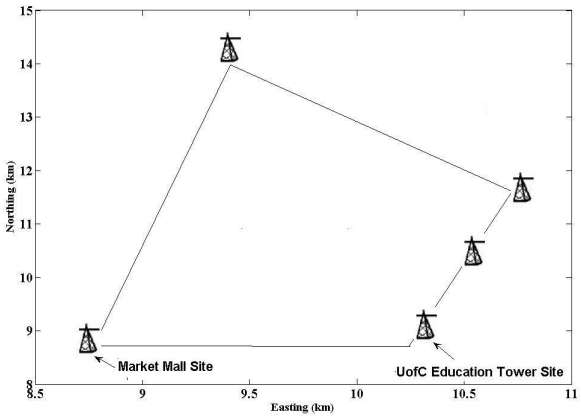

Figure 2.3: Telus BTSs in Calgary

2.4 TOA Method

The TOA method is the dominant method used in radiolocation. TOA is the measured time at which an RF signal first arrives at a receiver. The measured TOA consists of the propagation-induced time delay and also measurement errors which can be as simple as a fixed known bias or as complex as an unknown time variable source of error. After measuring the absolute signal propagation time between BTS and MS, the distance/range between the BTS and MS is estimated. The estimated ranges among different BTSs provide the required pieces of information for the traditional trilateration method. As shown in Figure 2.4, the MS position is the intersection of three circles centered at three BTSs. In a more general case, i.e., the multilateration method, more than three BTSs can be exploited to enhance the estimation procedure and to verify the reliability of the solution. Given the precise time synchronization of all involved fixed and mobile units, TOA based techniques provide reasonable accuracy. However, the absolute time synchronization must be at least as precise as the desired positioning accuracy. For example, a positioning error budget of ± 1 m requires absolute time synchronization significantly better than 3 ns. Since the transmitter timing has to be recovered and tracked in the MS unit, TOA leads to a prohibitively complicated and expensive architecture on the receiver side.

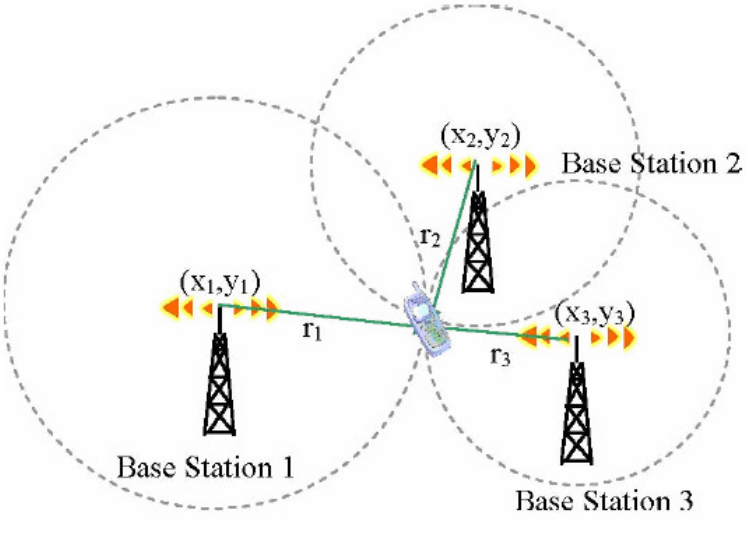

Figure 2.4: Illustration of TOA based method on three BTS's

The cornerstone of time-based techniques is the receiver's ability to accurately estimate the arrival time of the LOS signal. Even in the absence of a multipath signal, the accuracy of the arrival time has an innate limitation imposed by additive noise. This means that for a given bandwidth and SNR, the TOA estimate can only achieve a certain amount of accuracy. This type of analysis for investigating the performance boundaries is called the Cramer-Rao-Lower-Bound (CRLB) which is a mature field of study. It is well known that the CRLB sets a lower limit for the variance, or covariance matrix, in general, of any unbiased estimates of an unknown parameter. The bound is useful as a guideline for knowing the best an estimator can possibly do which in turn helps researchers to judge the estimator performance. Given a perfect timing recovery in the receiver, for the TOA positioning problem based on the transmitted signal, $s(t)$, in a multipath-free channel, it can be shown (Kay 1998 , Qi 2003) that the lower bound is as follows:

$$\mathrm{var}(\hat{\tau}) \geq \frac{1}{8\pi^2 \beta^2 SNR} \tag{2.3}$$

where $\hat{\tau}$, SNR and β^2 are estimated TOA, signal to noise ratio (SNR), and the effective mean square bandwidth of the signal, respectively.

$$\beta^2 = \frac{\int_{-\infty}^{\infty} f^2 |S(f)|^2 df}{\int_{-\infty}^{\infty} |S(f)|^2 df} \tag{2.4}$$

where *S(f)* is the single side Fourier transform of the transmitted signal, *s(t)*. Since the cellular network uses the CDMA signal, its spectral property can be incorporated to derive a closed form for TOA accuracy (CRLB) in an ideal case but with ambient noise as follows.

Consider a cellular CDMA system with chip rate T_s and carrier frequency F_c. The CDMA signal is deemed to have a flat spectrum within its bandwidth, *W,* which is approximately $\frac{1}{T_s}$. Given spectral flatness within bandwidth, β^2 can be approximated as:

$$\beta^2 = \frac{\int_{F_c-W}^{F_c+W} f^2 |S(f)|^2 df}{\int_{F_c-W}^{F_c+W} |S(f)|^2 df} \approx F_c^2 \tag{2.5}$$

Substituting Equation 2.5 into Equation 2.3, the CRLB for TOA (i.e., innate uncertainty due to the noise) is

$$\text{var}(\hat{\tau}) \geq \frac{1}{8\pi^2 F_c^2 SNR} \tag{2.6}$$

In the IS-95 cellular network, carrier frequency and chip rate are about 2 GHz and 1.2288 MHz, respectively. For a nominal value of $SNR=10$, the 1σ accuracy for TOA can be as

small as 0.018 nsec which, in terms of distance, is equal to 5 mm. This simple analysis does not include the probability of errors in a multi-hypothesis search. Notwithstanding, it emphasizes that the fundamental variance caused by only AWGN ambient noise is generally negligible in the LOS TOA scenario. What are not negligible, though, are the biases due to systematic error, clock offset, stability, and multipath.

The CRLB for more realistic scenarios taking into account the clock offset, multipath, and NLOS effect have been studied in many articles, e.g., Qi, et al. (2004) and Koorapaty (2004), and theses , e.g., Qi (2003). All that is needed to calculate CRLB is the statistical model with conditional PDF of the random measurement, i.e., $f(X \mid \theta)$ where X is the measurement and θ represents the parameters that are to be estimated from the measurements. After establishing the statistical model, any unbiased estimator, $\hat{\theta}$, must satisfy Equation 2.7, i.e.,

$$Cov(\hat{\theta}) \geq \left\{ E\left[-\nabla_{\theta} (\nabla_{\theta} \ln f(X \mid \theta))^{T} \right] \right\}^{-1} \tag{2.7}$$

where $Cov(\hat{\theta})$ is the covariance matrix (i.e., the statistics that represent the performance and dependence) of the estimated parameters, $E[.]$ indicates expected value, ∇_{θ} is the gradient operator over parameters θ, and the superscript T indicates the matrix transpose. Equation 2.7 has an intuitive interpretation as: If the negative curvature of the Fisher information (i.e., amount of information that an observable random variable, X, carries about an unknown parameter, θ, upon which the likelihood function, $f(X \mid \theta)$, depends) is very large, then the parameter can be accurately identified.

TOA range errors in multipath circumstances can be many times greater than those caused by additive noise alone. It was mentioned in Chapter 1 that multipath in the TOA measurement manifests itself in two ways:

1- Early-arriving multipath in which the multipath signals arrive in short delays after the LOS signal, and their contributions change the real TOA of the LOS signal.

2- NLOS in which the LOS signal is severely attenuated compared to late arriving multipath components; this leads to substantial positive range error.

Traditionally, correlation processing is used in CDMA positioning systems which will be explained in Chapter 3. Since the peak width of the autocorrelation function is inversely proportional to the signal bandwidth, to achieving greater temporal resolution in a multipath environment, a wider signal bandwidth is required. Hence, a narrow autocorrelation peak enhances the ability to pinpoint the leading edge of a signal and helps to isolate the LOS signal from the early-arriving multipath signals. Chapter 4 analyses and demonstrates the multipath and its impact on positioning based on field wireless cellular network measurements.

2.5 TDOA Method

TDOA is a modified version of TOA in which the relative signal transmission times between BTSs and MS are measured and converted to range (or pseudorange) differences. TDOA methods using range differences are widely used to deal with the bias at the receiver. Two mathematically equivalent approaches called hyperbolic positioning

and pseudorange positioning can be deployed to use the range differences or pseudoranges. Due to the equality of the hyperbolic and pseudorange methods, single point GPS positioning using pseudorange can be considered as an equivalent form of hyperbolic positioning in three dimensions (Lachapelle 1999). In pseudorange positioning, ranges are measured within the receiver time frame and bias, while in the hyperbolic mode, the distance differences at an unknown point from at least two known points (usually but not always transmitters) are measured. In general, using only two known points introduces ambiguity in the position fix process, however, it may be resolvable in some applications where transmitter positions are not uniformly scattered around the receiver (for example, long-range shore-based systems used for ship positioning). In cellular network positioning, at least three hyperbolae (i.e., four BSs) are needed to resolve the ambiguity when the distance between the BTSs are short.

The major advantages of the TDOA method are 1) its robustness to the common source of biases and errors in pseudoranges, and 2) its synchronization isolation of the MS and BTS. In other words, TDOA does not require that the MS be synchronized to the CDMA network, though BTSs still must be synchronized and use the same time reference. The major disadvantages for the TDOA mode are that more transmitters are required and a TDOA has a relatively rapid geometric dilution of precision (GDOP) degradation (Lachapelle 1999).

It is worthwhile to mention here that the positioning accuracy for all positioning techniques depends not only on the measurement accuracy but also on the geometry of the MS and BTSs. This is due to the fact that some non-linear transformations map measurements to the parameter of interest (i.e., position) and the measurement error is

therefore non-linearly propagated into the positioning error. The GDOP is commonly used to quantify the effective sensitivity of the position parameters to the measurement. If an estimator uses range measurements with common variance, σ_d^2, and achieves a position variance σ_l^2, then its GDOP is defined as $GDOP = \frac{\sigma_l}{\sigma_d}$. Greater GDOP leads to greater positioning error for the same set of measurements. TDOA and TOA give the same performance if all signals arrive simultaneously at all receivers because the transmission time does not add any information.

2.6 AOA Method

By providing information about the direction to the neighboring BTS rather than the distance to that BTS, AOA measurements provide position information complementary to the TDOA and RSS measurement. In the AOA technique, the MS is the intersection of the directional lines derived from AOA measurements as shown in Figure 2.5.

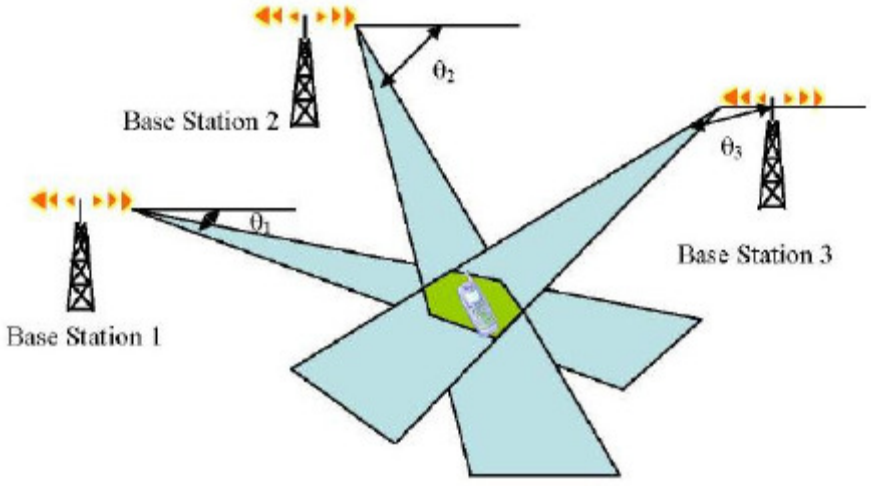

Figure 2.5: Illustration of AOA based method with three BTSs

The advantage of the AOA method is that only two BTSs are required to estimate the MS position in 2D. The aforementioned property is very helpful in cases where fewer than three BTSs are available (mostly rural areas). It was mentioned before that the TOA method requires strict timing synchronization between the BTSs and the MS. The TDOA method diminishes this restriction to only the BTS synchronization requirement. AOA moves another step forward in loosening the timing synchronization challenge as AOA does not even need synchronization within BTSs.

The accuracy of positioning from AOA measurements depends on the distance between the MS and BTS and also the AOA itself. The further the MS is from the BTS, the larger the positioning uncertainty. Figure 2.6 illustrates the dependency of the positioning error (i.e., dx) on measurement error (i.e., $d\theta$) and distance itself (i.e., R).

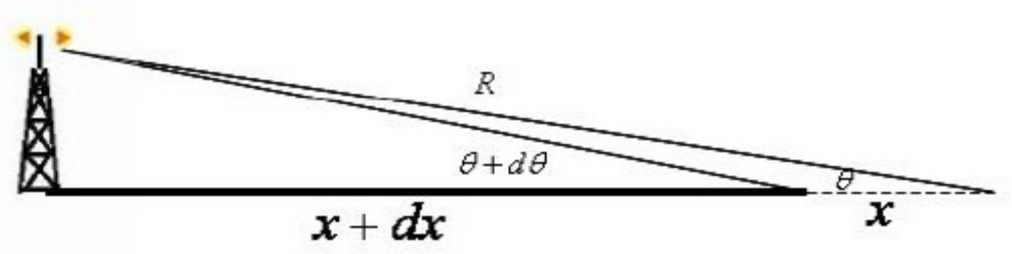

Figure 2.6: Positioning error in AOA

From Figure 2.6,

$$x = R\cos(\theta) \tag{2.8}$$

and an error in θ leads to an error in x as follows:

$$dx = -R\sin(\theta)d\theta \tag{2.9}$$

Equation 2.9 can be interpreted in another way: The AOA measurement leads to an equivalent GDOP proportional to distance.

The most common method for AOA estimation is to use an antenna array and exploit array processing techniques at the receiver. In this case, the receiver is comprised of two or more antennas whose relative locations are known by the receiver. The AOA is estimated from the difference in arrival times for a transmitted signal at each of the antenna elements. When the impinging signal bandwidth is much less than its carrier frequency (i.e., narrowband signal), then a time delay, τ, relates to a phase delay, ϕ, via the relation $\phi=2\pi F_c\tau$, where F_c is the centre frequency. Essentially, narrowband AOA estimators are often formulated based on phase delay. By measuring the phase delays, or equivalently the time delays among different antennas, AOA can be estimated using *a priori* knowledge of antenna geometry. A second approach to AOA estimation uses the RSS ratio between two or more directional antennas (Ash & Potter, 2004). By overlapping main beams, AOA can be estimated from the ratio of each individual RSS value.

Additive noise and multipath are two main sources for impairing AOA measurement. Due to the multipath around an MS, the AOA measurement contains different components corresponding to different directions. It is necessary to detect if the received signal direction is indeed a LOS component or a multipath component which imposes a potentially large bias on the position estimate. Hence, AOA estimation must be used with multipath mitigation techniques and assistance.

2.7 Performance Comparison in Different Radiolocation Systems and Approaches

Figure 2.7 depicts a rough performance (i.e., accuracy versus availability) overview of the aforementioned wireless positioning techniques compared to legacy GPS in different environments (Vosseik, et al., 2003).

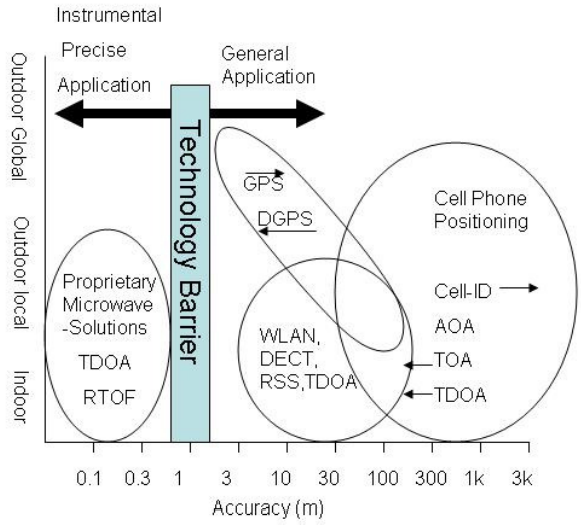

Figure 2.7: Overview of some wireless positioning system

The technology barrier discriminates between a precise positioning application (e.g., logistics, automation, process control, etc.) that requires accuracy significantly better than 1 m and less accuracy intensive applications.

It can be seen that GPS has its shortcoming in dense urban areas and inside buildings where heavy, and strongly-growing local wireless data transfer takes place. Taking advantage of cellular network backbones and infrastructure, cellular network schemes can be exploited to expand positioning-oriented applications into dense urban areas and indoor situations. Nevertheless, the expectation for achievable accuracy may not be as high as GPS performance in open sky.

This chapter provided the basic background to explain different schemes applicable to the cellular network positioning problem. Each individual aforementioned scheme is a complete field of research, hence, only general concepts and ideas were addressed. The following chapters will provide more details about one selected technique, namely TDOA, along with its challenges, analyses, and field positioning results.

Chapter Three: Signal Structure and PLAN Prototype Receiver Architecture

Chapters 4, 5 and 6 contain experimental results based on field measurements in the wireless cellular network. The field measurements and results are all based on the downlink IS-95 pilot signal which carries the timing information for the positioning system. Hence, the current chapter addresses the signal structure and hardware architecture by which the tests are conducted and raw IS-95 data is collected. Following that, some fundamental receiver challenges, impairments, and limitations in the hardware are characterized and reviewed. These ad hoc characteristics of the receiver will be considered in Chapters 4 and 5 when the notion of space-time observations is discussed along with some experimental results based on the PLAN prototype front end.

3.1 IS-95 CDMA Forward Link Pilot

By far, the most widely deployed CDMA technology is the IS-95-based cellular and PCS CDMA technology used in North and South America and Asia (Liberti & Rappaport, 1999). This technology, which includes the IS-95A standard for 800 MHz cellular systems and the JSTD-008 standard for 1900 MHz PCS systems, will be collectively referred to as IS-95.

Full duplex (i.e., two way) cellular communications relies on a variety of channels to ensure call connection and delivery. Control channels include paging channels that are used to notify subscriber units of incoming calls and access channels that let the subscriber initiate outgoing calls (Liberti & Rappaport, 1999). Traffic channels are used

to support customer voice calls and messages. In a CDMA network, all BTSs use the same frequency channel, or carrier. Each BTS is synchronized to CDMA system time which is derived from a precise time reference supplied by GPS satellites. In IS-95 CDMA, every BTS transmits a pilot signal on the downlink using the same pseudo-noise (PN) sequence. However, each pilot is offset in time from the others, allowing the subscriber to differentiate the signals. The offset is an integer multiple of 64 chips, or 52.08 μs equivalently. The pilot PN sequence is 32768 chips long, at a chip rate of 1.2288 Mchip per second, so that each PN sequence repeats every 26.67 ms. The IS-95 CDMA subscriber unit searches for pilot signals that are strong enough to be detected. Each CDMA subscriber unit can combine at least 3 independent forward traffic signals, using a rake receiver, to improve reception. In this case, since the subscribers are not distinctly attached to one BTS or the other, the subscriber is said to be in soft handoff. This state is quite useful, especially at the edge of the cell.

IS-95 BTSs typically use 10 to 20 watt (40 to 43 dBm) RF amplifiers to provide composite power of the pilot, sync, paging, and traffic channels (Liberti & Rappaport, 1999). Typically, 15-20% of the total transmitted power is reserved for the pilot. This is because the pilot is used for coherent demodulation of other channels and without adequate pilot power, the sync, paging, and traffic channels cannot be recovered.

Table 3.1 shows the power budget for different channels of a typical BTS in the IS-95 CDMA cellular network (Liberti & Rappaport, 1999).

Table 3:1 Percentage of Composite RF Power Assigned to Different IS-95 Channel

Channel	% of RF Power
Pilot	20%
Sync	2%
Paging	14%
All Traffic Channels	64%

Due to the substantial strength of the pilot channel in the IS-95, and also due to the dataless property of the pilot, it can be considered as a favourable signal part of IS-95 in cellular network positioning systems. In addition, there is no power control mechanism in the pilot channel, as opposed to the traffic segment, which leads to a better detectability than with the other channels.

3.2 Pilot Signal Generator

Figure 3.1 shows a quadrature spreading operation that is the final stage in generating the base band pilot sequence in the BTS. A quadrature-phase-shift-keying (QPSK) modulator then transfers the baseband signal to the RF centre frequency for RF propagation via the antenna.

An all zero input to the module emphasizes the fact that the pilot is not modulated with data. The two PN-sequences used for quadrature spreading are based on two maximum

length sequences (M sequence) that can be generated by two 15 tap linear-feedback-shift-registers (LFSR) using generator polynomials (Liberti & Rappaport, 1999):

$$G_i(x) = x^{15} + x^{13} + x^9 + x^8 + x^7 + x^5 + 1 \tag{3.1}$$

and

$$G_q(x) = x^{15} + x^{12} + x^{11} + x^{10} + x^6 + x^5 + x^4 + x^3 + 1 \tag{3.2}$$

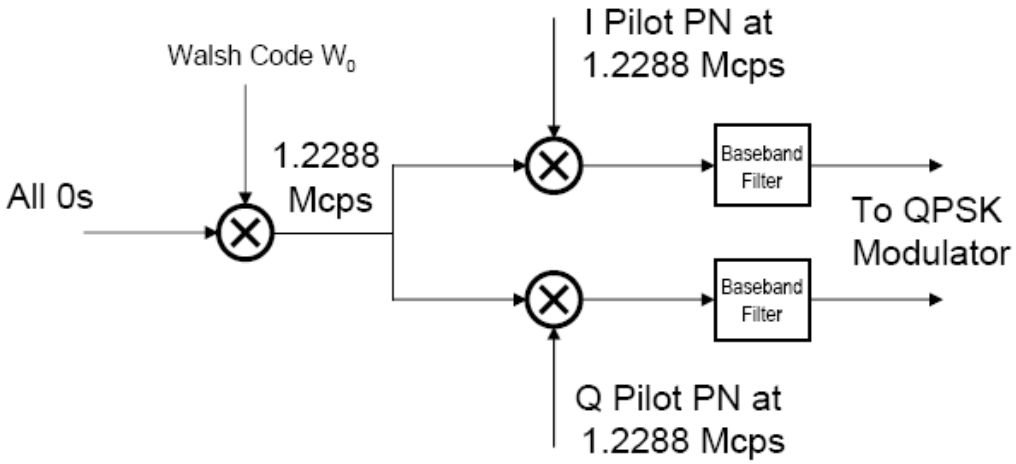

Figure 3.1: Quadrature spreading stage for the forward channel

The pilot PN sequences, *i(n)* and *q(n),* are generated by the following linear recursions:

$$i(n) = i(n-15) \oplus i(n-10) \oplus i(n-8) \oplus i(n-7) \oplus i(n-6) \oplus i(n-2) \tag{3.3}$$

$$q(n) = q(n-15) \oplus q(n-13) \oplus q(n-11) \oplus q(n-10) \oplus q(n-9) \oplus q(n-5) \oplus q(n-4) \oplus q(n-3)$$

where $i(n)$ and $q(n)$ for $1 \le n \le 32{,}767$ represent a binary value of 0 or 1, $i(15)= q(15)=1$, and $\oplus$ represents modulo -2 addition also known as exclusive OR.

The M sequences generated by these polynomials have length 2^{15}-1 and an extra zero is padded at the end of the sequences to give the total length 2^{15} = 32768 chips. As the chip rate in IS-95 is 1.2288 Mcps, each of the aforementioned sequences is 26.667 ms long which implicitly makes 75 repetitions every 2 seconds.

It was mentioned before that every BTS uses a different pilot PN sequence offset index separated by an integer multiplier of 64 chips, so that there are 512 offset indices in overall. The original PN sequence is designed such that different offsets corresponding to different BTSs do not cause considerable interference problems. In Figure 3.1, the Walsh code, W_0, is a sequence of all zeros for the pilot channel while it can be non-zero sequences for the other channels (i.e., sync, page, and traffic) to keep the orthogonality of the different segments and users.

In the cellular network, BTSs are presumably synchronized by utilizing the GPS reference time in their timing circuits, hence, timing information is consistently preserved in the transmitted pilot signals. If the receiver has access to the reference time of the transmitters, i.e., GPS time, the entire link between MS and BTS can be considered a synchronous network. In this case, TOAs corresponding to active BTSs include the transmission time in addition to intrinsic code offsets associated with each BTS. Measuring the transmission time is fundamental to this thesis, so the following subsection describes the primary processing module for extracting the parameter of interest, i.e., TOA, from the transmitted pilot signal.

3.3 Despreading Process

Channel Impulse Response (CIR) measurements are sufficient statistics (i.e., a pre-processed measurements which contain required information for estimation purpose) for estimating the signal delay because the propagation delay between each BTS and the MS can be observed from the CIR. Hence, CIR estimation indirectly leads to TOA/TDOA estimation as the parameter of interest. CIR also allows for further characterization of the LOS and NLOS multipath components for more accurate and robust timing assessments. Despreading the CDMA pilot is a conventional method for CIR estimation in a slow fading channel, where the channel is assumed to be stationary during observation. In the despreading process, the complex received signal (i.e., I and Q pair) is correlated with locally generated code and integrated over an interval. Figure 3.2 shows the despreading process applied to the received IF signal.

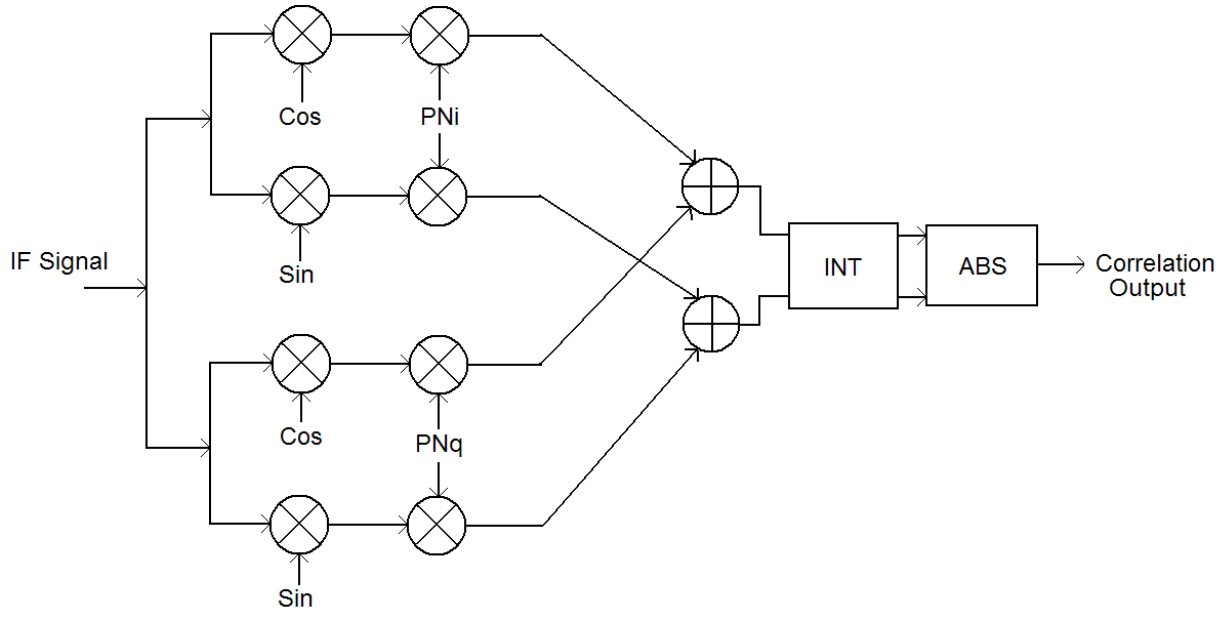

Figure 3.2: Despreading process of IS-95 CDMA signal

The correlation output conveys superimposed CIRs corresponding to different visible BTSs. There is some amount of degradation in detectability due to the non-ideal correlation properties of the pilot. Figure 3.3 shows a typical output (correlation magnitude) obtained by despreading the field IS-95 signal. Each strong peak in Figure 3.3 is a candidate for TOA/TDOA measurement. With access to GPS time in the receiver, absolute code offsets can be estimated by measuring the indices corresponding to strong peaks. It should be noted that the absolute code offsets include both BTS code offsets and gross TOAs as parameters of interest.

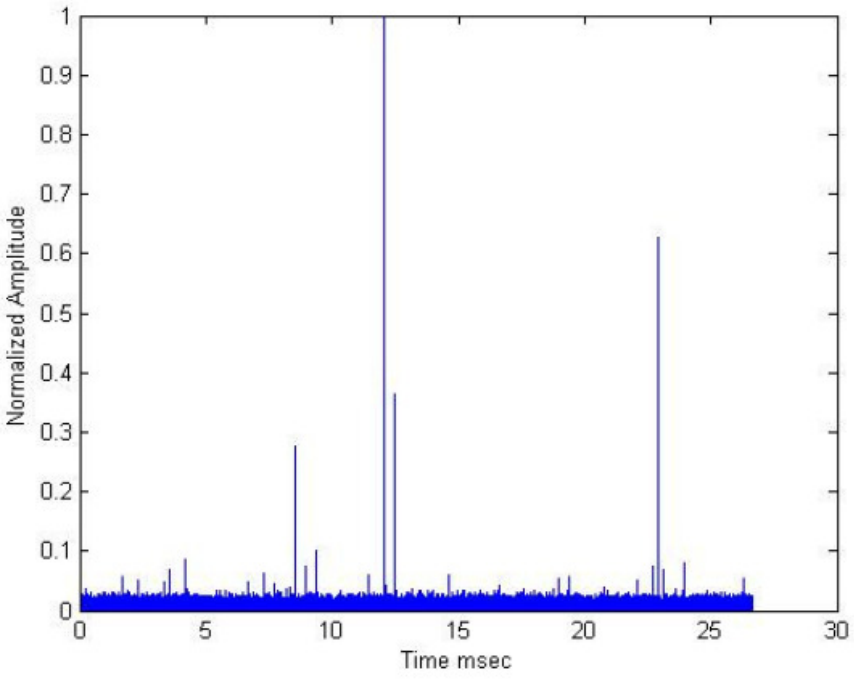

Figure 3.3: Despread IS-95 signal

Local timing offset in the receiver, Doppler frequency in dynamic mode, sample quantization, integration time, and autocorrelation properties of the PN code, all impact the despreading process output. The aforementioned parameters have been studied in the

literature, hence, they will not be addressed here in detail. The following discussion addresses an efficient method for the despreading process using an FFT.

3.3.1 FFT based Despreading Process

FFT-based correlation processing is an efficient method for despreading the CDMA signal. Let the received signal be $r(n)$, then the complex correlation between $r(n)$ and the locally generated sequence, $c(n)$, is given by:

$$R_{R,c}(m) = \frac{1}{N}\sum_{n=0}^{N-1} r(n)c^{*}(n-m) \tag{3.7}$$

Both $r(n)$ and $c(n)$ may be written in the following form:

$$r(n) = \sum_{f=0}^{N-1} R(f)\exp(j2\pi fn/N) \tag{3.8}$$

$$c(n) = \sum_{f'=0}^{N-1} C(f')\exp(j2\pi f'n/N) \tag{3.9}$$

where $R(f)$ and $C(f')$ are the Discrete Fourier Transform (DFT) of $r(n)$ and $c(n)$, respectively. Substituting (3.8) and (3.9) into $R_{R,c}(m)$ (3.7) yields the following:

$$
\begin{aligned}
R_{R,c}(m) &= \frac{1}{N}\sum_{n=0}^{N-1}\left(\sum_{f=0}^{N-1} R(f)\exp(j2\pi fn/N)\right)\left(\sum_{f'=0}^{N-1} C^*(f')\exp(-j2\pi f'(n-m)/N)\right) \\
&= \frac{1}{N}\sum_{n=0}^{N-1}\left(\sum_{f=0}^{N-1} R(f)\exp(j2\pi fn/N)\right) \\
&\quad .\left(\sum_{f'=0}^{N-1} C^*(f')\exp(-j2\pi f'n/N)\exp(j2\pi fm/N)\right) \\
&= \frac{1}{N}\sum_{f=0}^{N-1}\sum_{f'=0}^{N-1} R(f)C^*(f')\exp(j2\pi fm/N)\sum_{n=0}^{N-1}\exp(j2\pi(f-f')/N) \\
&= \frac{1}{N}\sum_{f=0}^{N-1}\sum_{f'=0}^{N-1} R(f)C^*(f')\exp(j2\pi fm/N)N\delta(f-f') \\
&= \sum_{f'=0}^{N-1} R(f')C^*(f')\exp(j2\pi f'm/N)
\end{aligned}
\tag{3.10}
$$

Equation (3.10) indicates that the cross correlation can be achieved by taking the Inverse Discrete Fourier Transform (IDFT) of the product of $R(f')$ and $C(f')$. Hence, its processing may be implemented as shown in Figure 3.4.

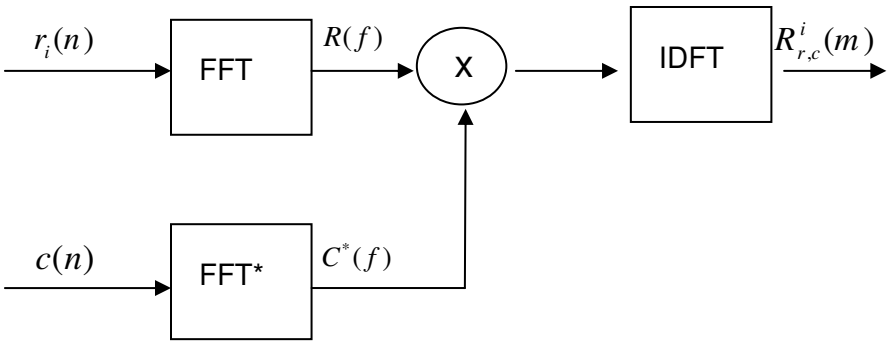

Figure 3.4: FFT-based Correlation Method

3.4 PLAN Prototype Receiver Architecture

The primary objective of this research is to utilize the space-time observations to enhance positioning and verify the scheme feasibility with field measurements. It is hoped that the proposed novel techniques will meet the required positioning accuracy in challenging multipath affected environments. For analyzing real phenomena and developing and verifying realistic positioning algorithms, an RF front end is exploited which was designed, tested, and developed in the PLAN group at the Geomatics Engineering Department of the University of Calgary. The PLAN RF front end has been tuned for ground-based radiolocation positioning system that is based on the interim standard-95A (IS-95A). While the system is designed around IS-95, it is equally applicable for any of the North American CDMA-based standards and can be quickly modified to be compatible with UMTS or arbitrary direct-sequence-spread-spectrum (DSSS) pilots.

The PLAN CDMA receiver demodulates five independent channels using five individual antennas simultaneously and provides the processing unit with spatially independent observations. The PLAN front end is designed (Lopez 2006) to achieve different objectives standard to a wireless receiver such as amplification, filtering, mixing, and demodulation. The single-conversion superhetrodyne architecture was the selected receiver structural design, since low power consumption and a highly integrated scheme were not the primary design objective. For the sake of convenience and flexibility, the timing circuit, including master oscillator, local oscillators, and frequency synthesizers, was fabricated in a separate board called the Synthesizer board in this thesis. Figure 3.5 illustrates the PLAN receiver. After demodulating five channels, five in-phase (I) and quadrature phase (Q) pairs are digitized by a multichannel digitizer with sampling frequency greater than the Nyquist rate. The multichannel digitizer for sampling the raw data is an Octopus CompuScope CS8280 manufactured by GAGE. The important parameters of the digitizer are given in Table 3.2.

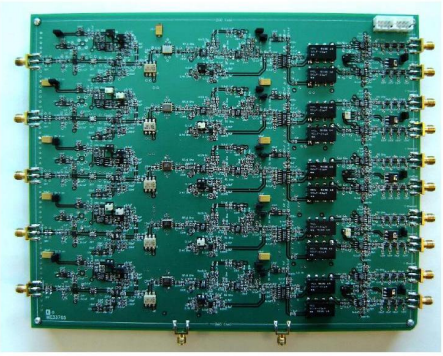

Figure 3.5: PLAN prototype 5 channel CDMA receiver

Table 3: 2 GAGE card specification

Digitizer Parameters	
Sampling Rate	≤ 10 MHz
Sampling Precision	12 bits
Number of Channels	8
Total on board Memory	128 MS
Interface with PC	Single-Slot PCI Card

Figure 3.6 shows the high level block diagram of the measurement set up including the RF front end, synthesizer board, GAGE card, and PC for post-mission processing. The entire PCS network is deemed to be synchronized to GPS time; hence, one GPS receiver providing the GPS time reference is connected to the digitizer to make the incoming CDMA signal synchronous to the entire network. It is worthwhile to mention that the sampling clock of the digitizer using a free run oscillator, is still asynchronous to the transmitters. However, due to the GPS auxiliary assistance, the start point of the captured streams is synchronously tight to the original timing of the transmitter.

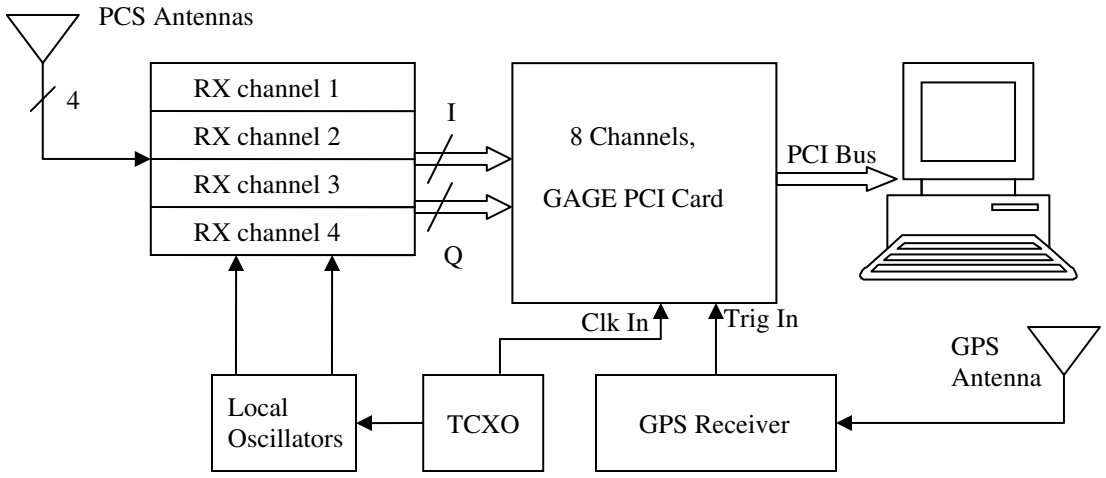

Figure 3.6: Overall architecture of the CDMA PCS receiver

3.4.1 Receiver Challenges

In this subsection, some characteristics of the PLAN receiver which directly influence the space-time processing and positioning accuracy based on antenna arrays, are discussed.

Figure 3.7 shows a test set up for analyzing different channel behaviours given the same incoming signal.

Ideally, it is preferable that all channels show the same power level after despreading the incoming signal. However, due to miscalibration, mostly as I-Q gain and phase imbalance, different channels show different power levels after despreading. A simple analysis and mathematical manipulation for the effect of phase imbalance is explained next.

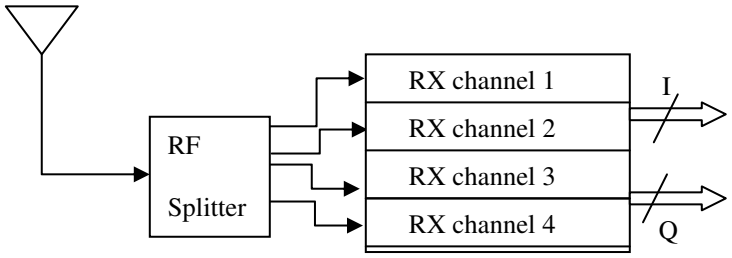

Figure 3.7: Test set up for investigating misbalance among different channels

3.4.1.1 Phase Imbalance

The incoming signal is demodulated by a quadrature demodulator which decomposes the incoming RF signal *R* into two orthogonal baseband components (i.e., I and Q). Due to the discrepancy among analog circuit components, there is some I-Q phase imbalance, θ, shown in Figure 3.8. Without losing generality, it is assumed that the gains in the I and Q branches of the demodulator are equal.

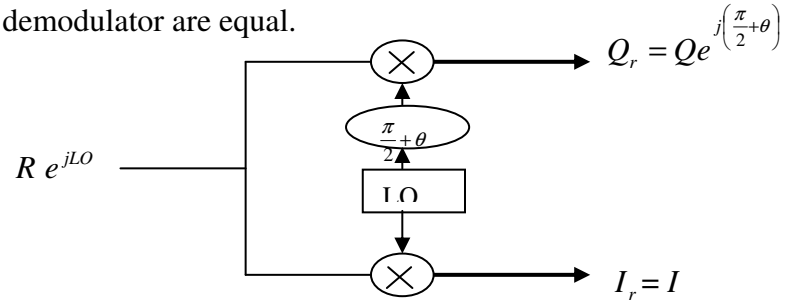

Figure 3.8: Phase imbalance

Conversely, in the despreading process, I and Q are assumed to be orthogonal. Hence, there is some amount of degradation in correlation processing performance due to this not quite perfect assumption. Figure 3.9 illustrates the effective operation of the complex despreading process.

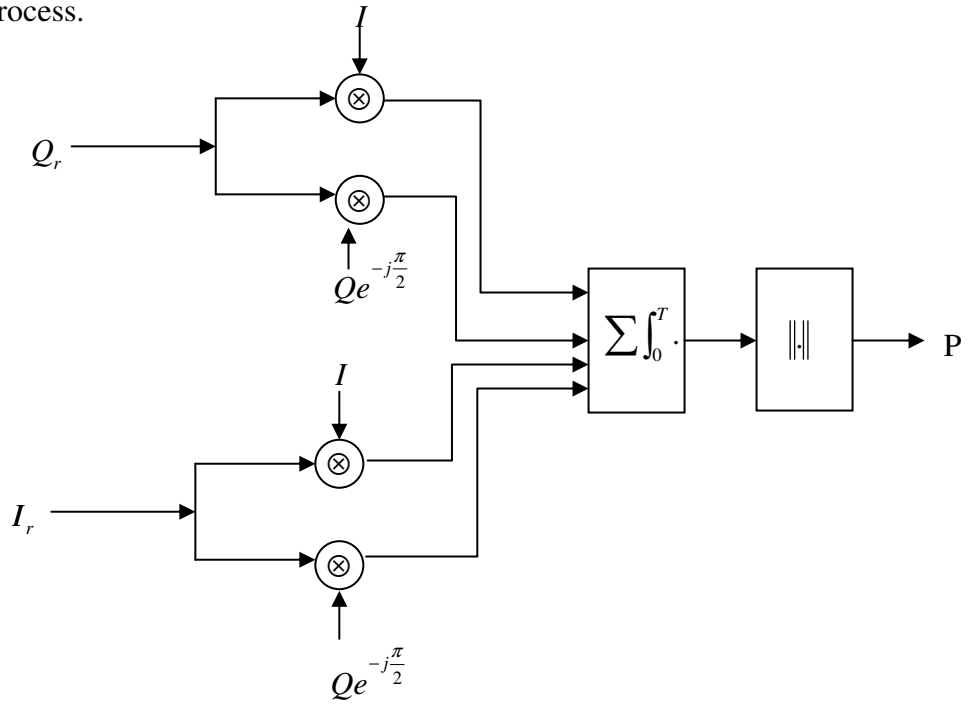

Figure 3.9: Complex despreading process

In Figure 3.9, $\sum\int_0^T .$ indicates integration over period T and summation among all branches and the $\|.\|$ operator gives the square magnitude of a complex signal. If the integration interval T is large, given the orthogonality of I and Q, i.e., $\int_0^T I(t)Q(t)dt \approx 0$, P can be given as:

$$P = \left\| \int_0^T \left(IQe^{j\left(\theta+\frac{\pi}{2}\right)} \right) dt + \int_0^T \left(Q^2 e^{j\theta}\right) dt + \int_0^T \left(I^2\right) dt + \int_0^T \left(IQe^{-j\frac{\pi}{2}} \right) dt \right\| = T\left\|1 + e^{j\theta}\right\| = T\sqrt{2(1+\cos\theta)} \tag{3.4}$$

where $I(t)^2 = Q(t)^2 = 1$.

If the demodulator is balanced, the maximum achievable gain is $2T$ accordingly; hence, the degradation curve (dB) in terms of I-Q phase imbalance, θ, is:

$$L_P = 20\log\sqrt{\frac{1+\cos\theta}{2}} \tag{3.5}$$

Figure 3.10 depicts correlation loss due to the phase imbalance. In conclusion, if the I and Q relative phases are not calibrated in a timely manner in different channels, there is a potential degradation in achievable processing gain which may be significant, especially in weak signal conditions.

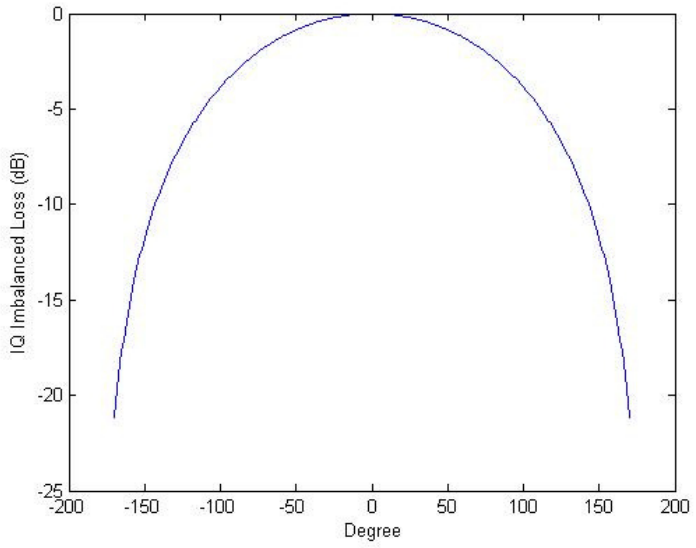

Figure 3.10: Phase imbalance correlation loss

Figure 3.11 shows the long term fluctuation of received power, in different channels, for a presumably LOS BTS during nearly 7 hours of data collection obtained by the PLAN front end. During data collection, one roof antenna and an RF splitter, similar to the configuration in Figure 3.7, were used to provide different channels with nearly the same amount of received signal power. It was also verified that different channels have the same amount of matching/mismatching toward the antenna-splitter output impedance.

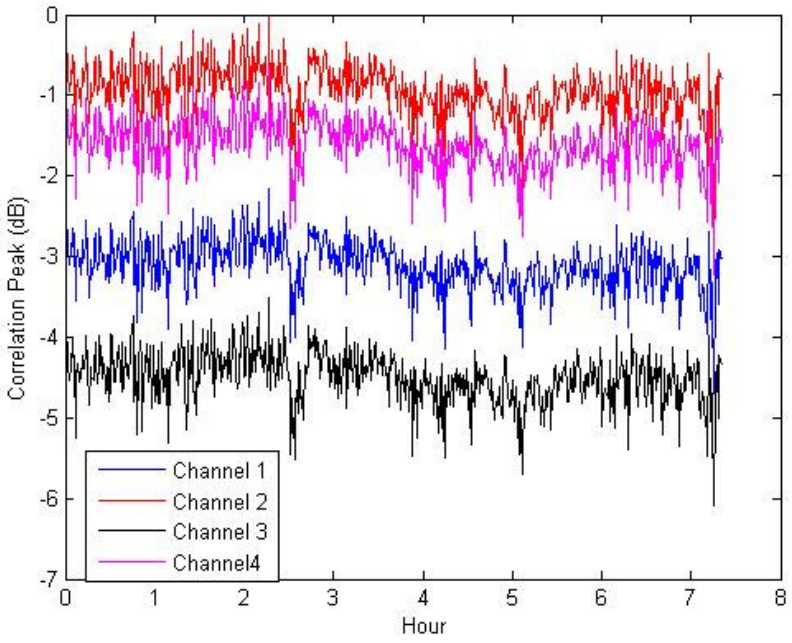

Figure 3.11: Measured power in different channels

As can be seen in Figure 3.11, measured powers in different channels are different. Fortunately, it seems that the discrepancies are constant over time and there is a high amount of correlation between different channels. Since the channels operate independently, the correlations imply that the fluctuations in the received power can be

associated with the transmitted power fluctuation and also variable multipath. Because the gains for different channels were set to an equal level per I and Q, there was almost no gain imbalance issue and the offsets mostly came from the I-Q phase imbalance of different channels.

Figure 3.12 shows a smoothed version of received power in Channel 2. This figure implicitly demonstrates gain stability in both transmitter and receiver during 7 hours of data collection. Fluctuations, although less than 1 dB, can be associated with variations in transmitted power of the BTS pilot as well as receiver characteristics during 7 hours of data collection.

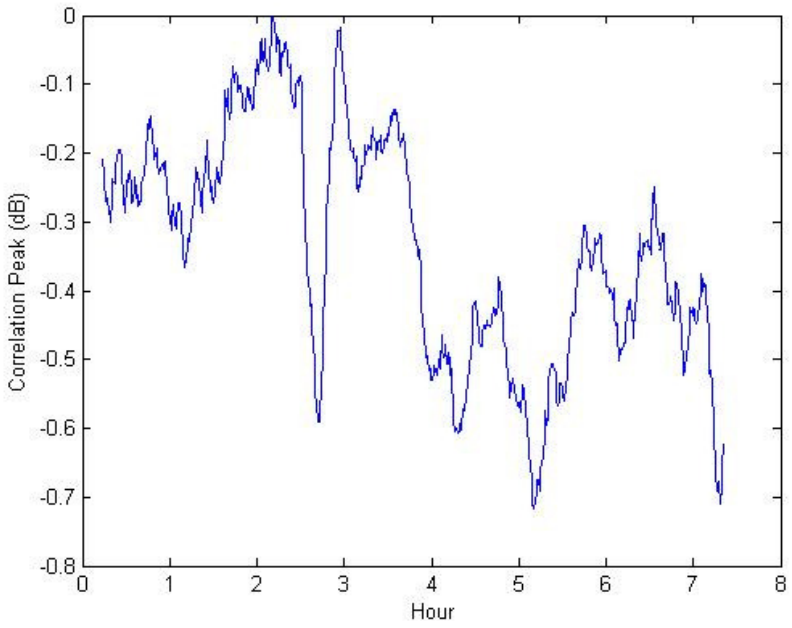

Figure 3.12: Long term behavior in measured power

3.4.1.2 Frequency Stability

Frequency stability of the receiver is another parameter that is partially analyzed here. The frequency stability issue is very critical, especially in lengthy correlation processing which is inevitable in weak signal circumstances. From the transmitter perspective, all BTSs in the CDMA cellular network attempt to be GPS synchronized. Nevertheless, there is always some small timing error due to the local oscillator short term stability, phase noise, drift, Doppler shifts, long-term aging, and variable distance from the mobiles to the BTS. Presently, the most common method of time distribution in BTSs is to locate a GPS clock, also called GPS timing receiver, at every BTS. The GPS system provides a reasonably accurate timing reference which is based on the global standard time scale i.e., universal-time-coordinated (UTC). This GPS time is available worldwide via GPS clocks at no cost for the service. In this case, GPS is being used as an infrastructure not for positioning but for timing. A GPS clock uses a high stability oscillator (ovenized quartz or rubidium cell) disciplined on GPS signals. The long term accuracy of GPS complements the short term stability of the crystal oscillator.

From the receiver perspective, in addition to the aforementioned timing errors, temperature level, vibration, shock, acceleration, and power supply fluctuation must be considered as sources of oscillator instability. Due to the non stationary nature of errors, both short term and long term, the classical variance metrics cannot take into account all phenomena. Thus, the level of random frequency error is characterized by the Allan variance, which is an interval-based variance metric. Figure 3.13 illustrates the Allan deviation (i.e., square root of the Allan variance) for a Rubidium oscillator and standard quartz oscillator (Moghaddam, et al., 2006).

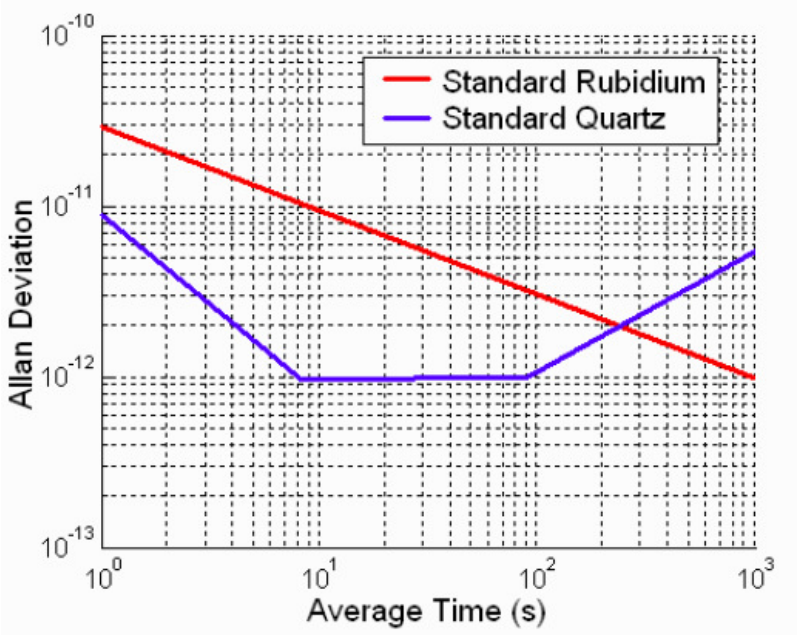

Figure 3.13: Short term stability of quartz and rubidium oscillator

In a coherent scenario for despreading the signal, any constant uncompensated frequency offset leads to effective power attenuation characterized by the well-known sync function, presented as Equation 3.6 below (Kaplan 2006).

$$L_{F_{err}} = \frac{\sin(\pi \Delta f T)}{\pi \Delta f T} \tag{3.6}$$

where Δf and T are frequency offset and integration time, respectively.

The prototype receiver on which all experimental results in this thesis are based (i.e., PLAN front end), uses a 10 MHz temperature-compensated-crystal-oscillator (TCXO) as the master clock for synthesizing the necessary frequencies such as RF and IF LOs as well as the sampling frequency. The TCXO frequency accuracy is about 0.5 part-per-million (ppm). Accordingly, for an RF carrier frequency of a nominal IS-95 provider

(e.g., 1.947 GHz used by Telus, approximately 2 GHz), a potential carrier frequency error of about 1 kHz is conceivable. From Equation 3.6, it can be shown that a frequency error, $\Delta f \approx \frac{0.44}{T}$, leads to 3 dB attenuation in correlation peak. Hence, if 3 dB attenuation is the ultimate budget for correlation loss, then the uncorrected spread CDMA signal cannot be integrated longer than 440 μs in a coherent correlation process. This integration time severely limits the achievable processing gain required for increasing detectability. Nevertheless, if the Allan variance of the TCXO in the PLAN receiver was sufficiently low such that the frequency offset was relatively constant, the attenuation effect could be lessened by a frequency de-rotation module. This de-rotation processing creates sufficiently long coherent integration times as required to process weak pilot signals.

Figure 3.14 shows coarse frequency offsets estimated from the strongest BTS during 7 hours of data collection. In Figure 3.14, estimated frequencies get a quantized value because the coarse estimation is performed by the FFT despreading process.

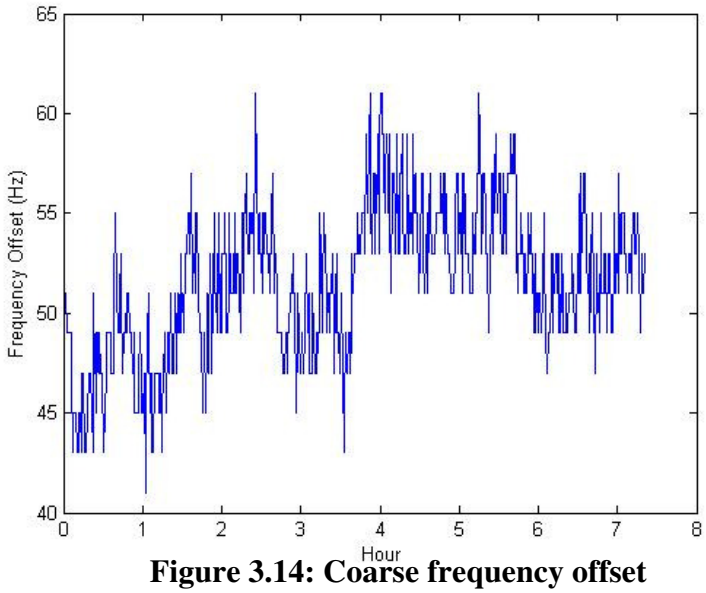

Figure 3.14: Coarse frequency offset

Mean and standard deviation for the above mentioned figure is 51.5 Hz and 3.67 Hz, respectively. Figure 3.15 shows a histogram of frequency offsets derived by a data set with 625 points. The histogram implicitly suggests a Gaussian PDF for frequency error with a negligible standard deviation of 3.67 Hz during 7 hours of data collection. Figure 3.14 may indicate that the PLAN prototype front end timing is stable enough in long term tests and that the measurement system does not have a severe clock instability problem which is crucial in positioning systems. The next chapter demonstrates some experimental positioning results obtained from the field IS-95 CDMA cellular network.

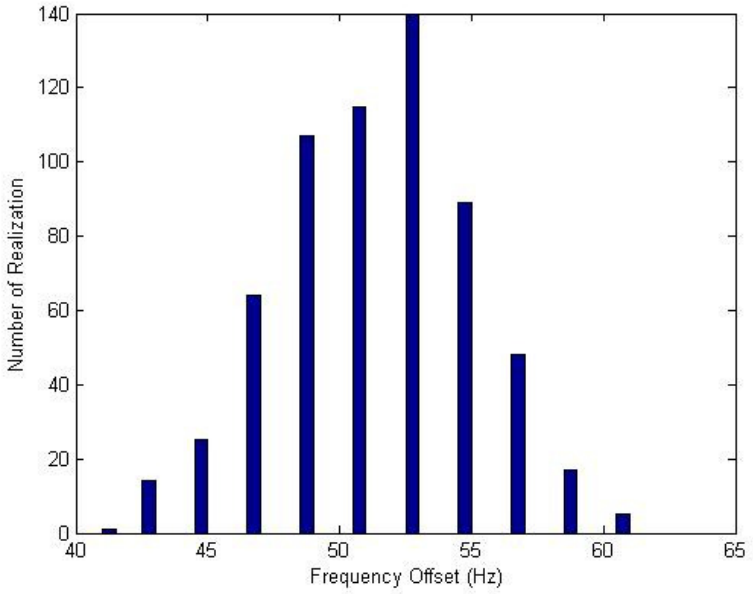

Figure 3.15: Frequency offset histogram

Chapter Four: Cellular Network Positioning Implementation and Test

This chapter demonstrates some IS-95 field positioning results along with corresponding analyses. The measurement setup, tools, and signal structure of the IS-95 were reviewed in Chapter 3. All results demonstrated in this chapter are derived in static mode. This chapter provides some practical insights toward challenges in wireless cellular network positioning and also helps the overall thesis in realizing the parameters affecting the positioning accuracy. In all the field tests of Chapters 4, 5 and 6, grid points and cell sites are assumed to lie in a horizontal plane. The position to be estimated is a two-dimensional, horizontal position. Hence, the heights of the grid points and cell sites are not accounted for. Due to its relevance, an abstract-theoretical non-coherent detection process is also derived in this chapter which is optimal in the Neyman-Pearson sense.

4.1 Positioning Method Selection

Estimating the range, or more accurately the pseudorange (due to the clock bias), from transmitters to the receivers is the first step toward TOA/TDOA positioning. Since the radio signal travels with the speed of light, there is a one to one relationship between time and distance. Therefore, ranges or radial distances between BTSs and MS can be estimated from TOA accordingly. Using range measurements, multilateration can fix the position as intersections of geometric loci which are circles in TOA methodology and hyperbolae in the TDOA counterpart.

It was mentioned before that all field measurements in this thesis are based on the PLAN prototype front end and GAGE card digitizer. In this set up, there are some sources which induce common timing bias in raw data. These sources originate mostly from analog elements such as filters, amplifiers, cables, tracks in printed-circuit-boards (PCBs), and also the sampling circuit. Fortunately, the TDOA method is not sensitive to common TOA biases. Hence, the TDOA approach is preferable for position fixing in this study. Since identifying code offsets corresponding to each BTS demands a network time reference (i.e., GPS time), another by-product of TDOA usage is its independence from this GPS time reference.

Given the same geometry of BTSs and MS, GDOP for TDOA is higher than the TOA method which leads equivalently to a higher positioning error. Therefore, there is some amount of degradation in achievable performance due to TDOA usage. Another disadvantage for TDOA usage, instead of TOA, is its sensitivity to the differential reference. It will be shown in this chapter that positioning accuracy changes if the TDOA reference measurement changes. Therefore, if the reference is corrupted by severe multipath, all TDOA measurements are affected severely by multipath.

4.2 Steps Toward TDOA Position Fix

Given received IS-95 base band samples, the following pre-processing must be done for estimating position: 1- Despreading the R_x, 2- BTS Detection, 3- BTS Identification, 4- Residual TOA derivation, and 5- Position Fix

Despreading the pilot code was explained in Chapter 3. It was mentioned that despreading the signal gives a sufficient statistic (i.e., channel-impulse-response, CIR) for timing information. Other steps are explained in detail in the following subsections.

4.2.1 Base Stations Detection and Identification

The position fix procedure needs geodetic BTS locations. Hence, the BTSs having strong signal power should be detected first and then associated with their corresponding *a priori* coordinates. These are the detection and identification steps, respectively. A decision making process can be conducted to detect the visible BTSs by comparing the despread signal to a fixed threshold. The higher the threshold, the more reliable the decision making process, since the probability of accepting ambient noise or interference as active BTS becomes less.

Figure 4.1 shows a decision-making process using a hard threshold applied to a despread received signal. Typically the threshold is a multiple of the surrounding noise variance and the scheme maintains a constant-false-alarm-ratio (CFAR) during the decision making process. Consequently the frequency of false identification can be controlled by changing the threshold. A falsely identified BTS leads to unpredictable behaviour and biases in positioning results. Fortunately, Figure 4.1 indicates that the noise level is very consistent and stationary; hence, it is possible to set a fixed threshold level given a tolerable false detection rate. Otherwise an adaptive threshold must be contrived to balance the signal power and noise. What is tolerable in this sense is highly dependent on the application and hence can only be arbitrarily set in this study.

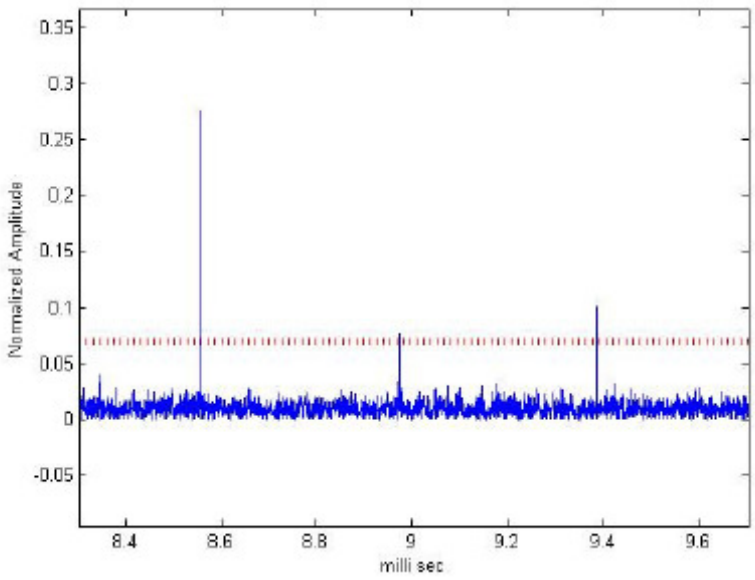

Figure 4.1: BTS detection

4.2.2 Optimum Noncoherent Processing for BTS Detection

In this subsection, the BTS detection process is further studied and an abstract optimum process in the Neyman-Pearson (NP) sense for detecting a complex baseband signal buried in additive-white-Gaussian noise (AWGN) is also detailed. The main focus in this attempt is to contrive a noncoherent process using pure signal amplitude instead of using both amplitude and irrelevant phase information as used in traditional coherent scenarios. The main advantage of noncoherent detection is to reduce the number of parameters involved. Given some unknown parameters in the received signal, the noncoherent detection scheme reduces the number of nuisance parameters which otherwise have to be either estimated or averaged in a generalized-likelihood-ratio-test (GLRT).

Although the noncoherent approach simplifies the detection process, there is some amount of degradation in terms of SNR due to the change in noise characteristics after taking the amplitude or energy of the signal.

In the following, the closed form for an optimum NP detector using amplitude is obtained and then an approximation for the analytical detector is derived. The approximation is useful in terms of computational efficiency and insight into the nonlinear process.

4.2.2.1 Analytical Derivation

A conceptual block diagram for a decision making process is shown in Figure 4.2.

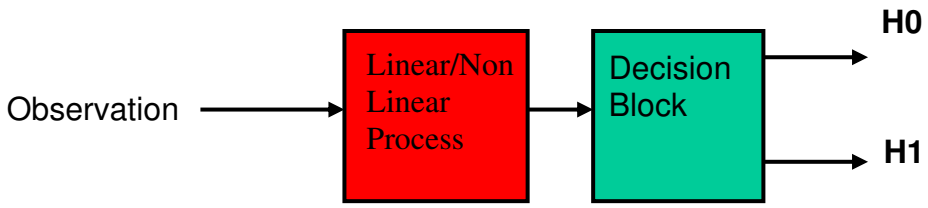

Figure 4.2: Decision Making Process

The observation is used by a process which combines data efficiently for detection purposes. The process provides optimal usage of *a priori* information about signal and noise stochastics. The Neyman-Pearson approach gives a process which has the best performance among all possible detectors (Kay, 1998). In NP, given a probability of false-alarm (i.e., misinterpretation of noise as the signal), the process using the

likelihood-ratio-test (LRT) has the best probability of detection among all possible processes. Hence, the optimum detector has a design form as in Equation 4.1,

$$LRT = \frac{P(X \mid H1)}{P(X \mid H0)} \geq \gamma \tag{4.1}$$

where X , $H1$ and $H0$ are observation vector, state of "Signal Present," and state of "Signal Not Present," respectively. It can be shown (Kay, 1998) that Gaussian noise ends up with an optimum detector which has a linear form in terms of observation samples. However, the linear form is not necessarily optimal if the noise is not Gaussian. Given a conceptual case of a complex value, A_c, buried in a circular zero mean complex Gaussian noise with equal variance, σ^2, in both real and imaginary parts, taking the amplitude of the observation yields two possible hypotheses:

$$\begin{aligned} &H1: \| A_c + n_c \| \qquad A_c = A_r + j * A_i = Ae^{j\phi} \\ &H0: \| n_c \| \end{aligned} \tag{4.2}$$

where n_c , A, and φ are complex circular Gaussian noise, $N(\bar{0}, \sigma^2 I)$, signal amplitude, and phase of arrival, respectively. It can be shown that the signal makes the observation a

random variable with Rician PDF while pure noise makes the observation a random variable with Rayleigh PDF.

$$P(X \mid H1) = \frac{X}{\sigma^2} e^{-(\frac{X^2+A^2}{2\sigma^2})} I_0(\frac{AX}{\sigma^2}) \quad A = \sqrt{A_r^2 + A_i^2}$$
$$P(X \mid H0) = \frac{X}{\sigma^2} e^{-(\frac{X^2}{2\sigma^2})} \tag{4.3}$$

It can be seen that H1 is described sufficiently by amplitude, *A,* and noise power, σ^2, but independent of φ. In Equation 4.3, $I_0(X)$ is a modified zeroth order Bessel function of the first kind which is presented in Equation 4.4.

$$I_0(u) = \frac{1}{2\pi} \int_0^{2\pi} e^{u\cos\varphi} d\varphi \,, \qquad I_0(u) = 1 + \frac{(\frac{u}{2})^2}{(1!)^2} + \frac{(\frac{u}{2})^4}{(2!)^4} + \cdots \tag{4.4}$$

Without losing generality, noise variance can be assumed to be unity (i.e., $\sigma = 1$). Substituting the PDFs into the LRT as NP suggests, the optimum detector structure for a noncoherent amplitude scenario is as follows:

$$GLRT = \frac{P(X \mid H1)}{P(X \mid H0)} = e^{-\frac{A^2}{2}} I_0(AX) \tag{4.5}$$

If A is known *a priori*, $I_0(AX)$ turns out to be a sufficient statistic for detection and the constant term, $e^{-\frac{A^2}{2}}$, can be dismissed. The process for the detector shows a non linear form which reemphasizes that in a non Gaussian process, the matched filter is not optimal in the NP sense. In another view, taking the amplitude of an AWGN complex process changes the stochastics of the process which consequently changes the optimality of the linear processing.

4.2.2.2 Analytical Approximation

The above derivation for a noncoherent detector assumes a single conceptual observation in the process. It can be further generalized into multiple observation scenarios as follows. Given $X = [X_1, X_2, \cdots, X_n]$ observations with identically-independent-distribution (IID) noise terms, the LRT suggesting the optimal process has an analytical form of Equation 4.6.

$$LRT = \frac{P(\overline{X} \mid H1)}{P(\overline{X} \mid H0)} = (e^{-\frac{A^2}{2}})^n \prod_{i=1}^{n} I_0(AX_i) \tag{4.6}$$

The analytical expression for the multiple observation case is mathematically accurate, but does not give any insight into the process. Instead of using the accurate expression, an approximation can be made which is less computationally intensive and also gives better insight toward the combination process.

Given a fixed n and $X >> n$, the modified Bessel function, $I_n(X)$, can be approximated as Equation 4.7.

$$I_n(x) \approx \frac{e^x}{\sqrt{2\pi x}} \tag{4.7}$$

$X >> n$ is not a stringent assumption because $n = 0$ and A is usually large due to the processing gain in the despreading process.

Given the signal vector $S = [S_1, S_2, \cdots, S_n]$ and X as observation vectors with IID noise terms, the LRT for non coherent amplitude processing can be approximated as Equation 4.8 using Equation 4.7.

$$LRT = \frac{e^{x_1 s_1 + x_2 s_2 + \ldots . x_n s_n}}{\sqrt{x_1\, x_2 \ldots x_n}} = \frac{e^{\bar{X}\,\bar{S}^T}}{\sqrt{\prod_{i=1}^{n} x_i}} \tag{4.8}$$

In the above expression, only sufficient statistics are shown and constants are dismissed. Interestingly, the numerator suggests a pattern similar to a matched filter which correlates the observation sequence with the known signal sequence. Nevertheless, the denominator emphasizes the non-linear nature of the optimal NP process in this noncoherent processing. In fact, due to the denominator, taking the logarithm of the analytical expression is not helpful in simplifying the process, whereas in traditional manipulation

for Gaussian process cases, the expression becomes simplified after taking the logarithm of LRT.

Optimality of the proposed non linear process can be verified via the receiver-operating-characteristic (ROC) curve which plots the probability of detection (P_{det}) versus probability of false alarm (P_{fa}). It is well known that the optimum detector in the NP sense has the largest value of P_{det} given a P_{fa}. Derived by an exhaustive Monte Carlo simulation, Figure 4.3 compares ROC curves corresponding to suggested LRT and a conceptual non-coherent matched filter for an artificially generated signal with rectangular pulse shaping. It can be seen that the derived LRT outperforms the matched filter because it fits more to the signal and noise stochastics.

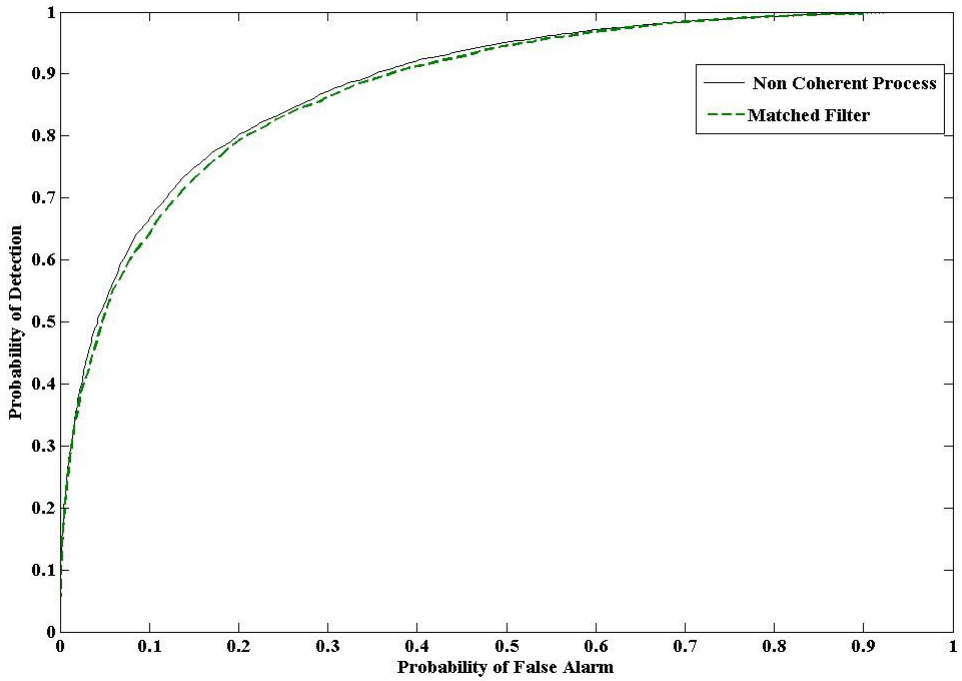

Figure 4.3: ROC curves for Matched filter processing and non linear processing

4.2.3 BTS Identification using GPS Time Reference

Given adequate code offset margins among adjacent BTSs, if the time reference upon which all BTSs are synchronous (i.e., GPS time) is available in the receiver side, each reliable peak in the despread sequence can be associated with a specific BTS unambiguously. This unique association of a peak into a BTS is called "BTS binding" in this thesis. It is worthwhile to mention that network specifications obligate code offset margins to be an integer multiplier of 64 chips between BTSs, which in the range domain equals more than 15 km. Due to wireless path loss, signals coming from 15 km, relative to the receiver, are too attenuated to be detected and therefore will not introduce an ambiguity into the BTS binding process.

A simple algorithm for BTS binding is suggested:

1- Segmenting the first full PRN region of despread signal (i.e., 26.666 msec) into 512 sub segments (512*64 = 32768)

2- Seeking for strong peaks in subsegments

3- Given a reliable peak in any subsegment, noting the segment index as BTS code offset.

Then, geodetic coordinates can be associated with the extracted code offset by referring to the data base belonging to the IS-95 CDMA cellular network provider. Figure 4.4 displays the above mentioned procedure.

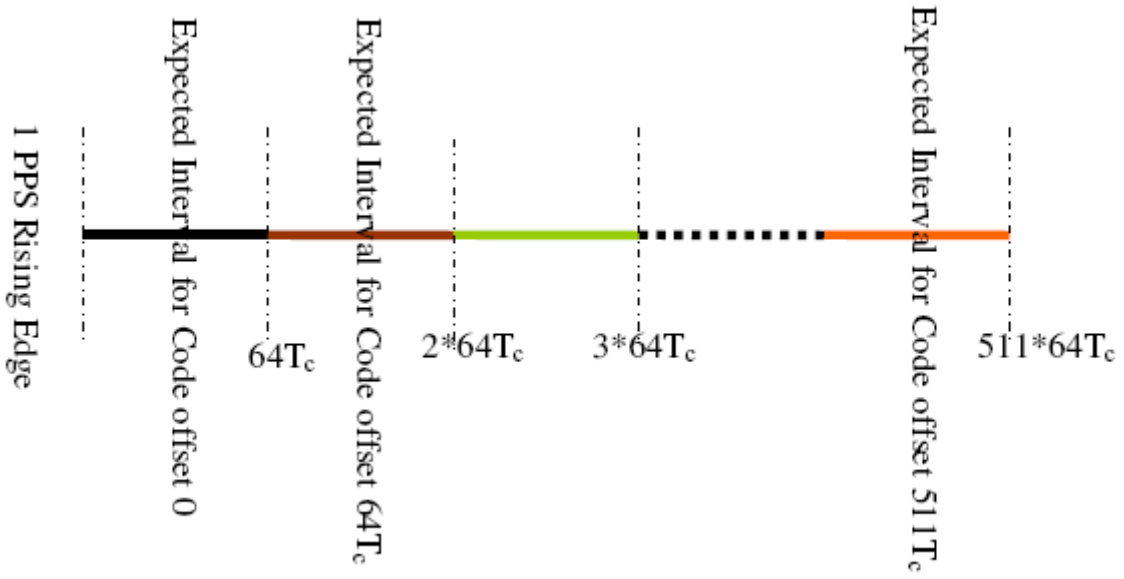

Figure 4.4: 64 Chip demarcations for successive BTS's

Given a specific provider, the code offsets are usually reused among remote BTSs. Hence, initial coarse position (cell accuracy is enough) for the MS is required to resolve possible BTS site candidates corresponding to each strong peak.

4.2.4 BTS Identification without using GPS Time Reference

If the GPS 1 pps pulse is not available in the MS side, there is an ambiguity in association of each strong-reliable peak to a physical geodetic coordinate. Two possible solutions to this ambiguity resolution are: 1) using the synchronization channel of the IS-95 signal; or 2) a brute force approach.

In the IS-95 cellular network, BTSs use a sync channel spread with Walsh code 32. The sync channel frame is 80/3 ms long, and its frame boundary is aligned to the pilot. The sync channel continually transmits a single message, the Sync Channel Message, which has a length and content dependent on the standard. The message is transmitted 32 bits per frame, encoded to 128 symbols, yielding a rate of 1200 bit/s. The Sync Channel Message contains information about the network, including the PN offset used by the BTS site-sector.

Demodulating the sync channel and decoding its data messages leads to a direct ambiguity resolution solution. However, sync channel usage increases the complexity of the receiver because a standalone CDMA soft receiver must be implemented in order to demodulate the message. Also, this method is only applicable if the BTS has a sync channel in addition to the pilot and the coding of the sync channel can be deciphered by the receiver.

In the second method, ambiguity is resolved by a brute force approach. In this exhaustive method, all possible hypotheses in terms of code offset are made to bind detected BTSs. Two cases can be conceived in this scenario: 1) having auxiliary or *a priori* knowledge about possible BTS code offsets, and 2) Cold start (GPS field terminology for starting "cold" with zero satellites acquired).

Given N detected active BTSs in the signal, *a priori* knowledge about mode (i.e., mathematical operator), and 64 of the code offsets in an ascending set $\{CO_1, CO_2, ...CO_N\}$, the following scenario can be suggested to bind each BTS to a corresponding code offset.

Given the earliest peak as reference, Equation 4.9 decomposes TDOAs into code offset parts and residual parts.

$$T_{BS_{i1}} = 64T_c I_{BS_{i1}} + TOA_{BS_{i1}} \; i = 2,3,..., N \tag{4.9}$$

where $I_{BS_{i1}} \in \{0,2,...,511\}$ and $TOA_{BS_{i1}}$ is net time difference of arrival for the parameter of interest. Given *a priori* knowledge of $\{CO_1, CO_2, ...CO_N\}$, N different auxilary sets can be contrived as in Equation 4.10.

$$\begin{aligned} &\Pi_i = \left\{H_i^1, H_i^2, ..., H_i^N\right\} \;\; i = 1,2,..., N \\ &H_i^p = \begin{cases} CO_p & 1 \le i + p - 1 \le N \\ CO_{N-p} & 1 \le i + p - 1 \le N \end{cases} \quad p = 1,2,..., N \end{aligned} \tag{4.10}$$

Based on the auxiliary Π_i s, the following sets can be constructed:

$$\begin{aligned} &J_{i1} = \left\{\Delta_i^2, \Delta_i^3, ...\Delta_i^N\right\} \;\; i = 1,2,..., N \\ &\Delta_i^q = \begin{cases} H_i^q - H_1^q & (H_i^q - H_1^q) > 0 \\ 512 + H_i^q - H_1^q & (H_i^q - H_1^q) < 0 \end{cases} q = 2,3,..., N \end{aligned} \tag{4.11}$$

The code offsets, $\{CO_1, CO_2, ...CO_N\}$, are associated with BTSs by comparing $\{I_{BS_{m1}} \mid m \in 2,3,...,N\}$ to all J_{i1} ordered sets and then seeking the best matched set.

The aforementioned algorithm requires *a priori* knowledge of $\{CO_1, CO_2, ...CO_N\}$. In a more general case, the number of members in the *a priori* information set, $\{CO_1, CO_2, ...CO_N\}$, exceeds the number of detected BTSs. In this circumstance, the two sets $J_{i1}, i = 1,2,...,N$ and $\{I_{BS_{m1}} \mid m \in 2,3,...,N\}$ do not have the same cardinality. Nevertheless, $\{I_{BS_{m1}} \mid m \in 2,3,...,N\}$ can be compared to different J_{i1} s in order to find the best set among J_{i1} that has more similarity in terms of orders and also members.

Without *a priori* knowledge of $\{CO_1, CO_2, ...CO_N\}$, all possible combinations of code offsets with cardinality *N*, having the relative distance property similar to $\{I_{BS_{m1}} \mid m \in 2,3,...,N\}$ should be enumerated.

$$\begin{aligned} &\Gamma_i = \{CO_1^i, CO_2^i, ..., CO_N^i\} \quad i = 1,2,....., L \\ &\mathrm{mod}(CO_p^i - CO_1^i, 512) = I_{BS_{p1}} \quad p = 2,3,...,N \end{aligned} \tag{4.12}$$

The value of *L* depends on the possible combinations among BTS code offsets which meet the above criteria. Hence, it is an observation dependent parameter (i.e., $\{I_{BS_{m1}} \mid m \in 2,3,...,N\}$). By selecting a set among different sets, $\Gamma_i \, i = 1,2,...,L$, which has the most reasonable score, ambiguity can be resolved. A simple measure for scoring Γ_i s

can be suggested as the cumulative distance between BTSs in different combinations. Given (X_p^i, Y_p^i) as the Cartesian coordinate corresponding to CO_p^i, the cumulative relative BTS's distance for each Γ_i is as follows:

$$\Psi_i = \sum_{v=2}^{L} ((X_v^i - X_1^i)^2 + (Y_v^i - Y_1^i)^2) \quad i = 1,2,...,L \tag{4.13}$$

The winner set for code offsets is Γ_o which meets Equation (4.14):

$$o = \min_i \{\Psi_i\} \tag{4.14}$$

Any other *a priori* information can be incorporated to build up an effective measure for scoring.

4.3 Fixing Position

Measuring time difference of arrivals, $T_{BS_{i1}} = 64T_c I_{BS_{i1}} + TOA_{BS_{i1}}$, $i = 2,3,...,N$, gives $I_{BS_{i1}}$ s and $TOA_{BS_{i1}}$ s which can be used for BTS identification and the position fix process, respectively. There are several well known approaches by which position is fixed based on range measurements. Maximum-likelihood (ML) and least-square (LS) solutions are among the famous ones which are explained in the following section.

4.3.1 Least Square Position Fix

The location equations expressed by TDOA measurements are nonlinear and must be linearized in order to give a traceable optimal solution. There are several proposed suboptimal LS algorithms which use Taylor-series-expansion (TSE) as an efficient method in solving non-linear equations. In most of them, e.g., Chan & Ho (1994) and Foy (1976), accuracy and robustness of equations rely on small measurement errors and a reasonable initial estimate for an entry point into some iterative procedures. If the already mentioned requirements are not well satisfied, numerical issues cause divergence in the iterations. Among different LS based methods, a TDOA location technique (Jin-Yu, et al., 2003) based on TSE has been chosen in this thesis which does not need an initial guess for fixing the position. The approach is as follows.

Given TDOA measurements and *a priori* knowledge of the geodetic Cartesian coordinates of BTS_i (X_i, Y_i), Equations (4.15) and (4.16) give the required vectors and matrices for the algorithm.

$$\begin{aligned} &d_{i,1} = cTOA_{BS_{i1}} \quad i = 2,...,N \\ &C_i^2 = X_i^2 + Y_i^2 \\ &X_{i,1} = X_i - X_1 \\ &Y_{i,1} = Y_i - Y_1 \end{aligned} \tag{4.15}$$

$$h_c = \frac{1}{2}\begin{bmatrix} d_{2,1}^2 - (C_2 - C_1) \\ d_{3,1}^2 - (C_3 - C_1) \\ \vdots \\ d_{N,1}^2 - (C_N - C_1) \end{bmatrix} \quad G_c = -\begin{bmatrix} X_{2,1}\ Y_{2,1}\ d_{2,1} \\ X_{3,1}\ Y_{3,1}\ d_{3,1} \\ \vdots \\ X_{N,1}\ Y_{N,1}\ d_{N,1} \end{bmatrix} \tag{4.16}$$

Equation 4.17 provides the entry point, $x^{(0)} = Z_c(1)$ and $y^{(0)} = Z_c(2)$ (Yu, et al., 2003), to the LS equation as:

$$Z_c = (G_c^T Q^{-1} G_c)^{-1} G_c^T Q^{-1} h_c \quad . \tag{4.17}$$

where Q is the noise covariance matrix. It can be shown (Yu, et al., 2003) that the estimation update, Δ, may be calculated as Equation (4.18).

$$D_i = \sqrt{(X_i - x_0)^2 + (Y_i - y_0)^2} \quad i = 1,2,...,N \tag{4.18}$$

$$\Delta = \begin{bmatrix} \Delta x \\ \Delta y \end{bmatrix} \quad h = \begin{bmatrix} D_{2,1} - (D_2 - D_1) \\ D_{3,1} - (D_3 - D_1) \\ \vdots \\ D_{N,1} - (D_N - D_1) \end{bmatrix}$$

$$G = \begin{bmatrix} \frac{(X_1 - x)}{D_1} - \frac{(X_2 - x)}{D_2} & \frac{(Y_1 - y)}{D_1} - \frac{(Y_2 - y)}{D_2} \\ \frac{(X_1 - x)}{D_1} - \frac{(X_3 - x)}{D_3} & \frac{(Y_1 - y)}{D_1} - \frac{(Y_3 - y)}{D_3} \\ \vdots & \\ \frac{(X_1 - x)}{D_1} - \frac{(X_N - x)}{D_N} & \frac{(Y_1 - y)}{D_1} - \frac{(Y_N - y)}{D_N} \end{bmatrix}$$

$$\Delta = (G^T Q^{-1} G)^{-1} G^T Q^{-1} h$$

In this case, Q is the covariance matrix of the TDOAs. Figure 4.5 shows a flowchart based on the aforementioned steps.

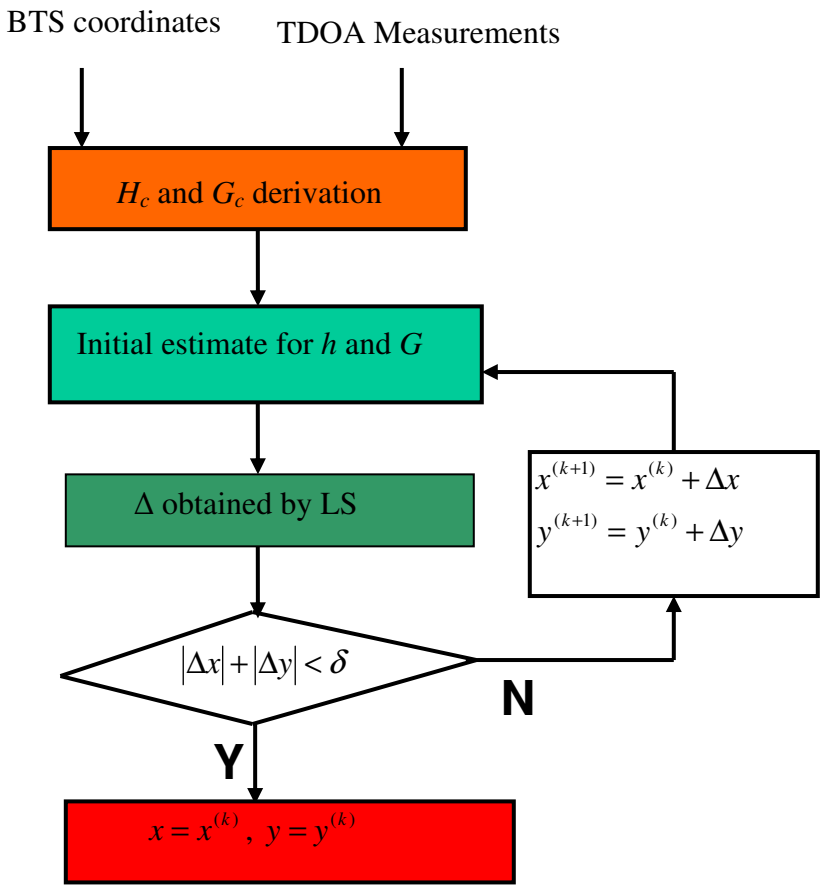

Figure 4.5: LS algorithm (Yu et al 2003)

Numerical and rounding errors may cause matrix singularity in the iterations which make LS susceptible to divergence and the local minimum trap.

4.3.2 Maximum Likelihood (ML) Position Fix

The maximum likelihood approach gives an optimum solution based on its innate exhaustive mechanism. Although ML is immune to the local minimum trap, its closed analytical form manipulation is prohibitively complicated. Nevertheless, numerical implementation of the ML is viable and is explained here. Given Gaussian measurement errors, the likelihood of hypothesis is proportional to the sum of squared residual errors in the measurements (Kay 1998). Hence, the numerical ML process is performed by evaluation of the residual errors in each cell (i.e., hypothesis) followed by an exhaustive search over the 2-D mesh for finding the minimum quadratic score as in the maximum likelihood hypothesis. Figure 4.6 shows a field IS-95 position fix result based on ML.

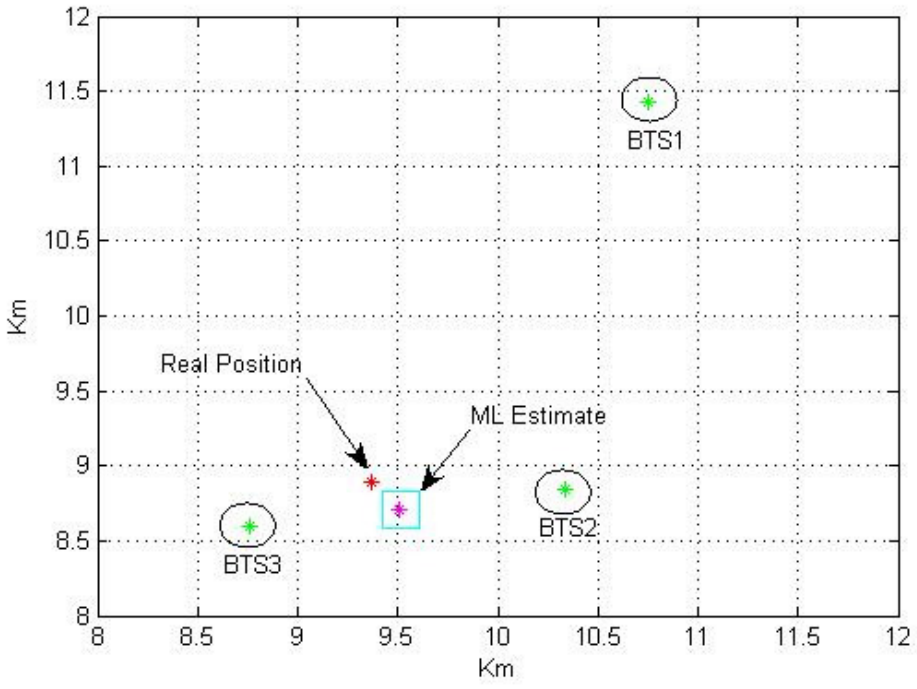

Figure 4.6: ML Position Fix

The map is divided into cells within a desirable resolution. Based on the errors between hypotheses and measurement, a likelihood can be assigned to each cell which then collectively form a likelihood fingerprint. Figure 4.7 illustrates the likelihood fingerprint corresponding to Figure 4.6.

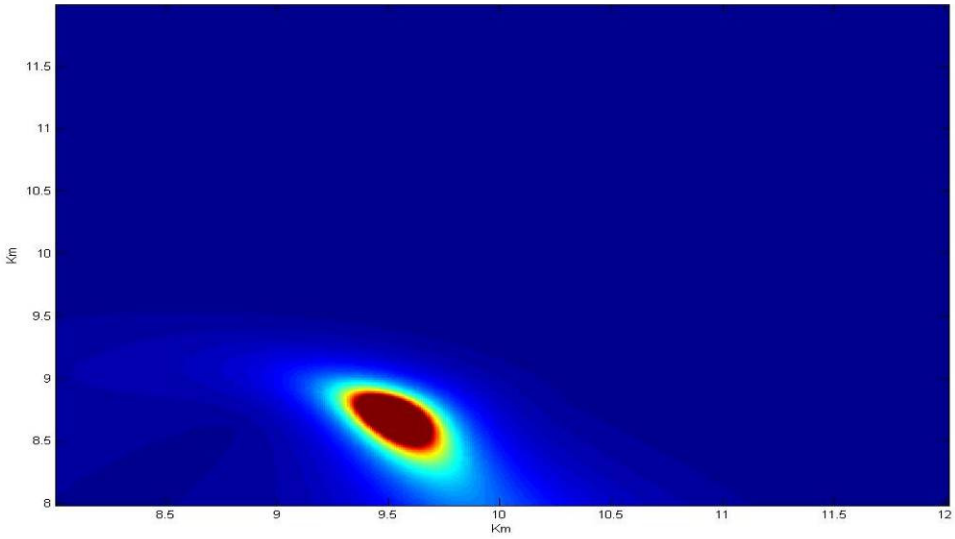

Figure 4.7:Likelihood fingerprint

4.4 Results and Analyses

In the following text, some positioning results obtained from the IS-95 field measurements are demonstrated. For characterizing the challenges, test scenarios start from the least multipath challenging (i.e., roof top) case and end with a challenging scenario (i.e., indoor circumstance). This subsection demonstrates preliminary results. Detailed statistical analyses and results will be presented in Chapters 5 and 6.

Figure 4.8 shows the hardware and tools during field data collection. The set up contains PLAN hardware as the IS-95 CDMA front end, GAGE card as the multichannel digitizer, and GPS receiver as the positioning benchmark and timing circuit.

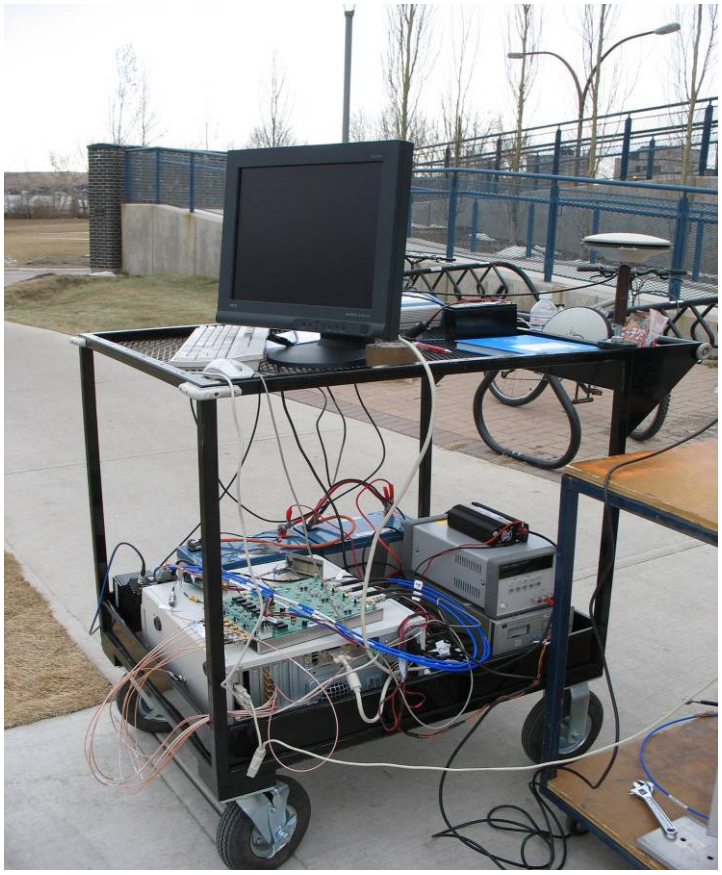

Figure 4.8: Field data collection set up

In the first experiment, the antenna was located on the roof top of the CCIT building where the incoming IS-95 CDMA signals were assumed to be less affected by multipath.

It is worthwhile to mention that due to the low elevation of the incoming signal in terrestrial positioning, the LOS condition is very difficult to achieve.

In all remaining figures, the origin for the Cartesian map is arbitrarily selected as a geodetic point corresponding to Latitude = 51^{o}; Longitude = -114^{o}, and Height = 1100 metres. In the first test case, the antenna was placed in the a position with (**51^{o} 4' 48.244"**) and (**-114^{o} 8' 1.36198"**) latitude and longitude, respectively. Figure 4.9 demonstrates the positioning results for 40 different epochs.

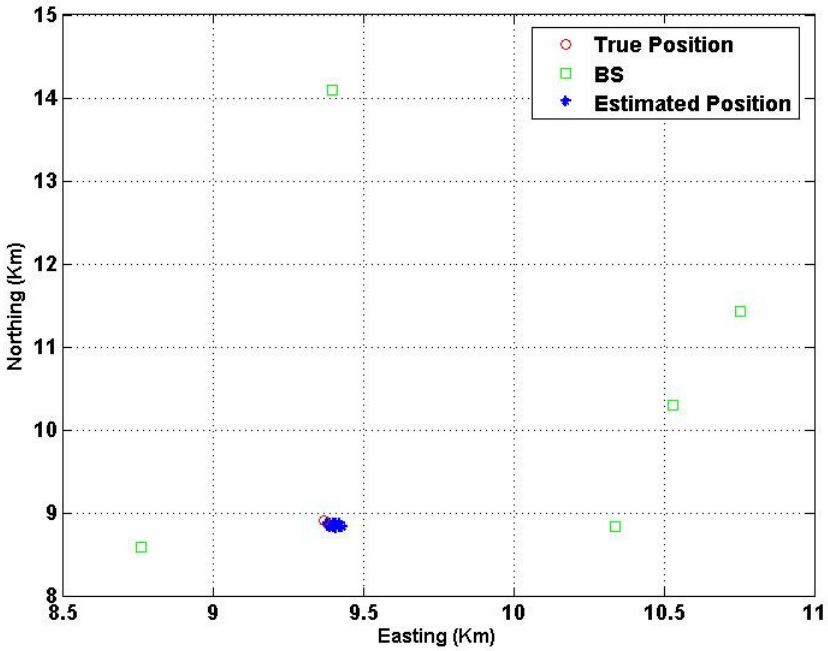

Figure 4.9: Scatter plot

The scatter plot indicates repeatability and stability of the hardware with a modest achievable accuracy.

Another test was conducted to verify the performance of the system in a more hostile multipath environment. In this test case, the antenna was located in an outdoor parking lot. Figure 4.10 shows a single epoch result corresponding to the campaign. Although the scatter plot could show the statistics better, a single epoch is shown here to analyze the impact of different scenarios addressed in the following subsections, given the same situation. Green, red, blue and black spots are BTSs, CCIT coordinate, real position, and estimated position, respectively.

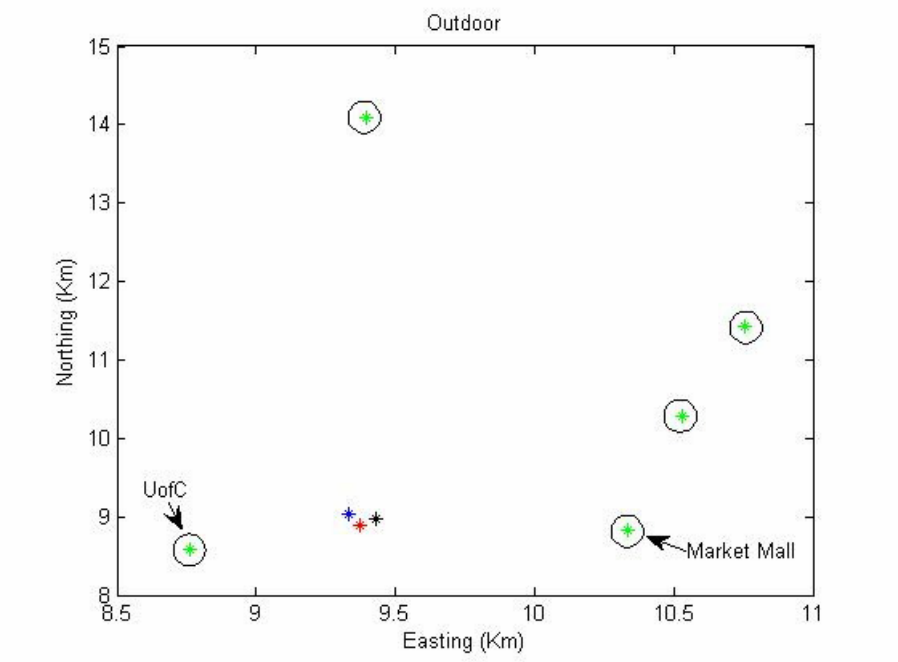

Figure 4.10: Parking lot result

Easting error and northing errors are 90 m and 50 m, respectively. In the above mentioned test, eight strong peaks corresponding to five BTS sites could be detected from the despread sequence. Usually, each BTS includes three different sectors with 120^0 azimuth angle separation. Hence, the excessive detected peaks corresponded to multipath reception of different sectors or a back lobe antenna pattern.

4.4.1.1 BTS–Sector Masking

Achievable accuracy of estimations can be partially changed or controlled by a selective approach among detected BTSs or sectors. A selective approach among detected BTSs effectively changes GDOP, thus controlling the positioning error sensitivity. On the other hand, a directive antenna pattern usually shows a considerable amount of attenuation in the back lobes. Hence, only one sector is deemed appropriate as a LOS provider. This suggests that a selective approach among available sectors corresponding to each BTS can potentially control multipath.

In conclusion, given a measurement, customizing detected BTS and sector set can effectively lead to a partial refinement or optimization in the achievable accuracy. Figure 4.11 compares positioning results in different scenarios, but all use the same data set as Figure 4.10.

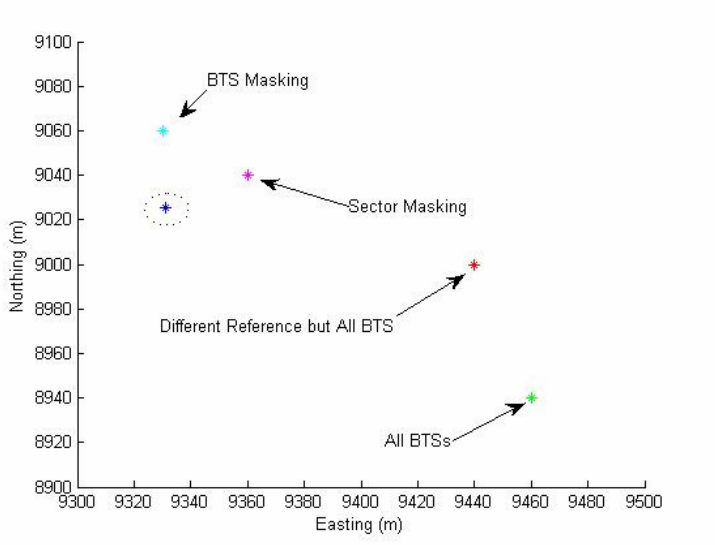

Figure 4.11: BTS-Sector masking results

In practice, the optimal BTS-sector set is not known *a priori*. Nevertheless, a least-cost approach among all possible sets seems reasonable with the LS error as criteria. Table 4.1 compares easting and northing errors from Figure 4.11.

Table 4.1: Northing - Easting errors

	Northing Error (m)	**Easting Error (m)**
All BTSs	-80	140
Sector Masking	14	30
BTS Masking	35	-1
Reference Alteration	-20	120

In the final test case, an indoor environment was investigated. In indoor environments, the received signal consists of substantial amounts of specular and diffused multipath. Indoors, GDOP is poor due to the high attenuation from all angles except regions subtended by window openings. Figure 4.12 shows an indoor result obtained by PLAN hardware.

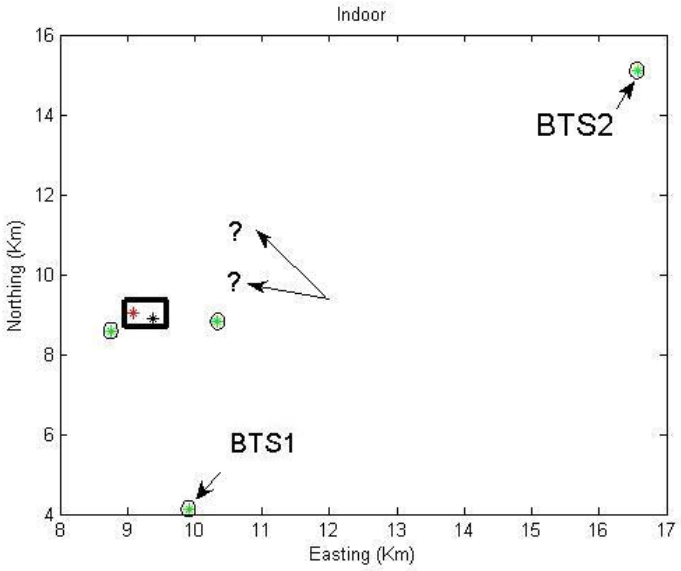

Figure 4.12: Indoor result

It can be seen in Figure 4.12 that due to the indoor blockage issue, two BTSs observed in previous test cases (i.e., question marks) have not been detected. Instead, two new remote BTSs show up which had not been observed in the roof top test case. Easting and northing errors are 300 m and 120 m, respectively.

4.4.1.2 Reference Selection

Essentially, fixed reference differential positioning needs a clean common reference to which all the measurements are compared. Since TDOA measurement accuracy depends indirectly on reference quality, altering the reference can potentially affect substantial change especially in the indoor environment. In summary, changing the reference BTS changes both the GDOP in TDOA position fix and also sensitivity to multipath affected measurements. Figure 4.13 shows the effect of reference alteration for the set of indoor observations used in Figure 4.12. It can be observed that, in the best case, northing-easting errors can be less that 100 m for this specific data set.

This chapter demonstrated preliminary results and analyses for IS-95 cellular network positioning. All results in this chapter were based on a single channel-static receiver. Upcoming chapters open the notion of time-space observations and show more detailed positioning results and analyses.

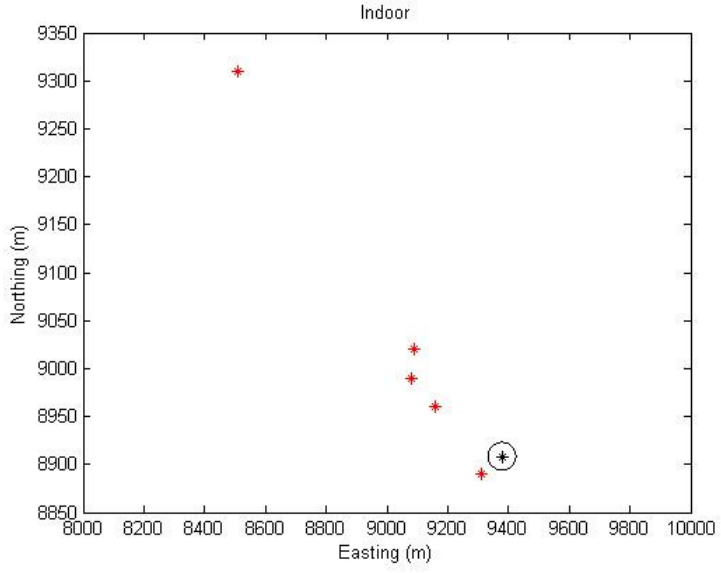

Figure 4.13: Reference alteration (measurement point surrounded by a circle)

Chapter Five: Positioning Enhancement using Space-Time Observations

It was briefly addressed in Chapter 4 that cellular network positioning is always susceptible to multipath. Even on an open field roof top, grazing effect (i.e., reflection from ground) exists. Northing-easting positioning errors are within hundreds of metres in some static field tests. Since the multipath is not necessarily common among different BTSs, differential techniques cannot alleviate the bias problem incurred by the impaired measurements. This chapter and Chapter 6 propose two solutions for mitigating the effect of multipath. Proposed approaches exploit one fundamental property of the multipath phenomenon. This property assumes that the multipath components of the signal become statistically decorrelated in different spots which are far enough from each other. Usually, one half wavelength is considered to be enough (Rappaport, 1999) in terms of distance. However, the decorrelation rate depends on the environment. Given one half wavelength as the approximate coherency distance and given that a typical carrier frequency in the cellular network is roughly 2 GHz, points which are farther from each other than 3e8/(2*2e9) = 7.5 cm introduce statistically decorrelated multipath terms.

The aforementioned property for multipath becomes more valid whenever the sources of multipath are small random objects causing dispersive environments. In some situations, for example, sparse environments having large buildings and obstacles as in Figure 5.1, dominant specular multipath components are correlated in amplitude and multipath delay over large spans. Hence, multipath decorrelation is very difficult to achieve in these environments. The rest of this chapter assumes dispersive behaviour in the multipath source. This implies that multipath becomes decorrelated if the observations are acquired from far enough distant locations.

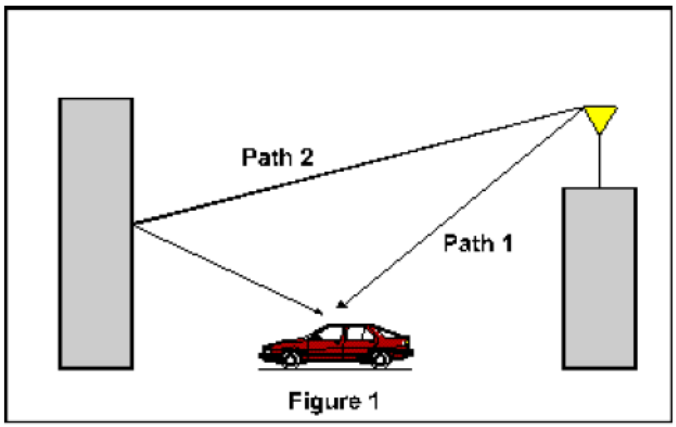

Figure 5.1: Specular-correlative multipath

5.1 Multipath Induced Bias

When the received signal contains severe multipath terms (e.g., in foliage, urban canyon, or any dense building areas), leading edge components derived from estimated CIRs are susceptible to severe biases corresponding to hundred metres error in positioning. Figure 5.2 shows the channel impulse response obtained in an indoor setting. Pseudorange estimation becomes extremely biased using a global peak detector.

Since $F_s = 2.5\,MHz$ during data collection, the pseudorange error corresponding to Figure 5.2 is around 480 m (i.e., four samples) because of the incorrect estimation of the leading edge index.

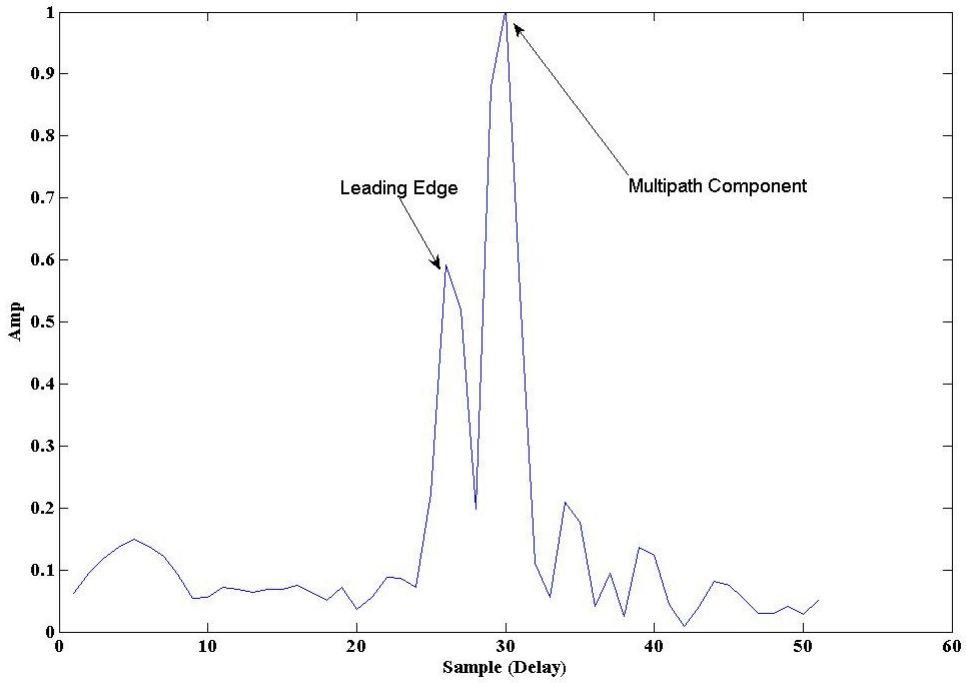

Figure 5.2: Large bias due to strong indoor multipath

5.2 Space – Time Paradigm

For mitigation of the undesirable multipath effect (i.e., falsifying the leading edge), diversity of the multipath both in space using multiple well separated antennas and in time using a slowly moving receiver seems feasible, at least under LOS conditions. The idea assumes that the LOS part of the incoming signal is correlated in space and time, whereas the multipath components are independent in terms of phase of arrival and delay. For a given BTS, Figure 5.3 demonstrates indoor field CIRs corresponding to four different antenna elements spaced about 7.5 cm apart (i.e., one half wavelength). The corresponding environment shown in Figure 5.4 is a typical indoor lab with no access to

LOS and a large number of small objects and reflectors. It can be observed from the figure that different antenna elements show different CIR profiles especially in the lag regions. This property suggests spatial diversity usage in static mode using antenna elements.

Equivalently, if the antenna is in motion, multipath starts decorrelating in different spots. This property suggests temporal diversity usage using motion. This type of diversity is called temporal diversity in this thesis; contrary to spatial diversity addressed above.

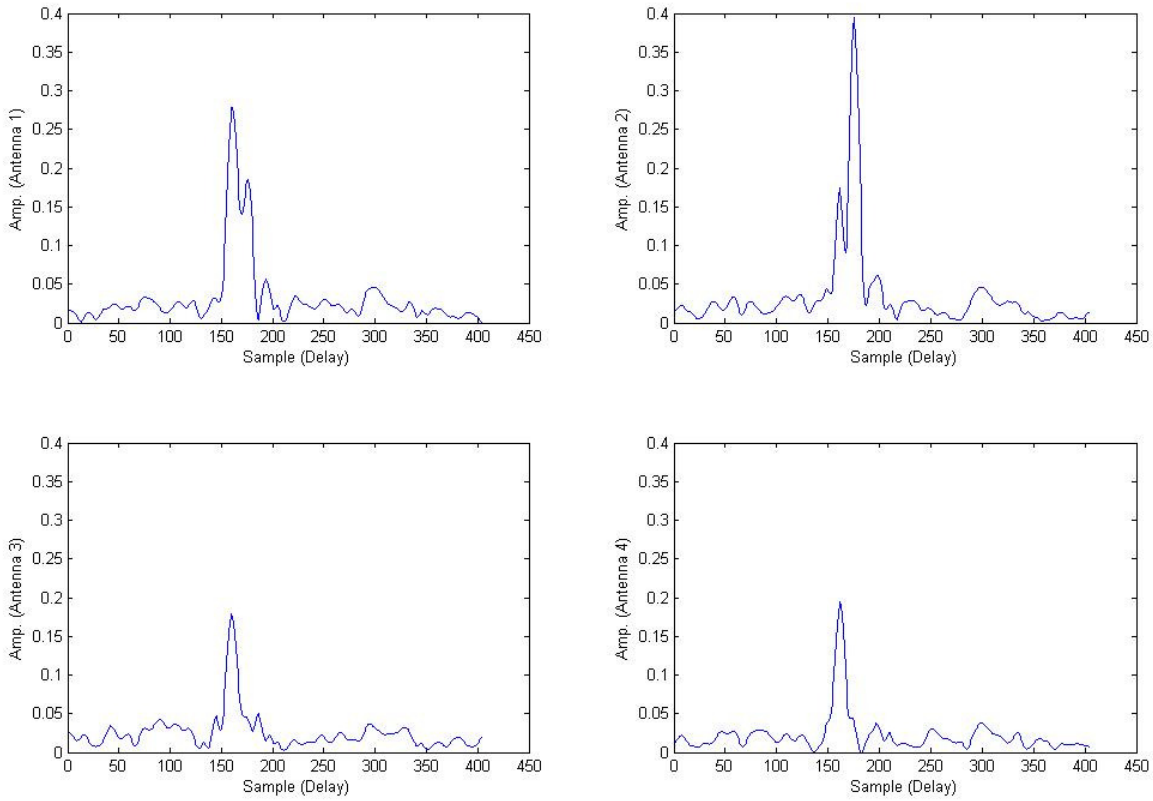

Figure 5.3: BTS1-CIR profiles from different antenna elements (space diversity)

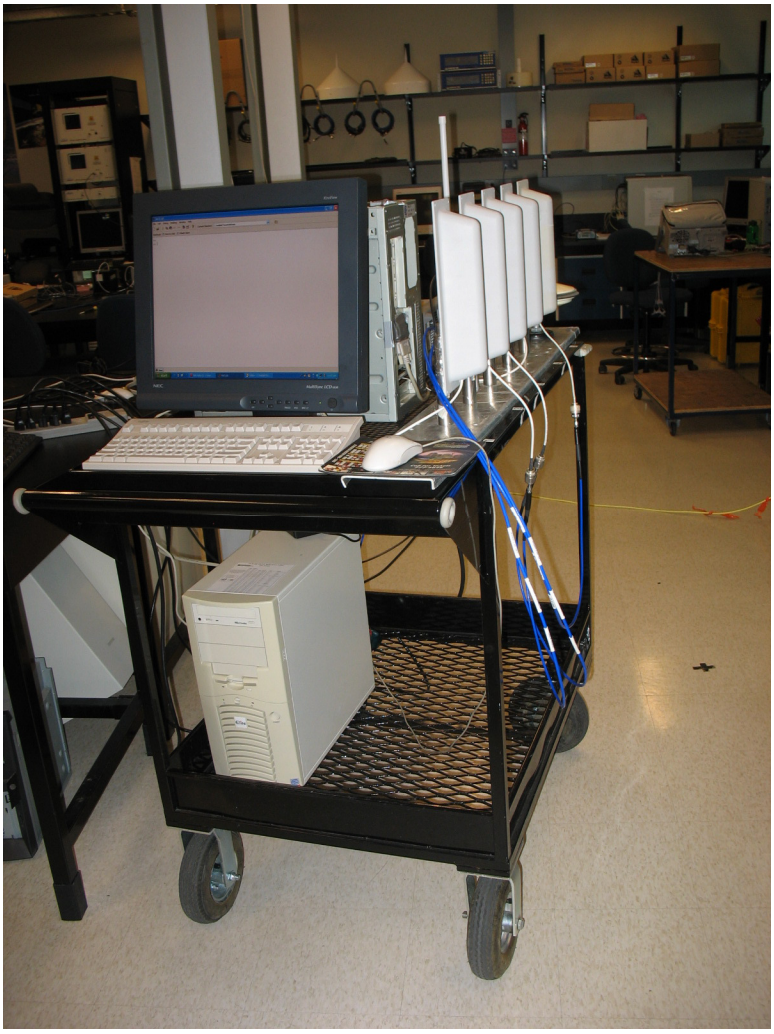

Figure 5.4: Indoor environment during data collection

Figure 5.5 demonstrates indoor CIR profiles corresponding to one antenna moving slowly. This environment is the same as that of Figure 5.4 (i.e., a typical indoor lab) and the speed is on the order of a walking person. In the figure, different positions corresponded to at most 3 metres displacement. Integration time for the CIR estimation was chosen to be 26.6 ms.

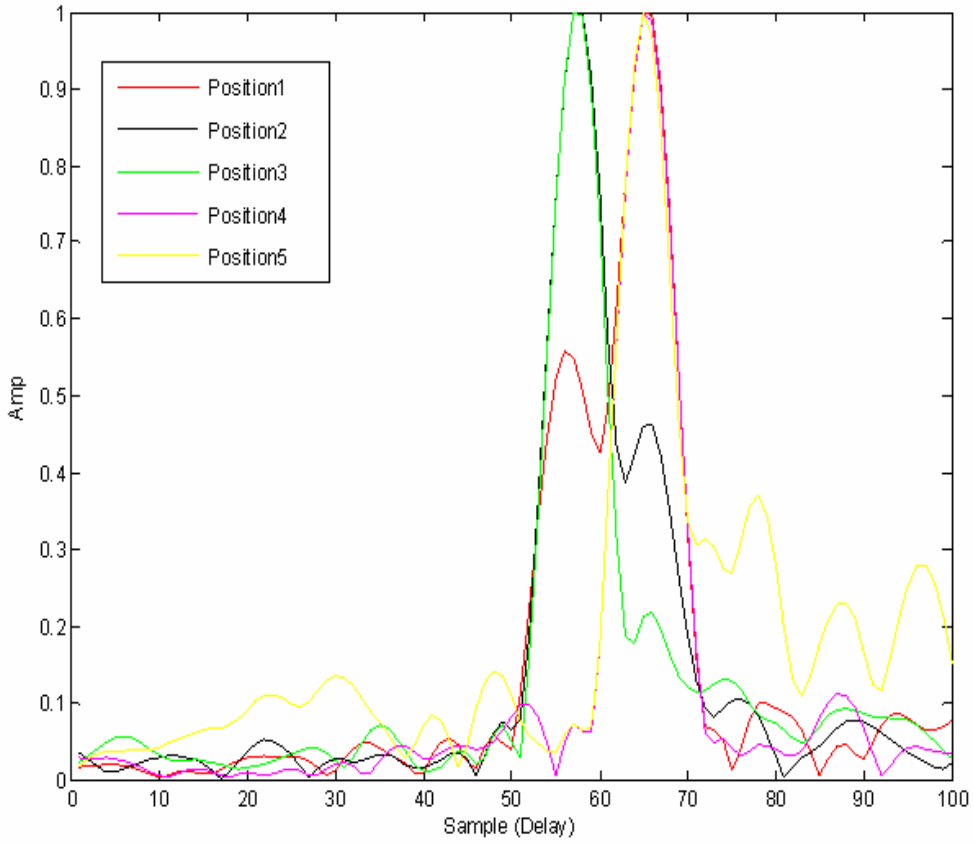

Figure 5.5: BTS1-CIR Profiles in different spots (time diversity)

Since dispersive multipath becomes independent approximately every half wavelength, the multipath decorrelation rate is deemed to be proportional to the speed of the MS. The higher the speed, the higher the decorrelation rate. In this thesis, all observations corresponding to temporal diversity are assumed to have a low dynamic range within a small area (i.e., within several metres) in order to keep the signal of interest (i.e., leading edge) correlated.

In the following subsection, it is shown that CIRs can be combined coherently to diminish the overall strength of multipath. In this coherent scenario, LOS and specular dominant multipath remain, whereas the dispersive multipath components induced by small objects can effectively be mitigated.

5.2.1 Coherent Combining of the Spatial Observation

Given the aforementioned model for the spatial-temporal observations in which the LOSs are correlated and the MPs are independent, if relative phases of arrival corresponding to different channels are denoted as $\varphi_{21}, \varphi_{31}, \varphi_{41}$, then the signal corresponding to different antenna elements can be modeled as:

$$Rx_i = (LOS + MP_i)e^{jw+\varphi_{i1}} + n_i \quad i = 1,2,4,5 \quad , \varphi_{11} = 0$$

where LOS, MP_i and ω are the correlative part, uncorrelative parts, and the residual frequency between BTSs and MS, respectively. Correlative parts include leading edge components and specular correlative multipath terms. Given $\varphi_{21}, \varphi_{31}, \varphi_{41}$, it can be shown that the signal $RX = Rx_1 + e^{-\varphi_{21}} Rx_2 + e^{-\varphi_{31}} Rx_3 + e^{-\varphi_{41}} Rx_4$ is statistically less affected by multipath terms. An arbitrary measure for multipath content of a signal can be defined as signal to multipath ratio (SMR), i.e.,

$$\frac{LOS\{RX\}}{MP\{RX\}} \geq \frac{LOS\{Rx_i\}}{MP\{Rx_i\}} \quad i = 1,2,3,4 \tag{5.1}$$

in which *LOS* and *MP* are operators giving the line-of-sight and multipath part of the signal, respectively. Therefore, given the compensation for inter-channel relative phases, superimposing CIRs corresponding to different channels can potentially mitigate the effect of dispersive multipath. The aforementioned approach implicitly uses spatial observations. Nevertheless, the concept can be extended to the temporal case in low dynamic situations. Using this spatial-temporal paradigm, the number of observations contributing to positioning enhancement can be tremendous.

5.2.2 Obstacles toward Coherent Combining of the Space-Time Observations

Some issues must be resolved in coherent combination of the CIRs, otherwise the approach can degrade the ultimate performance. The obstacles can be categorized as: 1)Residual frequency, 2) Clock drift, 3) Different inter-channel time delays, 4) Phase imbalance (i.e., offset between I and Q), and 5) Inter-channel coupling. The following subsections analyse the obstacles and give a solution for the challenges.

5.2.2.1 Residual Frequency

Residual frequency causes the rotation of the complex CIR in time with a rate proportional to residual frequency. This rotation precludes the coherent combining of the CIRs during long term intervals. The mechanism is similar to the Doppler frequency impact on the despreading process. Figures 5.6 and 5.7 show field complex CIRs in a

static receiver for two different time epochs. It can be seen that the I and Q are interchanged during the two depicted epochs and this is due to the residual frequency.

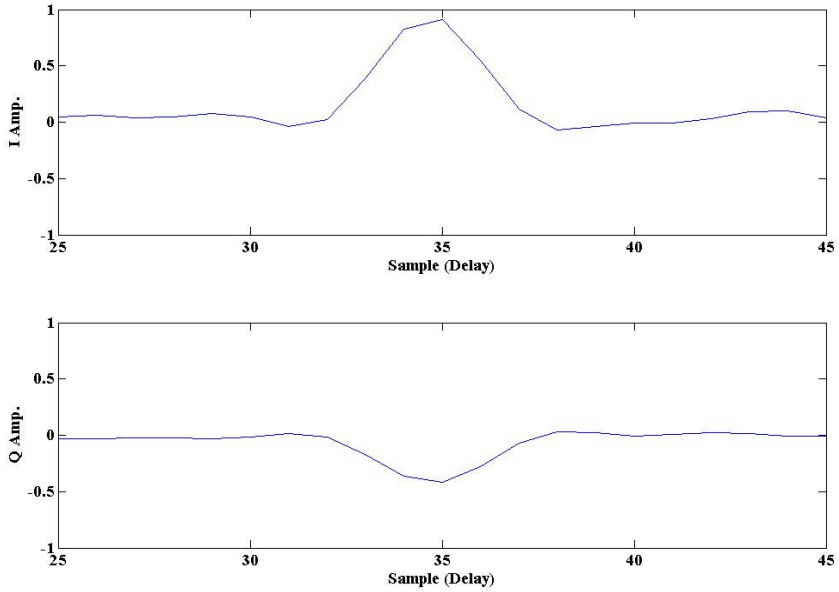

Figure 5.6: Complex CIR (Epoch 1)

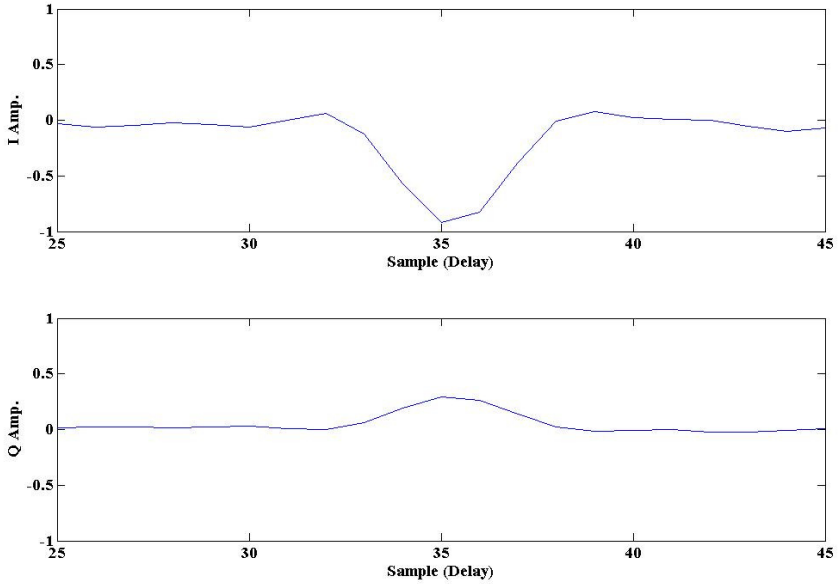

Figure 5.7: Complex CIR (Epoch2)

The residual frequency can be estimated by measuring the rate of change of phase for each individual point in the complex CIR. The accuracy of estimation depends on the local SNR corresponding to that point. The higher the strength, the lower the noise effect and the better the residual frequency compensation.

Let the M[th] tap of the CIR corresponding to time epoch *n* be denoted as $CIR^n(m)$. The following equation gives the phase evolution corresponding to tap M during epoch transition from *n* to *n+1*.

$$\theta_{err} = Arg\{CIR^{n+1}(m)\} - Arg\{CIR^n(m)\} \tag{5.2}$$

Due to the observation noise, smoothing can be done using a low pass filter which settles asymptotically to the residual frequency. In the aforementioned approach, only one delay among the entire CIR taps is utilized for estimating residual frequency. A more robust scheme can be proposed using all of the complex CIR taps. Intuitively, if more taps are incorporated into the estimation process, the effect of noise can potentially be lessened. The approach can be considered as a brute force search for finding the best phase correction among different phase hypotheses. The phase correction aims at aligning complex CIRs corresponding to different epochs for coherent combination purposes.

Given $CIR^n(m)$ and $CIR^{n+1}(m)$, $m = 1,2,...,M$, as M tap CIRs corresponding to time *n* and time *n+1,* respectively, the following equation gives a brute force estimation for

phase, θ (i.e., phase evolution due to the residual frequency), between two consecutive epochs *n* and *n+1*:

$$\theta_{err} = Max_{\theta}\left\{\left\langle CIR^{n}.CIR^{n+1}e^{j\theta}\right\rangle\right\} \tag{5.3}$$

In Equation 5.3, $\langle . \rangle$ denotes the cross correlation-integration between $CIR^{n}(m)$ and $CIR^{n+1}(m)$ over the CIR span $m = 1,2,...,M$ and $e^{j\theta}$ denotes the phase wipe off term. This estimator uses more information than the first one proposed in estimating the residual frequency. Hence, it is expected to show better stability and accuracy.

5.2.2.2 Clock Drift

Due to the asynchronicity between the transmitters and receiver, the locally generated code starts sliding relative to its correct position even in static circumstances. This effectively causes CIRs to slip over time. CIR slippage due to the sampling clock offset precludes coherent combining of the CIRs in different time epochs. Hence, for preserving the coherency among different CIRs, compensating the clock offset/drift is a must. Clock offset can be compensated indirectly by estimating the residual carrier frequency and then generating the compensated local despreading code in the receiver. This is justifiable due to the coherency between carrier and clock frequency in the transmitter. Clock offset can also be estimated directly using some well-known conventional methods. For example,

the delay-locked-loop (DLL) is a fully-digital implementation of a synchronization circuit which utilizes a phase discriminator, a numerically-controlled-oscillator (NCO), and a loop filter.

If the sampling circuit uses a short-term stable clock, given the usage of CIRs over short intervals, clock drift does not cause substantial degradation in the coherent combination process. The field CDMA signal used in this thesis is sampled by an oscillator board with a 10 MHz TCXO as the reference clock. The TCXO specification imposes at most 0.5 ppm static offset, which can be compensated directly after its estimation (e.g., by FFT method). Besides static offset, short term stability of the TCXO is another crucial parameter to be considered. Short-term stability is usually characterized by the Allan variance which is defined by one half of the time average over the sum of the squares of the differences between successive readings of the frequency deviation sampled over a given time interval. Lu (2007) practically measured the Allan deviation (i.e., square root of Allan variance) of the TCXO corresponding to the utilized hardware in this thesis. Table 5.1 shows the results for some arbitrary intervals.

Table 5.1: Allan Deviation for Front End Master Clock (TCXO)

Time interval	Specifications	Measured Values
τ = 1 s	1e-11	1e-10
τ = 10 s	1e-12	6e-10
τ = 100 s	1e-12	9.5e-10
τ = 1 hr	3e-11	2.5e-10

Even though the measured result for this particular TCXO is not as good as the specifications, it is stable enough for this research. For example, if the TCXO stability is 1e-10 in one second, then the frequency change at RF 1.9 GHz will be 0.19 Hz which is sufficiently small for this application. Therefore, given a compensating residual frequency, uncompensated clock offset local code can be generated to result in the CIRs which can then be coherently combined together if the continuous data set is collected in less than approximately a 1 sec time interval. This is due to the fact that the 0.5 ppm accuracy causes, in the worst case, a 0.614 chip slippage during one second. This residual misalignment is not critical, because there still remains some partial correlation between the different CIRs.

Another scheme for synchronization is to use the 1 pps signal as a trigger point in the sampling circuit whenever the CIRs are deemed to be combined during long-term intervals. This scheme readjusts the starting point of the data stream whenever the 1 pps pulse arrives. Hence, long term observations, however defragmented, are achievable on the receiver side.

5.2.2.3 Variable Inter-Channel Delays

Filters, amplifiers, and automatic-gain-control (AGC) units can introduce significant time-variable delays and phase offsets of the order of microseconds. Without hardware calibration, different channels can have different delays because of the discrepancy in RF component characteristics. Ideally, gains, delays, and phase offsets corresponding to different channels should be calibrated for effective coherent combination of the CIRs.

The calibrations were performed offline during data collection in this thesis. Nevertheless, an adaptive-on the fly scheme is worth studying as future work.

5.2.2.4 Inter-Channel Coupling and Leakage

Coherent combining of the CIRs for multipath mitigation relies fundamentally on the independence of each channel among antenna elements, though different channels are not perfectly independent. Mutual coupling is a concern in antenna arrays especially in short spacing scenarios. The electromagnetic leakage among different antennas causes different channels to be correlated in terms of signal contents. Electrical leakage between tracks and signal flows in the printed-circuit-board (PCB) and elements is another issue which imposes correlated observations. Figure 5.8 illustrates coupling among different channels in a typical field data set. During the data collection, samples corresponding to one antenna element were collected and the other channels were connected to ground by 50 Ω matched-terminator resistors. It should be emphasized that in Figure 5.8, the vertical scales for antennas 2, 3 and 4 are different than the scale for antenna 1 (i.e., unit is 10 times less). The correlation between different channels is obvious, however, the magnitude is not enough to be a critical concern. Hence, the signal contents corresponding to different channels are deemed to meet the prerequisite for the coherent combining process. In the following subsection, some preliminary results and analyses are performed to show the applicability of the algorithm. In Chapter 6, another extension of the space-time paradigm using MUSIC is suggested. Space-time MUSIC must also deal with the aforementioned challenges regarding the space-time observations.

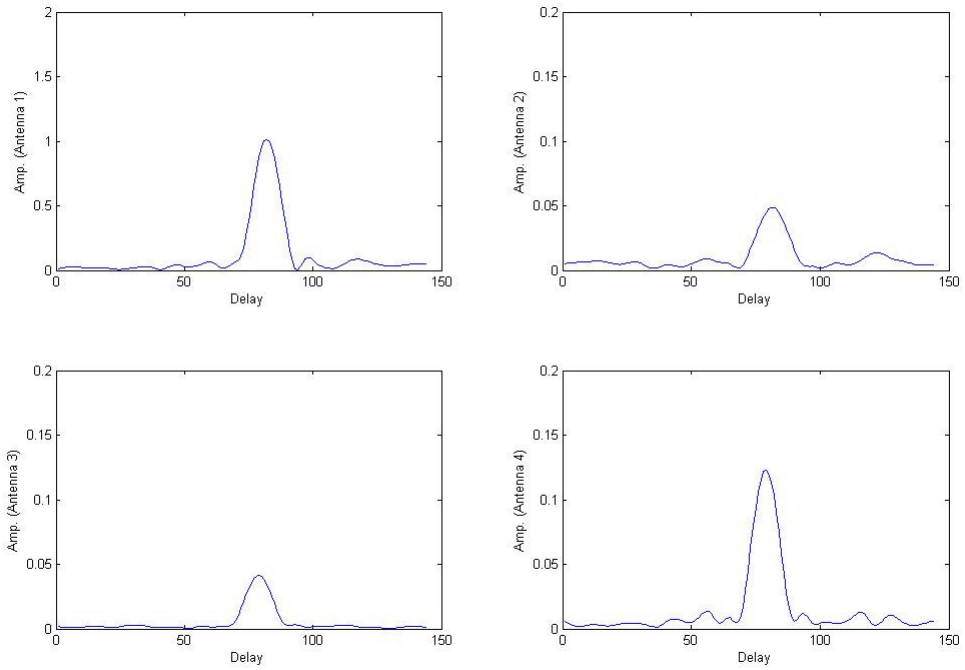

Figure 5.8: Inter-channel leakage

5.3 Analyses and Results

Combining the space-time CIRs, after resolving the previously stated challenges, yields observation sets containing enhanced-resolvability properties. These properties lead to a more robust and reliable leading edge identification process. Figures 5.9 and 5.10 show the CIR and enhanced CIR (26.6 ms as integration time) using temporal diversity observations in a pseudostatic mode. The field data was derived on the roof top of the CCIT building at the University of Calgary with BTS LOS accessibility (Market Mall site). During data collection, the antenna element had a low dynamic range (i.e., several metres) with the speed of a normal pedestrian. The data collection was performed over 13

seconds with a sampling frequency of 2.5 MHz and 12 bits resolution. Due to the hardware capture size limitation, the observation time could not go beyond 13 seconds. The consistency of the results, however, had already been tested using separate data sets under comparable conditions. It can be seen from Figure 5.9 that for some epochs, multipath contains stronger content than the leading edge part. Hence, the first components become susceptible to falsification, if the leading component is assumed to be the index corresponding to maximum amplitude in the CIR or if the threshold is kept high for decreasing the false alarm condition in the detection process. This falsification introduces incorrect peaks as leading components, which effectively makes the positioning biased. On the contrary, Figure 5.10 illustrates that combined-compensated CIRs give a sufficient statistic with a better property. It can be observed from Figure 5.10 that correlative components including leading edge and specular multipaths are resolved. This leads collectively to a more smoothed and robust CIR for detection purposes. This limited data set shows that dispersive multipath can be mitigated by this space-time manipulation, whereas the specular multipath still remains in the CIR. This is due to the coherency of the specular multipath among temporal observations. In fact, specular multipath uses the same property as the leading edge which is not favourable.

After the enhancement process, the resolvability of the components depends on the innate resolution in the despreading process. In Chapter 3, it was mentioned that the band limited CDMA signal cannot resolve components which differ in time by less than the chip rate. In Chapter 6, another technique based on MUltiple-Signal-Classification (MUSIC) will be proposed which both mitigates the multipath effect and improves the resolvability of the remaining components.

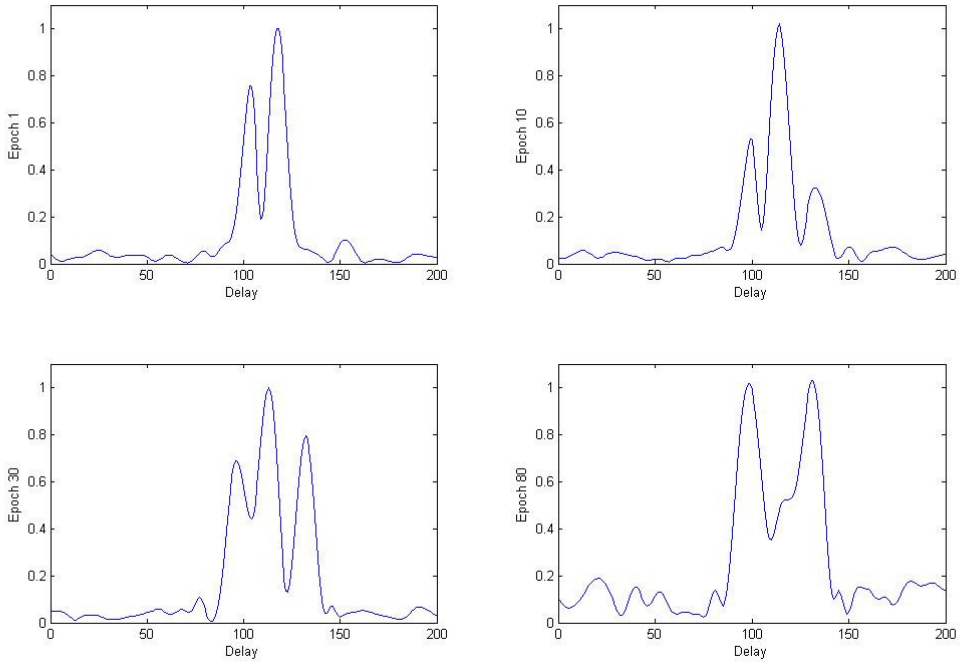

Figure 5.9: CIR in different epochs (pedestrian walk)

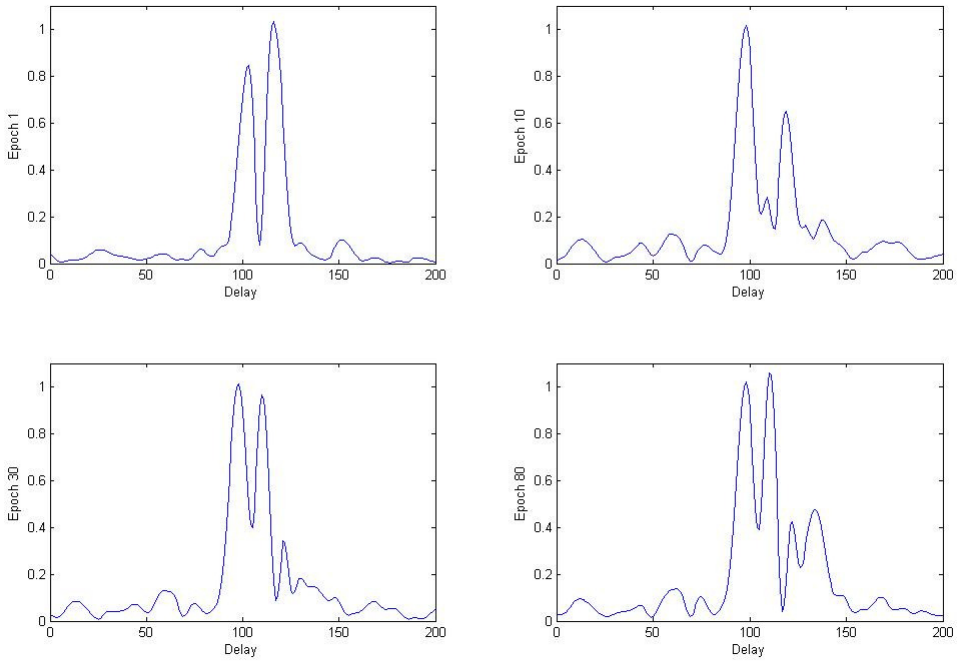

Figure 5. 10: Enriched-combined CIR in different epochs

Analyzing the leading component derived from the combined CIRs suggests that the combining is not merely smoothing, as might seem obvious from the beginning. Figure 5.11 shows, for given BTSs, different TOAs corresponding to different epochs in both the original CIRs (top) and the enhanced-combined CIRs (bottom). The thick base line (true TOA) is shown for better interpretation. It can be inferred from the figure that the enhanced-combined TOAs are not merely moving average replicas of the original TOAs. There are some apparent outliers in the original TOAs which come from false detection of the leading component.

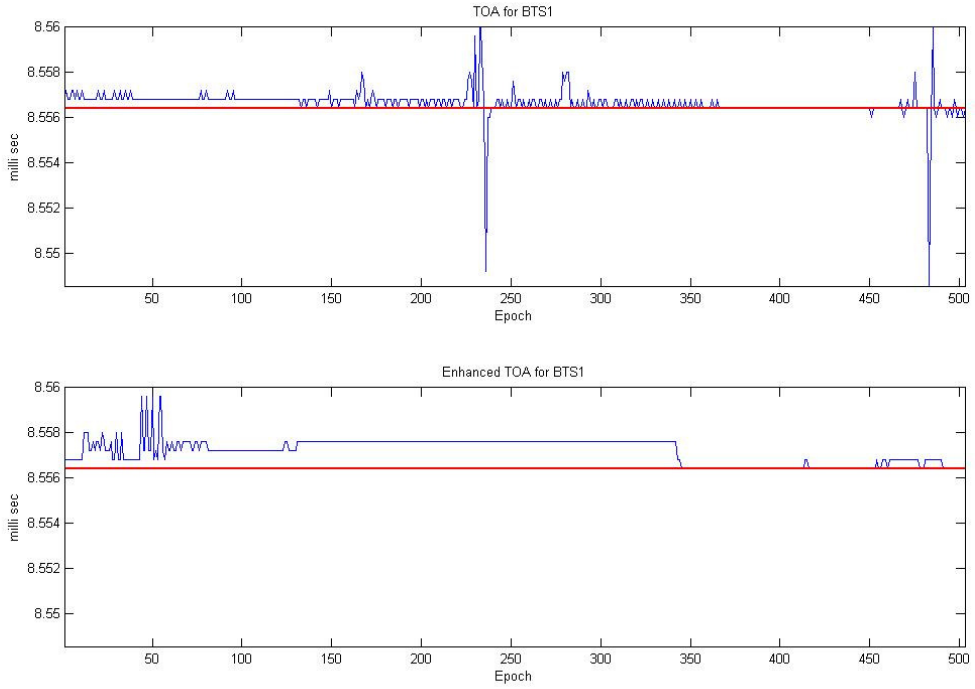

Figure 5.11: TOA (top) and enhanced-combined TOA (bottom)

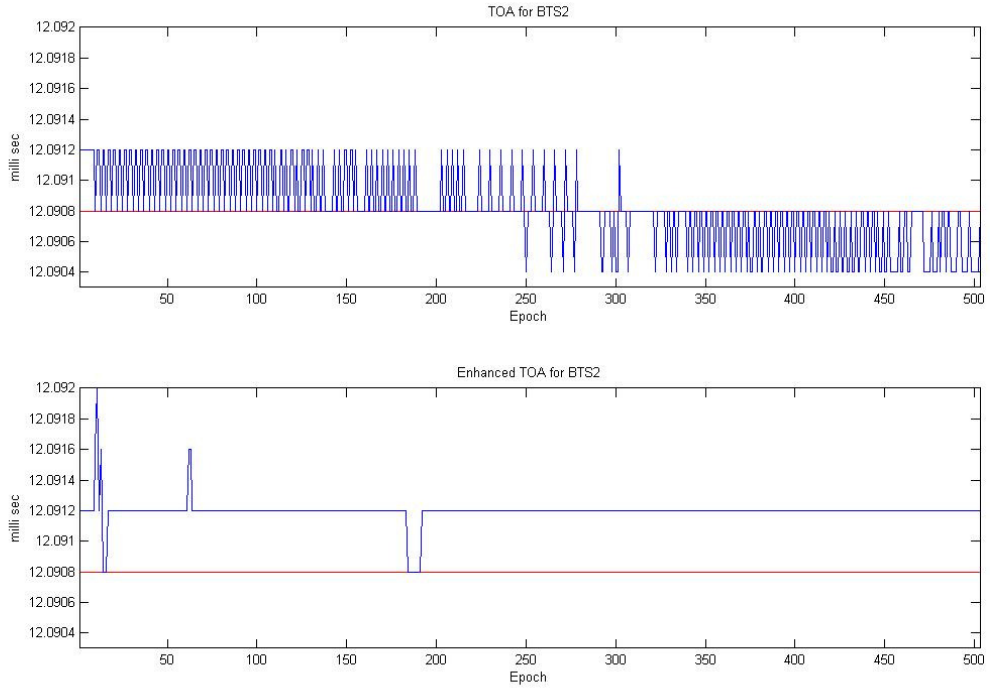

Figure 5.12: TOA (top) and enhanced-combined TOA (bottom) for BTS2

This is due to either signal blockage or strong multipath components as in Figure 5.2. For another BTS, Figure 5.12 shows TOAs and enhanced-combined TOAs. Positions were fixed with the same data set as in Figures 5.9, 5.10, 5.11 and 5.12 and compared for both scenarios, i.e., using original CIRs and also enhanced-combined CIRs. Figure 5.13 shows a scatter plot corresponding to the last 200 epochs of the total 500 epochs using original CIRs. It can be observed that the estimated positions are spread over a wide range due to both the multipath effect and also fragile BTS detectability.

In the plot, smoothed positions using a median filter are also depicted. The median filter, intended for removing outliers, discards 20 positions from both sides of the sorted

ensemble. Moreover, RP and EP stand for real-position (true position) and estimated-position, respectively.

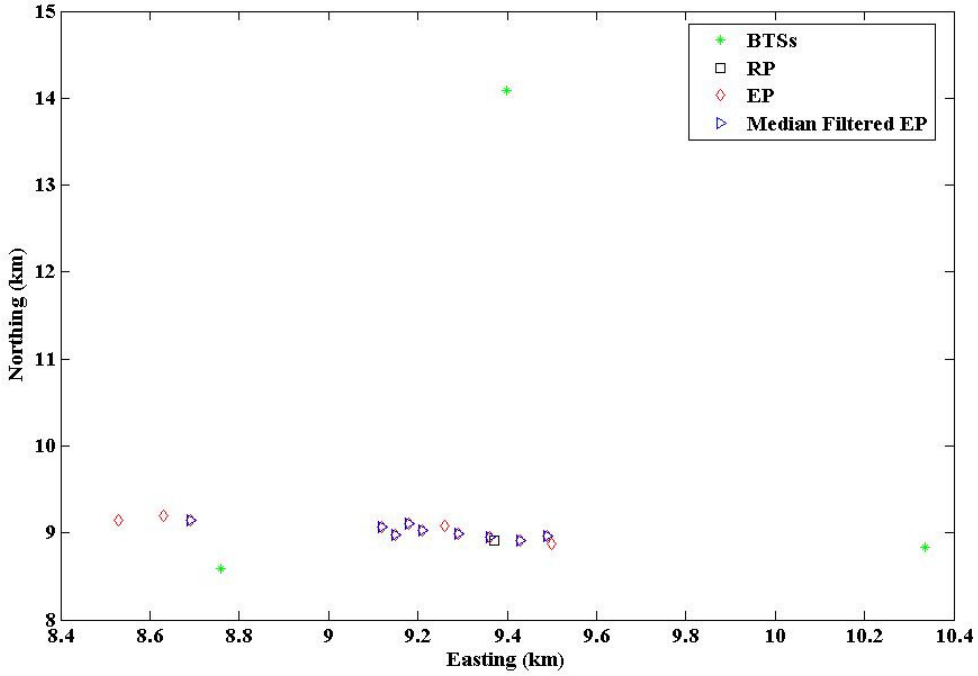

Figure 5.13: Scatter plot using original CIRs

After removing residual frequency and then combining different CIRs corresponding to each BTS, enhanced CIRs were obtained. The enhanced CIRs evolve over time and have better leading edge properties as a function of time. Figure 5.14 shows the scatter plot corresponding to the enhanced-combined CIR approach using the same data set as Figure 5.13.

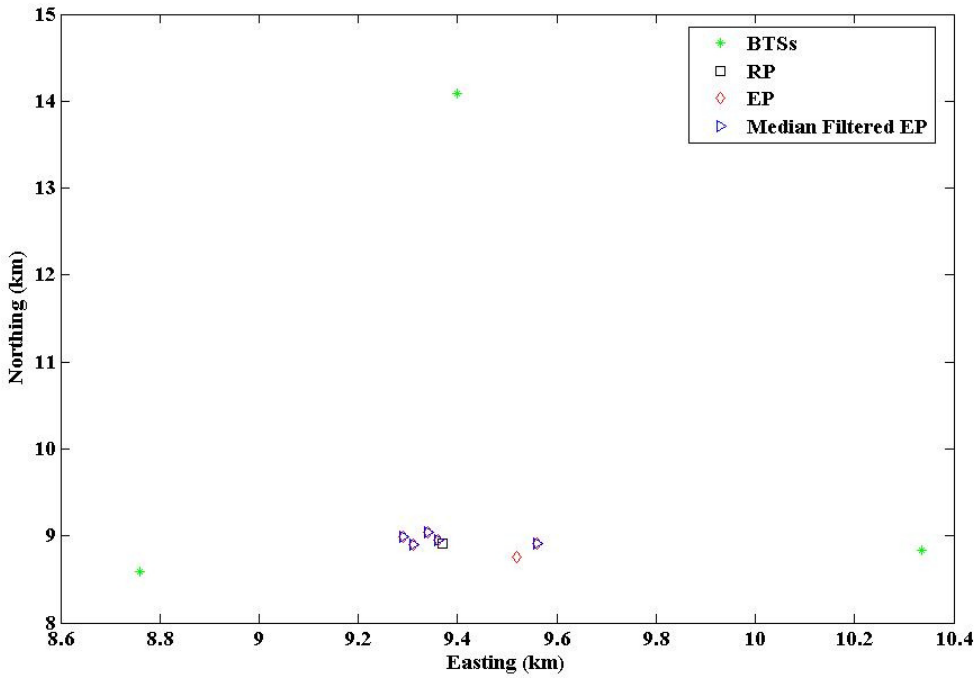

Figure 5.14: Scatter plot using enhanced-combined CIRs

It can be confirmed from Figure 5.14 that the scatter plot is more clustered using the enhanced-combined CIRs. In other words, the leading edge estimation becomes more robust and less susceptible to multipath components. It should be emphasized that the number of points in Figure 5.14 is the same as in Figure 5.13, namely 200 epochs. However, as the Maximum-likelihood brute force search with the limited amount of bin size in northing and easting (10 m) is used to estimate the positions, there is a quantization effect leading to a sparse plot in the resultant scatter. Table 5.2 compares easting-northing error mean (observation coordinates were precisely surveyed) and STD corresponding to the original CIR and enhanced-combined CIR usage. It can be inferred that the enhanced-combined CIR usage leads to more significant robust solutions in the position fix process.

Table 5.2: Easting-Northing Error Statistics

		Mean (m)	STD (m)
Easting	Original Error	-215.6	210.5
	Enhanced-Combined Error	-27.0	92.2
Northing	Original Error	130.6	65.0
	Enhanced-Combined Error	75.8	43.6

Comparing the means and STDs, the enhancement in the easting direction is more significant than the northing. This can be attributed to the different error sensitivities in the different directions. For quantifying the relative sensitivities, the unscaled error covariance matrix of the unknowns (i.e., easting and northing), based on the measured TDOAs is derived as (Lachapelle, 1999):

$$C' = \left(A' * A\right)^{-1} \tag{5.4}$$

where

$$A = \begin{bmatrix} F_2^x & F_2^y \\ \vdots & \vdots \\ F_N^x & F_N^y \end{bmatrix}$$

$$F_i^x = \frac{x - x_i}{\sqrt{(x - x_i)^2 - (y - y_i)^2}} - \frac{x - x_1}{\sqrt{(x - x_1)^2 - (y - y_1)^2}} \qquad i = 2,3,..,N \tag{5.5}$$

$$F_i^y = \frac{y - y_i}{\sqrt{(x - x_i)^2 - (y - y_i)^2}} - \frac{y - y_1}{\sqrt{(x - x_1)^2 - (y - y_1)^2}}$$

and $(x,y),(x_i, y_i)$ and N are Cartesian coordinates of the observation, Cartesian coordinates of the BTSs, and number of BTSs, respectively. Given the geometric configurations in Figures 5.13 and 5.14, the unscaled error covariance matrix is as follows:

$$\hat{C}_e = \begin{bmatrix} 0.3948 & -0.3521 \\ -0.3521 & 0.7516 \end{bmatrix} \tag{5.7}$$

Equation 5.7 implies that the positioning geometry is slightly worse in northing than in easting. Therefore, the actual difference in accuracy between easting and northing seen in Table 5.1 is not due to a difference in geometry but is instead likely due to multipath.

In the aforementioned test case, only temporal observations in a low dynamic scenario were used to demonstrate the applicability of diversity in positioning enhancement. Nevertheless, the idea is extendable to spatial diversity and also to joint spatial-temporal diversity scenarios. If spatial diversity is utilized, the inter-channel (i.e., between antenna elements) and intra-channel (i.e., within an antenna) calibrations become very crucial. In this realization, any miscalibration affects the overall performance in terms of achievable processing gain.

The next chapter gives a generalization of the MUSIC method using space-time diversity which takes advantage of both resolvability in MUSIC and also independent contents in the space-time observation.

Chapter Six: Space-Time Paradigm in MUSIC

Chapters 4 and 5 examined the applicability of independent spatial-temporal observations for use in mitigating the multipath effect. In all the aforementioned results corresponding to field measurements, TDOAs were derived based on correlation processing. The gain inherent in the correlation process gives this process an advantage over other methods. The advantage is its immunity to interference from other wireless systems operating in the same or overlapping frequency bands. The drawback of the conventional correlation method is that the time resolution is limited to the chip interval of the PN sequence. With a chip rate of 1.2288 MHz in the IS-95 cellular network, the resultant resolution is limited to several hundred metres which is not sufficient to analyze the normal IS-95 wireless channel with delay spread equivalent to tens of micro seconds (i.e., on the order of kilometres), even in outdoor circumstances. Hence, high-resolution delay profiles are necessary to isolate the multipath components from the leading edge in a CDMA cellular network.

Super-resolution techniques were originally studied in RADAR-SONAR signal processing literature for spectral estimation and angle of arrival (AOA) estimation using antenna/sensor arrays. During recent decades, a number of researchers have adapted super-resolution spectral estimation techniques for the time-domain analysis. Lo, et al., (1994) employed the super-resolution technique in the frequency domain to estimate multipath time dispersion parameters such as mean excess delay and root-mean-square delay spread. Morrison and Fattouche (1998) used the parametric harmonic signal model format to model indoor radio propagation channels. There are different varieties of super-resolution techniques, such as minimum-norm (Pallas and Jourdian, 1991), root multiple-

signal-classification (Dumont, et al., 1994), and total least square-estimation of signal parameters via rotational-invariance techniques (TLS-ESPRIT) in Saarnisaari (1997). Klukas (1997) demonstrated some experimental results using MUSIC for positioning in the cellular network. In his research, Klukas used a network-centric architecture (as opposed to a mobile-centric architecture as used in this thesis) and the system was operating under the Advanced-Mobile-Phone-Service (as opposed to the IS-95 CDMA signal). Meanwhile, space-time observations were not utilized to improve the accuracy of the positioning.

In this chapter, MUltiple SIgnal Classification (MUSIC), an eigenspace-based super resolution technique for estimating delay profiles, is discussed. MUSIC, in the context of delay estimation, is based on the eigen decomposition of the correlation matrix in the frequency domain. It will be shown that the applicability of MUSIC in resolving the components of the incoming signal requires the independent signal components. This condition is difficult to satisfy in multipath circumstances, where different arrivals of the transmitted signal are coming from the same source. Given the fundamental assumption of Chapter 5 in which the signal-multipath parameters (i.e., phase of arrival, amplitude) are deemed to be independent among different observations, a space-time paradigm for MUSIC is proposed (subsection 6.4.1) to satisfy more of the required conditions for the MUSIC technique. In the proposed technique, delays corresponding to signal and multipath components are assumed to be constant among space-time observations; hence, the method is implicitly suitable for static and pseudo-static scenarios where there is no substantial change in TOAs during data collection. The outcome of space-time MUSIC is enhancement of the resolvability of the multipath which directly affects the positioning

accuracy in multipath wireless channels. Performance, applicability, and sensitivity to involved parameters are demonstrated by real field data sets and measurements along with different statistical analyses in the end of the chapter.

6.1 MUSIC Technique

The multipath radio propagation channel is normally modeled as a complex lowpass equivalent impulse response, i.e.,

$$h(t) = \sum_{k=0}^{L_p-1} \alpha_k \delta(t - \tau_k) \tag{6.1}$$

where L_p is the number of multipath components, and $\alpha_k = |\alpha_k| e^{j\theta_k}$ and τ_k are the complex attenuation and propagation delay of the *k*th path, respectively. It is assumed that $\tau_m < \tau_n$ for $m < n$. Therefore, τ_0 denotes the propagation delay of the LOS or leading edge, which is the parameter of interest for the purpose of radiolocation. The Fourier Transform (FT) of Equation (6.1) is given as:

$$H(f) = \sum_{k=0}^{L_p-1} \alpha_k e^{-j2\pi f \tau_k} \tag{6.2}$$

It can be seen from Equation (6.2) that the role of time and frequency variables in the frequency domain is interchangeable. Utilizing the aforementioned duality property, Equation (6.2) can be expressed as

$$H(\tau) = \sum_{k=0}^{L_p-1} \alpha_k e^{-j2\pi f_k \tau} \tag{6.3}$$

Equation (6.3) is the well known harmonic signal model in the spectral estimation context. Hence, any spectral estimation technique that meshes with the harmonic signal model can be adapted here to perform the time-domain analysis. It is assumed that the sampling rate is sufficient to satisfy the Nyquist theorem. Hence, the frequency domain sampling interval, $\Delta f = f_{k+1} - f_k$, is bounded by the condition $1/\Delta f \geq 2\tau_{\max}$, where $\tau_{\max} = \tau_{L_p-1}$ is the maximum propagation delay (Li and Pahlavan, 2004). The discrete frequency-domain channel response is given by Equation (6.4).

$$x(l) = H(f_l) + w(l) = \sum_{k=0}^{L_p-1} \alpha_k e^{-j2\pi(f_0 + l\Delta f)\tau_k} + w(l) \tag{6.4}$$

where $l = 0,1,\cdots,L-1$ and $w(l)$ denotes additive white measurement noise with zero mean and variance, σ_ω^2. Equation (6.4) in matrix form can be expressed as Equation (6.5),

$$\begin{aligned}
&X = H + W = Va + W \\
&X = [x(0)\ x(1)\ \cdots\ x(L-1)]^T \\
&H = [H(f_0)\ H(f_1)\ \cdots\ H(f_{L-1})]^T \\
&W = [w(0)\ w(1)\ \cdots w(L-1)]^T \\
&V = \begin{bmatrix} 1 & 1 & \cdots & 1 \\ e^{-j2\pi\Delta f\tau_0} & e^{-j2\pi\Delta f\tau_1} & \cdots & e^{-j2\pi\Delta f\tau_{L_p-1}} \\ \vdots & \vdots & \cdots & \vdots \\ e^{-j2\pi\Delta f(L-1)\tau_0} & e^{-j2\pi(L-1)\Delta f\tau_1} & \cdots & e^{-j2\pi(L-1)\Delta f\tau_{L_p-1}} \end{bmatrix} \\
&a = [\alpha_0'\ \alpha_1' \cdots \alpha_{L_p-1}']^T \\
&\alpha_k' = \alpha_k e^{-j2\pi f_0 \tau_k}
\end{aligned} \tag{6.5}$$

which is a well known harmonic signal model with delays as the unknowns. To super-resolve the multipath arrival times using MUSIC, it is necessary to obtain the covariance matrix, R_{XX} , of the frequency response observation. This is written as:

$$R_{XX} = E\{XX^H\} = VAV^H + \sigma_\omega^2 I$$
$$A = E\{aa^H\} \tag{6.6}$$

In the original derivation, parameters α_k and τ_k are assumed to be constant; however, the phase of the complex attenuation, θ_k , is assumed to be random with a uniform probability density function, $U(0,2\pi)$. The subscript H denotes the Hermitian (i.e., conjugate transpose) operator.

Let λ_i and e_i be the eigenvalues and corresponding normalized eigenvectors of R_{XX} with λ_i in decreasing order. As the column vectors of the Vandermonde matrix, *V,* are linearly independent, V has full rank. Given the randomness of θ_k , the $L_p \times L_p$ covariance matrix A is nonsingular. Assuming $L > L_p$, the rank of the matrix, VAV^H , is L_p and the $L - L_p$ eigenvalues of R_{XX} are all equal to σ_ω^2.

The basic idea of the MUSIC algorithm is the exploitation of the orthogonality property to form a null spectrum. The *L* dimensional subspace that contains the signal vector *X* can be split into two orthogonal subspaces, known as the signal subspace and noise subspace. The range space, *V,* is called the signal space and it is within the space vector spanned by

the first L_p eigenvectors of R_{XX}. Two projection matrices using signal EVs and noise EVs (i.e., eigenvectors (EVs) corresponding to $L - L_p$ smallest eigenvalues if the SNR is above one) can be contrived by decomposing the signal vector *X* into its signal space and noise space parts. The projection matrix of the noise subspace is then determined by Equation (6.7).

$$P_w = Q_w Q_w^H \tag{6.7}$$

where $Q_w = \left[q_{L_p}, q_{L_p+1}, \cdots q_{L-1}\right]$ and q_k, $L_p \le k \le L-1$ are noise EVs. Since the vector $v(\tau_k) = \left[1\ e^{-j2\pi\Delta f\tau_k} \cdots e^{-j2\pi(L-1)\Delta f\tau_k}\right]^T$ (i.e., so called steering vector when τ is arbitrary) must lie in the signal space, or equivalently in the null space of P_w as:

$$P_w v(\tau_k) = 0 \tag{6.8}$$

Thus, the L_p multipath delays, $\tau_k, 0 \le k \le L_p - 1$, can be determined by finding the delay values at which the following MUSIC pseudospectrum achieves maximum value:

$$S_{MUSIC}(\tau) = \frac{1}{\left\|P_w V(\tau)\right\|} = \frac{1}{\sum_{k=L_p}^{L-1} \left|q_k^H v(\tau)\right|^2} \tag{6.9}$$

Figure 6.1 shows the power delay profile for a synthesized multipath model which consists of two discrete paths, the first of which is at delay number 14 and the second of which differs from the first by 1 chip. It is worthwhile to mention that in the simulation

the oversampling rate is 2; hence, the next location for the second component is equivalently 14+2 = 16. SNR is chosen as 40 dB. In Figure 6.1, signal components are depicted as solid thick lines and estimated CIR after despreading the code by correlation processing is depicted as a dashed line. It can be seen that due to band limitation (i.e., non-infinitesimal chip duration), the peaks corresponding to different paths overlap with each other. These two overlapping paths form a spurious single modal peak around tap number 15 due to destructive and constructive interference mechanisms. This example demonstrates that power delay profiles measured by the conventional PN correlation method with insufficient resolution margin may be delusive in some cases. In Figure 6.1, the MUSIC pseudospectrum is depicted as a solid thin line. The pseudospectrum suggests two strong components (i.e., two local peaks) as two components of the signal. This means that the super-resolution post-processing applied to the estimated CIR can improve the resolution of the delay profile. However, it can be inferred from Figure 6.1 that there are some bias issues after resolving the peak. The bias sources come from the practical implementation issues and inherent bias in the MUSIC approach which will be briefly addressed later.

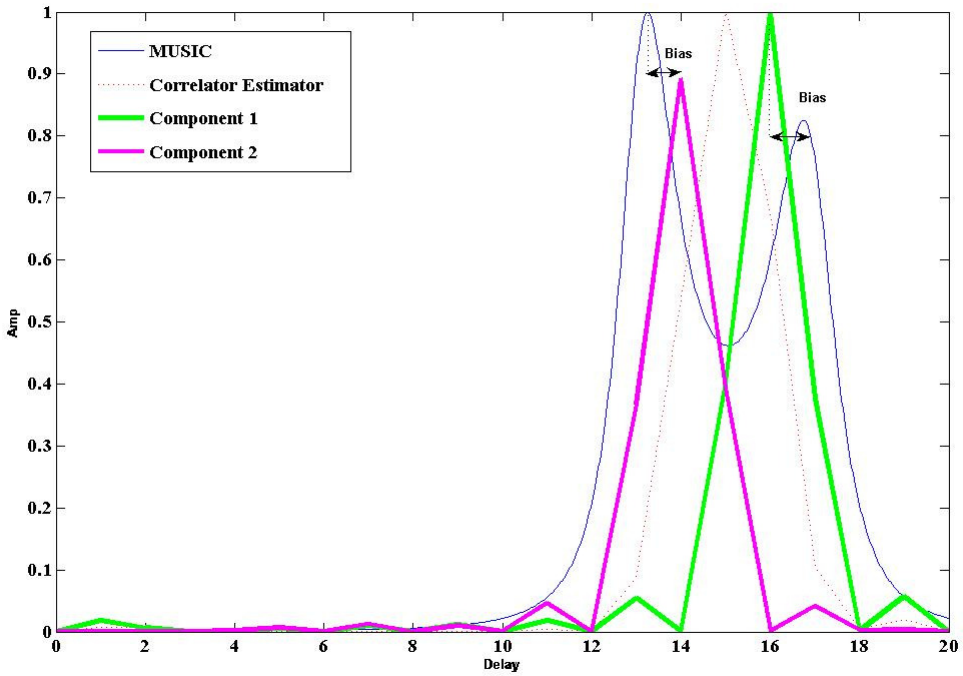

Figure 6.1: Power delay profile of two path signal

6.2 Practical Implementation Challenges

6.2.1 Covariance Matrix

In the preceding derivation of the MUSIC algorithm, the theoretical correlation matrix, R_{XX}, is required. In practice, the correlation matrix must be estimated from the finite data samples. Having access to P streams of measurement data, the averaged estimate of the correlation matrix is obtained as:

$$\hat{R}_{xx} = \frac{1}{P}\sum_{k=1}^{P} X^{(k)} X^{(k)H} \tag{6.10}$$

It should be emphasized that each individual data stream must convey some randomness in the signal space (e.g., θ_k) in Equation (6.9); otherwise the matrix A is susceptible to becoming degenerated (i.e., not full-rank). If only one data stream is available, Equation (6.10) is not applicable.

Having access to only one stream of measurement data with length N, the data sequence is divided into M consecutive segments of length L and then the correlation matrix is estimated as:

$$\hat{R}_{xx} = \frac{1}{M}\sum_{k=0}^{M-1} X^{(k)} X^{(k)H} \tag{6.11}$$

where $M = N - L + 1$ and $X^{(k)} = \left[x(k) \cdots x(k+L-1)\right]$. Figure 6.2 shows the covariance matrix estimation implemented by Equation (6.11). The matrix is called the forward-correlation matrix (FCM) in this thesis. The technique is also called spatial smoothing in array processing.

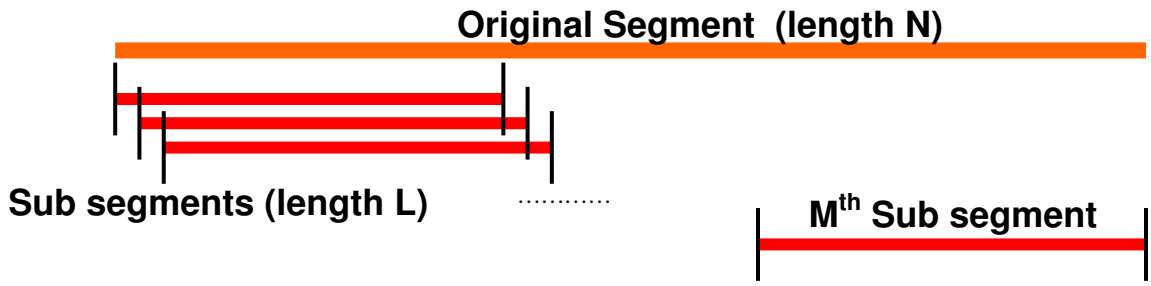

Figure 6.2: Covariance matrix estimation using forward method

The estimate of the correlation matrix can be improved using the forward-backward correlation-matrix (FBCM) below:

$$\hat{R}_{XX}^{FB} = \frac{1}{2}\left(\hat{R}_{XX} + J\hat{R}_{XX}^{\ *}J\right) \tag{6.12}$$

where J is the $L \times L$ exchange matrix whose components are zero except on anti-diagonal locations. Essentially, the estimate of the correlation matrix, R_{XX}, is based on the small finite length measurement data; hence, it is not necessarily Hermitian and Toeplitz as is the case with stationary random process correlation matrices. However, it can be seen that $\hat{R}_{XX}^{FB}$ is presymmetric, that is, $J\hat{R}_{XX}^{\ FB}J = \hat{R}_{XX}^{\ FB*}$ and its elements are conjugate symmetric about both main diagonals (Xinrong and Pahlavan, 2004).

The aforementioned estimation expressions for the covariance matrix have decorrelation effects for correlated signal components. This effect is highly desirable; otherwise, the MUSIC algorithm does not work properly. This is due to the fact that when using one stream of measurement data in estimating the correlation matrix R_{XX}, the rank of the correlation matrix A degenerates to one and the matrix becomes singular. It is worthwhile to mention that the decorrelation effect of the forward estimation method (i.e., Equation (6.11)) depends on the number of segments M, the frequency sampling interval Δf , and time delay difference between different signal components. For the forward-backward

method, the correlation coefficient also depends on the length of segment L, phase difference of different signal components, and the lowest frequency of the spectrum, f_0.

Cheung and Murch (1997) proposed an improved spatial smoothing technique as

$$\hat{R} = \frac{1}{M}\left(\sum_{i=1}^{M} R^{ii} + \sum_{j=1}^{m} \sum_{i=1}^{M-j} \left(R^{i(i+j)} + R^{(i+j)i} \right) \right) \tag{6.13}$$

where $R^{ij} = X^{(i)} X^{(j)H}$ is the cross-covariance matrix of the ith and jth sub-vectors and m is an integer smaller than the subvector size. The major advantage of Cheung's technique is that there are more matrices for averaging in order to decorrelate the coherent signals. It can be shown that this improved spatial technique is better able to resolve multipath than the FB technique alone.

6.2.2 Segment Size

Given one data stream set of length N, there is a tradeoff between resolution and stability of the algorithm affected by changing the number of samples in each segment. With large values of segment size (i.e., L), higher resolution is achievable which, in array signal processing, is equivalent to increasing the number of antenna elements-sensors in the subarrays and hence, increasing the aperture which in turn makes synthesizing a narrower beam width possible. However, increasing the segment size decreases the number of

available segments (i.e., M) which in turn causes a less reliable estimated covariance matrix and lessens the decorrelation effect of the subarray processing. Given a fixed N, different values for L are suggested (Xinrong and Pahlavan, 2004) as $N/2$, $N/3$, $3N/4$, $3N/5$ and $2N/3$.

6.2.3 Number of Multipath Components

The MUSIC pseudospectrum assumes *a priori* knowledge of the signal space dimension (i.e., number of multipath components, L_p) in its expression. However, L_p is neither known *a priori* nor can it be precisely determined by using estimated eigenvalues of the correlation matrix. The information theoretic criteria for detection and determination of the number of sources, including Akaike information theoretic criteria and Rissanen minimum-descriptive-length criteria (MDL), are applied to this problem (Wax and Kailath, 1985). The MDL criterion of estimation for L_p based on the estimated forward covariance matrix can be represented as:

$$L_p = \arg_k \left\{ \min \left\{ MDL(k) = -\log \left(\frac{\prod_{i=k}^{L-1} \lambda_i^{1/L-k}}{\frac{1}{L-k}\sum_{i=k}^{L-1}\lambda_i} \right)^{M(L-k)} + 0.5k(2L-k)\log M \right\} \right\} \qquad (6.14)$$

where $\lambda_i, 0 \le i \le L-1$ are the eigenvalues of the correlation matrix in descending order. The MDL criterion is slightly modified in Equation (6.15) for the FB covariance matrix.

$$L_p = \arg_k \left\{ \min \left\{ MDL(k) = -\log \left(\frac{\prod_{i=k}^{L-1} \lambda_i^{1/L-k}}{\frac{1}{L-k}\sum_{i=k}^{L-1} \lambda_i} \right)^{M(L-k)} + 0.25k(2L-k+1)\log M \right\} \right\} \quad (6.15)$$

Another suboptimum solution for determining the number of sources is to overestimate the model order. In this scenario, the number of sources is assumed to be a large and fixed value. Since the MUSIC pseudospectrum uses noise space eigenvectors, by overestimating the L_p, the number of noise space eigenvectors involved in Equation (6.9) is reduced which sacrifices the optimality of the MUSIC. However, the overestimation guarantees that there is no signal space eigenvectors in the projection matrix.

It also has been shown (Johnson and Degraaf, 1982) that modifying pseudospectrum as in Equation (6.16) can lead to a delay profile estimation process that is less sensitive to inaccurate estimation of the parameter L_p, which is highly desirable in a practical implementation when the correlation matrix is estimated from a limited number of data samples.

$$S(\tau) = \frac{1}{\sum_{k=L_p}^{L-1} \frac{1}{\lambda_k} \left| q_k^H v(\tau) \right|^2} \quad (6.16)$$

6.2.4 Estimation Bias

When SNR or the number of stream sets is not sufficiently large, MUSIC performs as a biased estimator of delay. This bias also affects the resolvability of MUSIC and is larger

than or comparable to the standard deviation in or right above the resolution threshold region (Xu, 1992). The bias depends on SNR, number of antennas (in array processing), stream sets, and source correlation. The rigorous statistical analyses of MUSIC are based on consideration of the estimated MUSIC null spectrum from which estimates are obtained. The estimated MUSIC null spectrum is a highly nonlinear function of its parameters and a quadratic function of the estimated subspace eigenvectors; so, most of the approaches in manipulating the null spectrum characteristics use Taylor series expansion and drop higher order derivatives of the null spectrum.

It was previously mentioned that the basic idea of the MUSIC is to exploit the orthogonality between noise eigenvectors and the steering vector, $v(\tau)$. The MUSIC pseudospectrum is a function of noise eigenvectors and parameters (i.e., delay profile). Because the noise eigenvectors, $\hat{Q}_w$, are derived from the estimated correlation matrix, $\hat{R}_{XX}$, if $\hat{Q}_w$ is perturbed from its true value, the MUSIC pseudospectrum will also be perturbed. This causes a perturbation of both the local maxima levels and positions. The perturbation in positions of the local maxima causes an error in delay profile estimates. For the sake of bias analyses, it is more convenient to represent the MUSIC pseudospectrum based on signal subspace eigenvectors.

Given $\hat{Q}_s = \left\lfloor \hat{q}_0\, \hat{q}_1 \cdots \hat{q}_{L_p-1} \right\rfloor$ as estimated eigenvectors corresponding to signal subspace where q_k, $0 \le k \le L_p - 1$ are signal EVs and $\hat{q}_k$ their estimated counterparts, the null spectrum of MUSIC defined by Equation (6.17) can be rewritten as Equation (6.18):

$$D_{MU}(\tau, Q_w) = v^H(\tau) Q_w Q_w^H v^H(\tau) \tag{6.17}$$

$$D_{MU}(\tau, Q_s) = v^H(\tau)\left(I_L - Q_s Q_s^H\right) v^H(\tau) \tag{6.18}$$

With the local minima at $\tau_0, \tau_1, \cdots, \tau_{L_{p-1}}$, the stochastic of $\hat{D}_{MU}(.)$ is quadratically related to $\hat{Q}_s$. Kaveh and Barabell (1986) derived the asymptotic statistics of the estimated signal eigenvector error, $\Delta q_i = \hat{q}_i - q_i$, as follows:

$$\begin{aligned}
AE\{N\Delta q_k\} &= -\frac{1}{2}\sum_{i=0, i\neq k}^{L-1} \frac{\lambda_k \lambda_i}{(\lambda_k - \lambda_i)^2} q_k \\
AE\{N\Delta q_k \Delta q_l^H\} &= \delta_{kl}\left\{\sum_{i=0, i\neq k}^{L_p-1} \frac{\lambda_k \lambda_i}{(\lambda_k - \lambda_i)^2} q_i q_i^H + \frac{\lambda_k \sigma_w^2}{(\lambda_k - \sigma_w^2)^2}\left(I_L - Q_s Q_s{}^H\right)\right\} \\
AE\{N\Delta q_k \Delta q_l^T\} &= -\frac{\lambda_k \lambda_l}{(\lambda_k - \lambda_l)^2} q_l q_k{}^T (1 - \delta_{kl})
\end{aligned} \tag{6.19}$$

where *AE* denotes asymptotic mean, *N* is the number of independent snapshots for estimating the correlation matrix, R_{XX}, and δ_{kl} represents the Kronecker delta. A rigorous bias analysis to drive an accurate and concise bias expression was performed in Liang Xu (1992). The analysis is based on the second order Taylor series expression, properties of the null-spectrum, and the statistics of the estimated signal eigenvectors. Given $\Delta\tau_i = \hat{\tau}_i - \tau_i, i = 0,1,\cdots, L_p - 1$, it is shown that the τ_i estimate has the following statistics:

$$\mathrm{var}\{\Delta\tau_i\} \approx \frac{1}{N} \frac{\sum_{k=0}^{L_p-1} \frac{\lambda_k \sigma_w^2}{\left(\lambda_k - \sigma_w^2\right)^2} \left| v^H(\tau_i) q_k \right|^2}{\ddot{D}_{MU}(\tau_i, Q_s)} \tag{6.20}$$

and,

$$E\{\Delta\tau_i\} \approx -\frac{1}{N} \frac{2\sum_{k=0}^{L_p-1} \frac{(L - L_p - 1)\lambda_k \sigma_w^2}{\left(\lambda_k - \sigma_w^2\right)^2} \mathrm{Re}\left[\dot{v}^H(\tau_i) q_k q_k^H v(\tau_i)\right]}{\ddot{D}_{MU}(\tau_i, Q_s)} - \frac{\dddot{D}_{MU}(\tau_i, Q_s)}{6\ddot{D}_{MU}(\tau_i, Q_s)} \mathrm{var}\{\Delta\tau_i\} \tag{6.21}$$

where

$$\ddot{D}_{MU}(\tau_i, Q_s) = 6\,\mathrm{Re}\left\{\ddot{v}^H(\tau_i)\left(I_L - Q_s Q_s^H\right)\dot{v}(\tau_i)\right\} \tag{6.22}$$

The results suggest that, for high SNR conditions, although asymptotically, the bias can be ignored in comparison with STD, whereas for low SNR circumstances, the bias can potentially become larger than or comparable to STD and critically affect resolvability as well as fidelity of the estimator.

Equation (6.20) also implies that overestimating the number of multipath components increases the estimation variance. This is due to the fact that given R_{XX} positive definite, eigenvalues are positive (i.e., $\lambda_i > 0$); hence if $O \geq P$,

$$\sum_{k=0}^{O} \frac{\lambda_k \sigma_w^2}{\left(\lambda_k - \sigma_w^2\right)^2} \left| v^H(\tau_i) q_k \right|^2 \geq \sum_{k=0}^{P} \frac{\lambda_k \sigma_w^2}{\left(\lambda_k - \sigma_w^2\right)^2} \left| v^H(\tau_i) q_k \right|^2 \tag{6.23}$$

The impact of overestimation in the bias expression of Equation (6.21) cannot be deduced directly as it implies more convoluted terms. Nevertheless, it is worth following up the bias analyses with future work.

6.3 Field Measurement Results

In this subsection, some field data delay profiles obtained by MUSIC are demonstrated. Figure 6.3 shows the functional block diagram for estimating delay profiles based on MUSIC super-resolution along with a sub-block diagram corresponding to the pseudospectrum module.

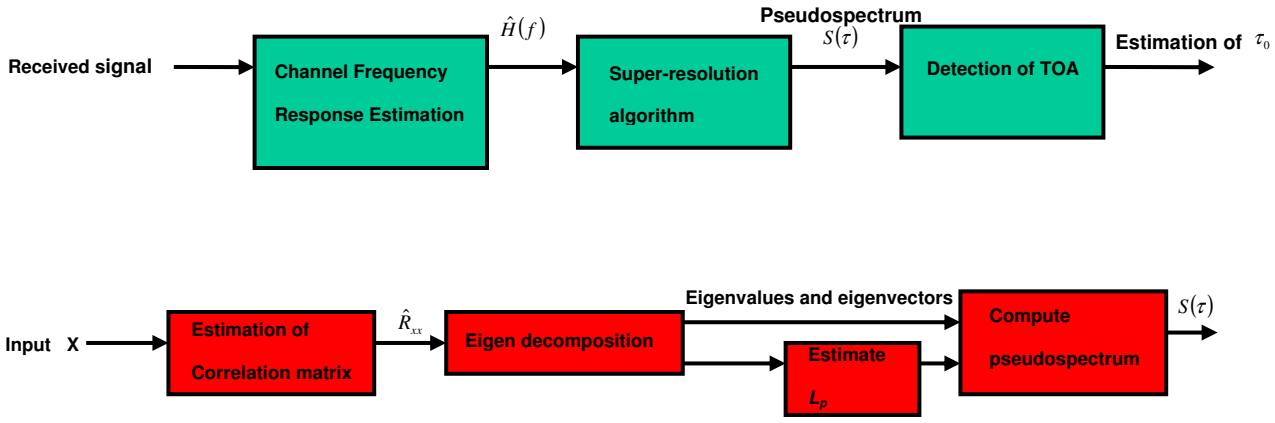

Figure 6.3: Functional block diagram for MUSIC delay profile

Estimation of the correlation matrix is performed by the forward technique which has a favorable intrinsic decorrelation effect. Field CDMA signals were digitized by the PLAN front end and the sampling rate was 2.5 MHz. Figure 6.4 compares delay profiles obtained by MUSIC and by the conventional despreading process for some BTSs. In the test, the static receiver was located on a roof top with moderate access to LOS. Subarray size (i.e., L), number of subarrays (i.e., M), and number of multipath components (i.e., L_p) are 30, 124 and 4, respectively. The number of multipath components was chosen as a fixed number 4 for all BTSs and MDL was not used in order to simplify the implementation. Although a fixed number for all BTSs in all epochs among different antennas is not an optimal configuration in the MUSIC context, it still imposes the same situation and fair comparison among different schemes addressed in the following. If the actual multipath number is greater than four, there is a severe degradation in resolvability of MUSIC, because the signal space eigen vectors are falsely considered as noise space eigen vectors in the MUSIC pseudo spectrum expression. If the multipath number is less than four, the signal components remain resolvable because the noise space eigen vectors are used in the MUSIC pseudo spectrum. Nevertheless, in the former case, there is some amount of bias in the estimated parameters due to the discrepancy between modeled and received signals

To increase the resolution of the frequency response (i.e., Δf), the original CIR window with size 51 was zero padded by a zero padding factor of 2. A zero padding factor indicates that the original 51 taps for temporal CIR were padded by 2*51 = 102 zeros before taking the FFT as a channel frequency estimator.

It can be observed that MUSIC delay profiles manifest more discernable sharp peaks in the pseudospectrum which can potentially be associated with the LOS and multipath components. Contrary to the artificially-simulated signal, in which the parameters are known *a priori*, fidelity of the profiles obtained by MUSIC in the field data is very difficult to verify. Nevertheless, LOS fidelity can be scrutinized by fixing position and then comparing the outcomes with conventional methods.

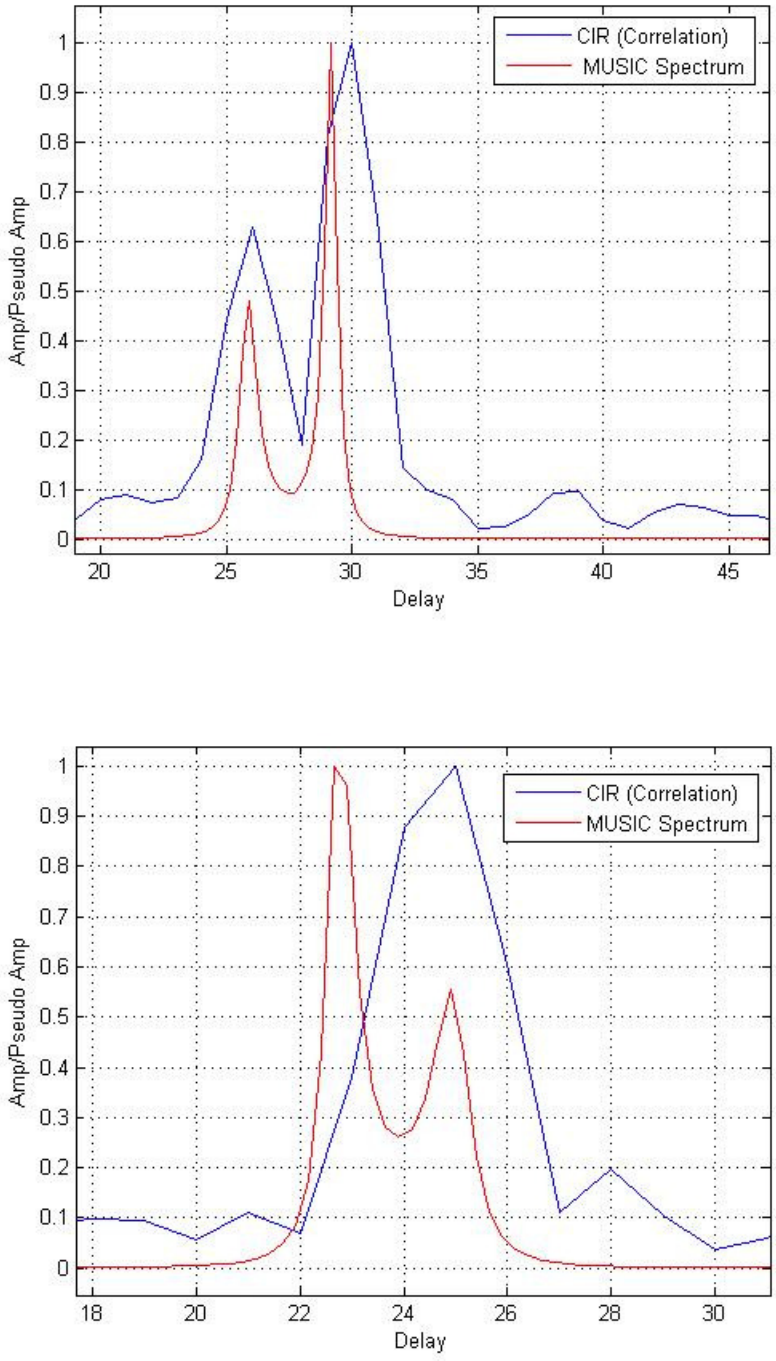

Figure 6.4: Delay profiles obtained by MUSIC and conventional despreading process

6.3.1 Positioning Results using Conventional Correlation Technique

Figure 6.5 shows the scatter plot corresponding to an IS-95 CDMA field measurement on a roof top (CCIT roof top) under pedestrian dynamics. In the figure, smoothed scatter obtained by removing outliers is also shown. The outliers were removed using a median filter applied to the ensemble estimated positions. RP and EP points are the real position and estimated positions, respectively.

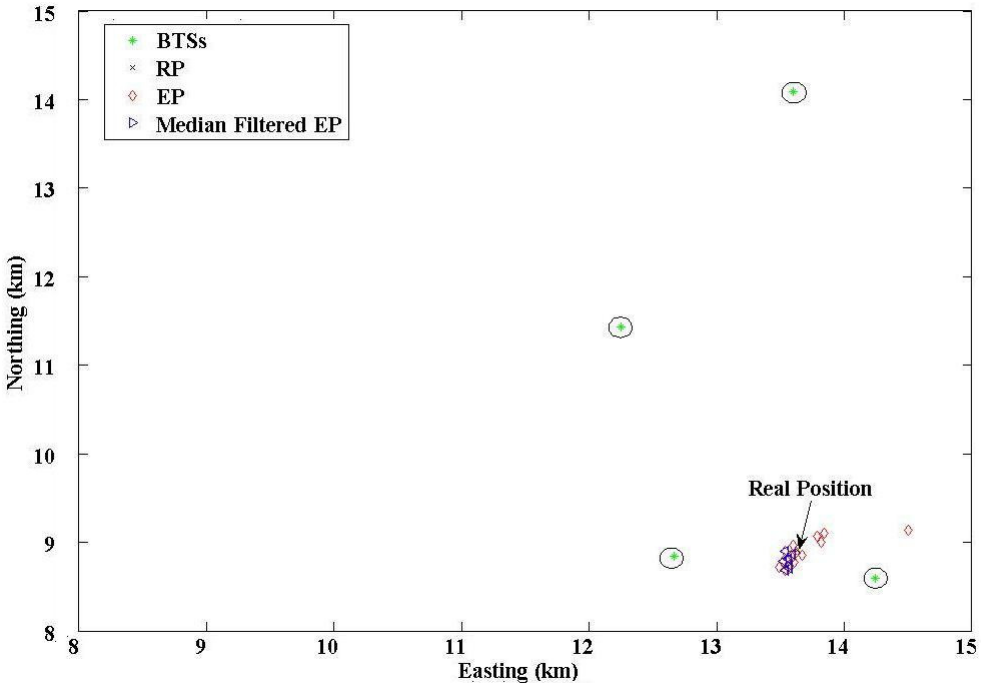

Figure 6.5: Scatter plot – Pseudoranges obtained by conventional correlation method

The range corresponding to each BTS was derived by applying a hard threshold to the estimated CIR using a despreading process (26.67 ms integration time) and then choosing the first above threshold index as the leading edge.

Since the antenna is moving around by several metres on the roof-top, the CIR corresponding to each BTS is changing. The signal strength for some BTSs might also be degraded during antenna movement. If this condition happens for a specific BTS, the pseudorange corresponding to this BTS is not reliable enough to be used in the position fix process. Rejecting this BTS also changes the GDOP in a given configuration. Therefore, the outliers in the scatter plot can be associated with this degenerated signal power, in addition to multipath.

Figure 6.6 shows the BTS availability status for the five BTSs corresponding to the above test case. The measure for availability (i.e., value 1) is the signal strength of a given BTS. Signal amplitude corresponding to the first epoch for a given BTS is set as a reference level. If the amplitude is degraded by 50% relative to this reference level, a not available status (i.e., value 0) is transmitted. This approach may not convey a rigid framework for verifying the BTS availability; however, it partially shows drastic power drop during data collection.

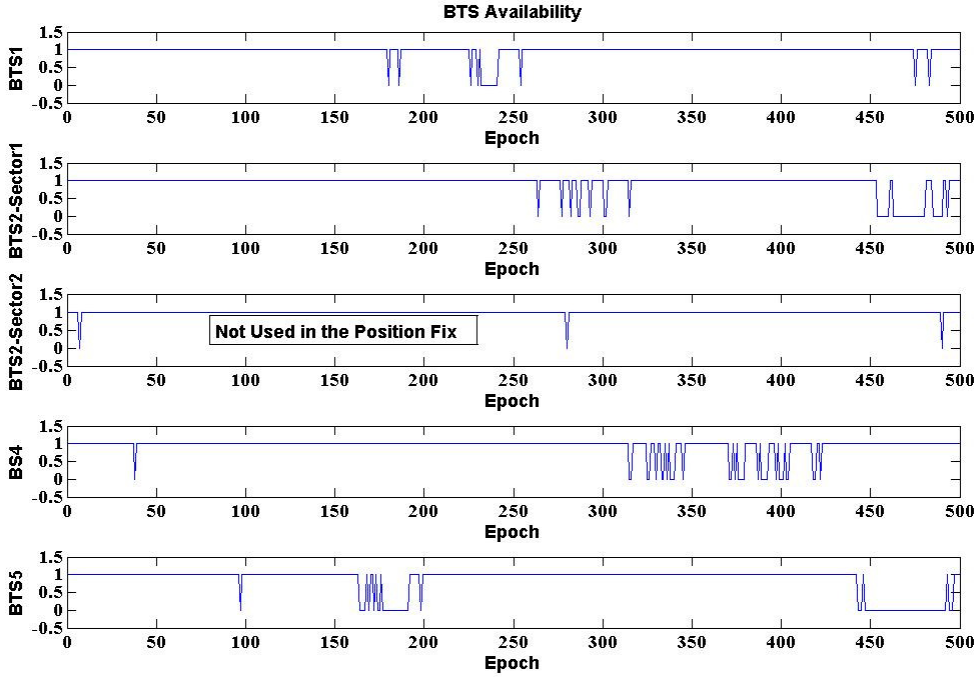

Figure 6.6: BTS availability

Since the BTSs transmit the CDMA signal through the air via three different directive antennas, it is worthwhile to mention that the second and third subplots in Figure 6.6 are different antenna sectors for the same BTS site. Figure 6.7 shows the northing and easting positioning errors for different epochs. There is a -800 m outlier in the easting-error for one epoch. By inspecting Figure 6.6, this outlier can be associated with a signal strength drop of BTS5 at the same epoch.

Figure 6.8 demonstrates estimated ranges for different BTSs involved in the position fix procedure in different epochs. The aforementioned outlier coming from BTS5 is evident as an outlier in the estimated range corresponding to BTS5.

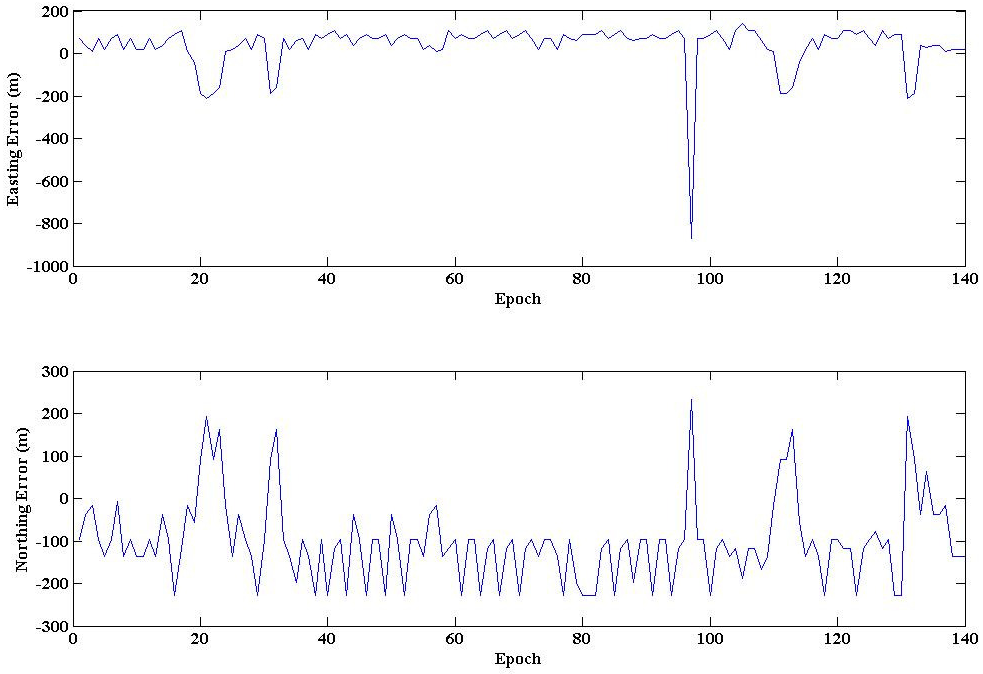

Figure 6.7: Easting and Northing errors (conventional)

After removing outliers, the easting error mean and standard-deviation (STD) are 55.4 m and 56 m, respectively, and the northing error mean and STD are -114 m and 79.5 m, respectively. The quantized behaviour of the range originates from the coarse despreading process with the resolution of sampling rate (i.e., 2.5 MHz) which equivalently conveys 120 m (3e8/2.5e6) range quantization.

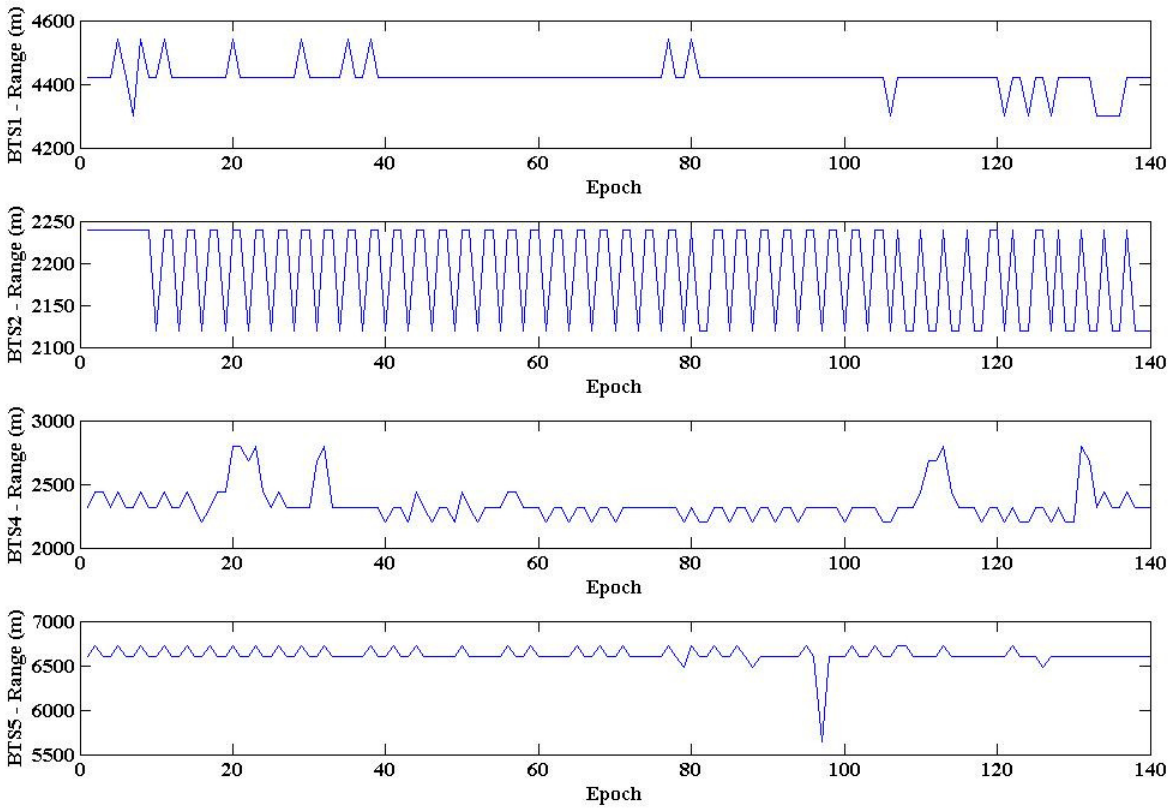

Figure 6.8: Estimated ranges for different BTSs (conventional)

Figure 6.9 shows histograms of easting and northing errors after removing outliers. Because the median filter, intended for removing outliers, discards 20 samples from both sides of the sorted data, estimated values are reduced to a 120 point data set out of the 140 point original data set including outliers. The histogram does not follow a Gaussian distribution; hence, the STD and mean do not have 1σ reliability meanings (67% realization probability within 1σ range) as Gaussian random processes would have. Usually multipath imposes a non-Gaussian distribution on positioning error; hence, the histogram characteristics of Figure 6.9 could possibly be due to the multipath effect.

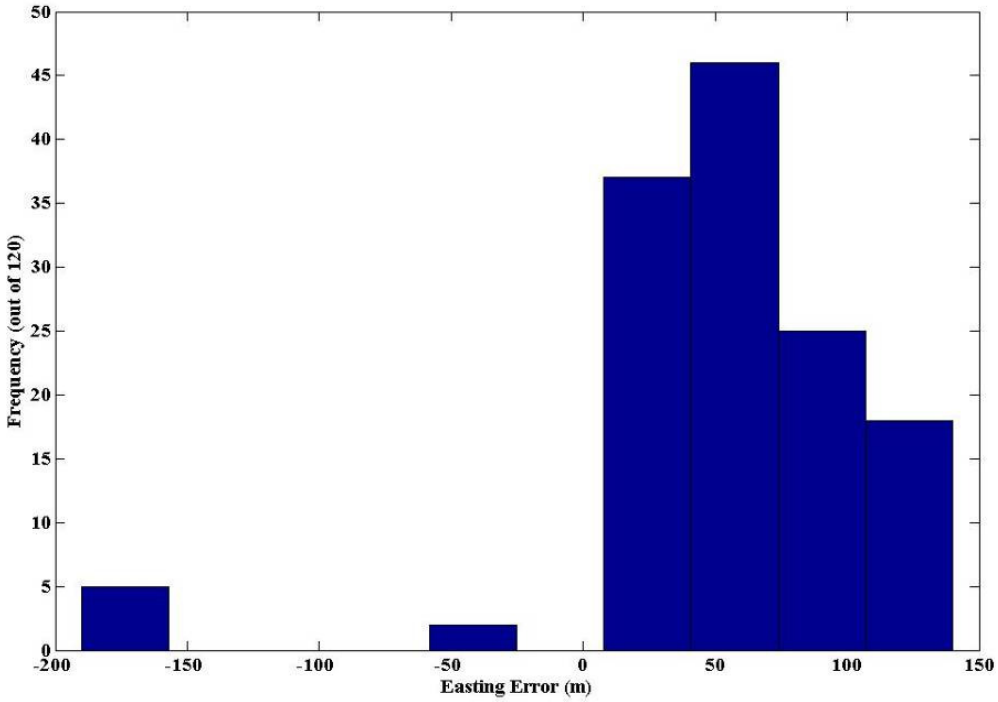

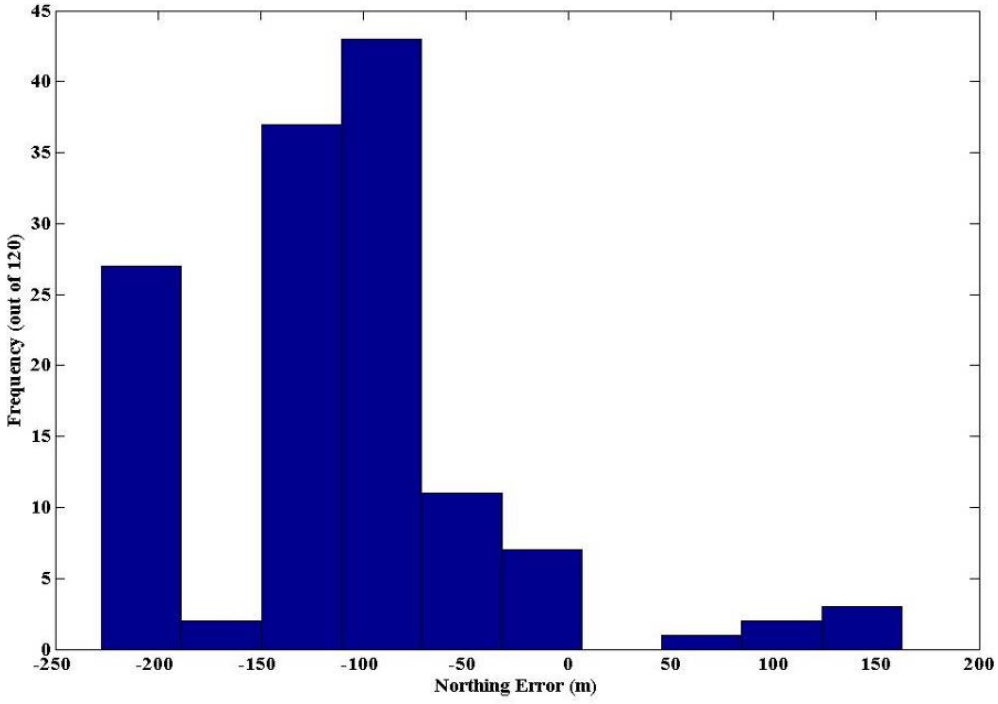

Figure 6.9: Easting-northing error distribution (conventional)

6.3.2 Positioning Results using MUSIC Technique

Figure 6.10 shows the scatter plot corresponding to the same set of IS-95 CDMA field measurements as shown in Figure 6.5. Here, the range corresponding to each BTS was derived based on applying a hard threshold to the estimated MUSIC pseudospectrum delay profile and then choosing the local maximum index nearest to the point right above the threshold as the LOS part. Subarray size, number of subarrays (i.e., M), and number of multipath components are 30, 124 and 4, respectively.

The higher resolution in MUSIC leads to the denser scatter plot compared to Figure 6.5. Figure 6.11 illustrates MUSIC northing and easting positioning errors for different epochs.

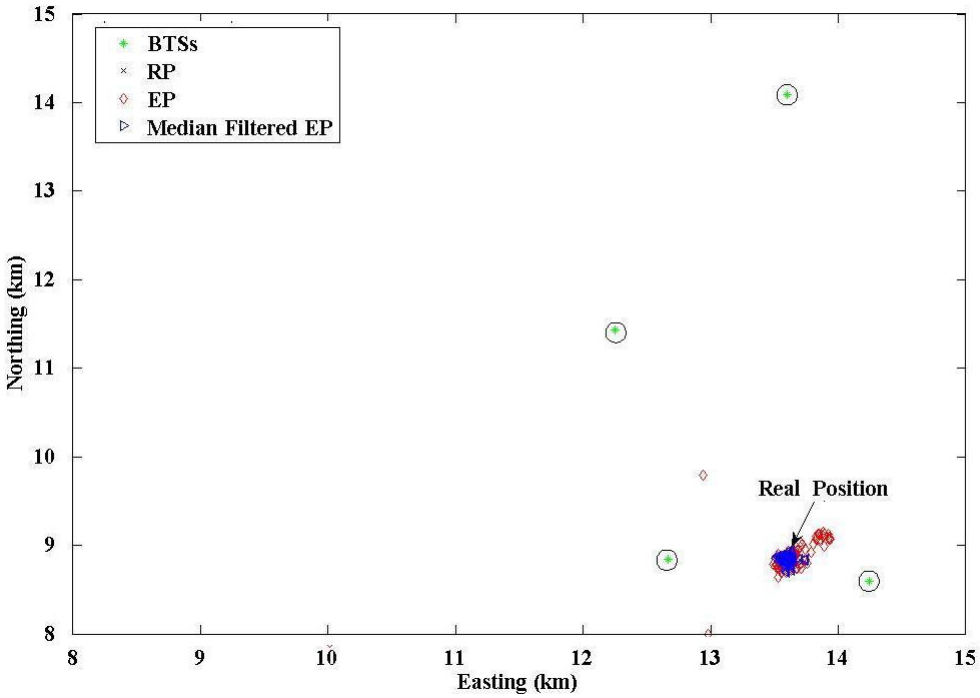

Figure 6.10: Scatter plot – Pseudoranges obtained by MUSIC pseudo spectrum

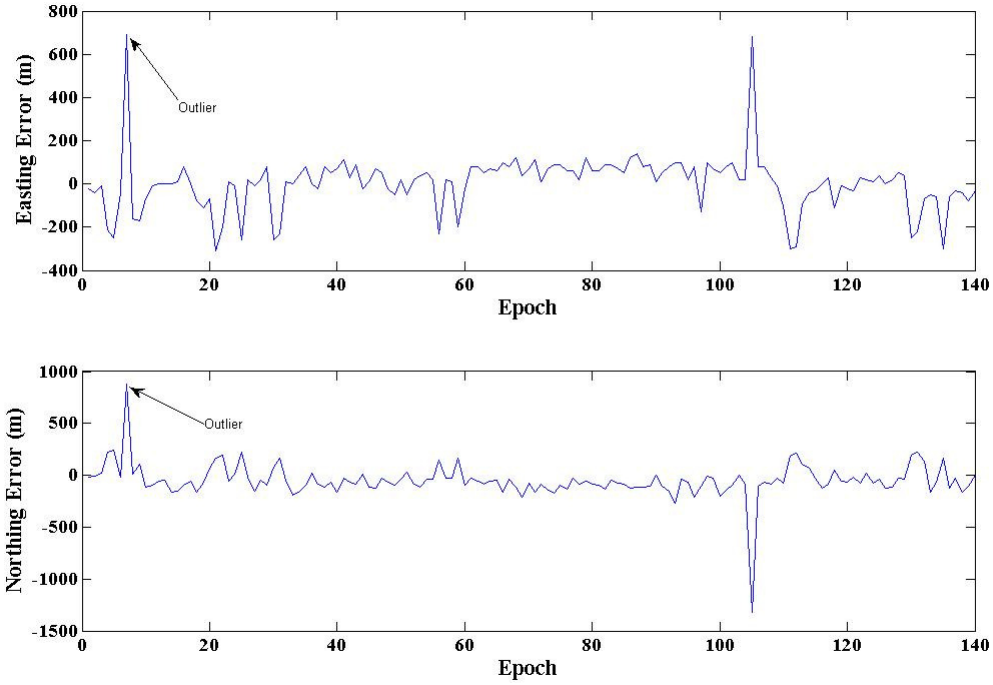

Figure 6.11: Easting and Northing errors (MUSIC)

For a better understanding of the pinpointed outlier origin, Figure 6.12 shows estimated pseudoranges using MUSIC for different BTSs involved in the position fix procedure.

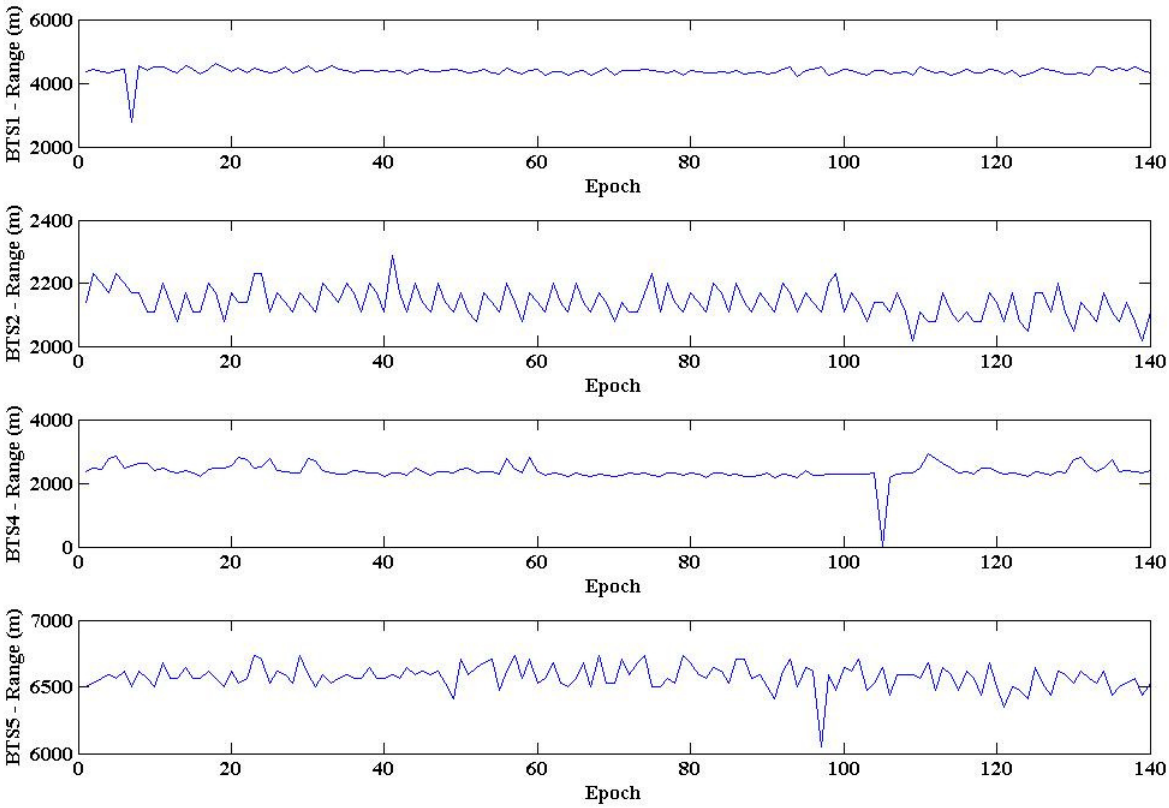

Figure 6.12: Estimated ranges for different BTSs (MUSIC)

The source of the outliers shown can be associated with the false alarm condition in the estimated range of BTS1. Figure 6.13 shows the delay profile corresponding to the outlier epoch of BTS1.

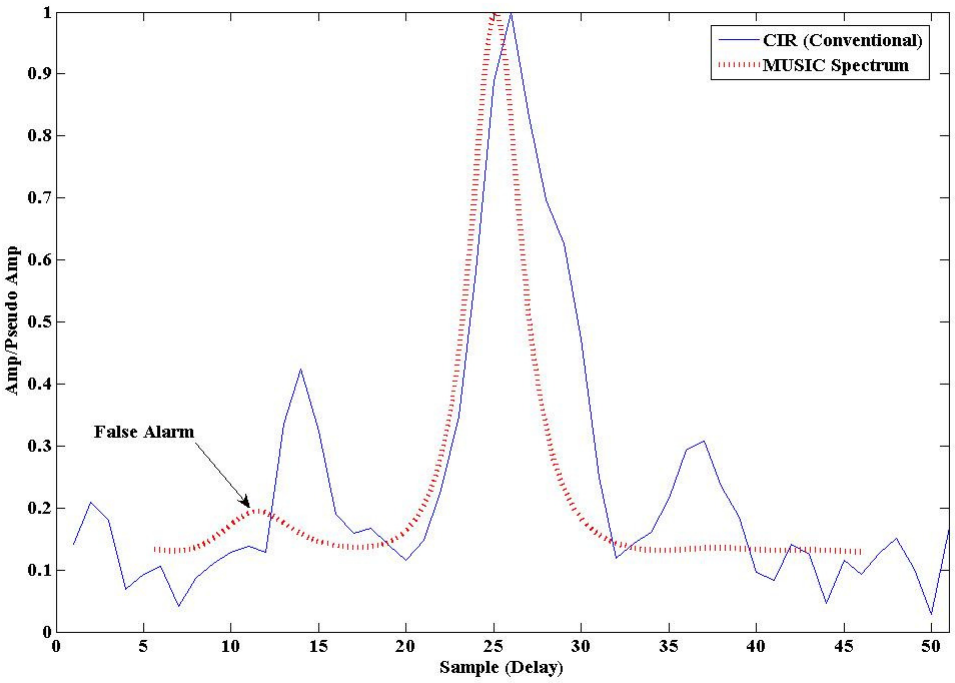

Figure 6.13: False detection of LOS component

As can be seen, there is a false local peak which passes the threshold of 0.2 set for detecting the LOS component and effectively causes an outlier to form in the estimated range. Other outliers are also observable from Figure 6.12 for different epochs and different BTSs. After removing outliers using a median filter, the easting error mean and STD are 6 m and 86 m, respectively, and the northing error mean and STD are -59 m and 88 m, respectively.

Figure 6.14 shows histograms of easting and northing errors after removing outliers. A histogram illustrates the statistical distributions for the errors.

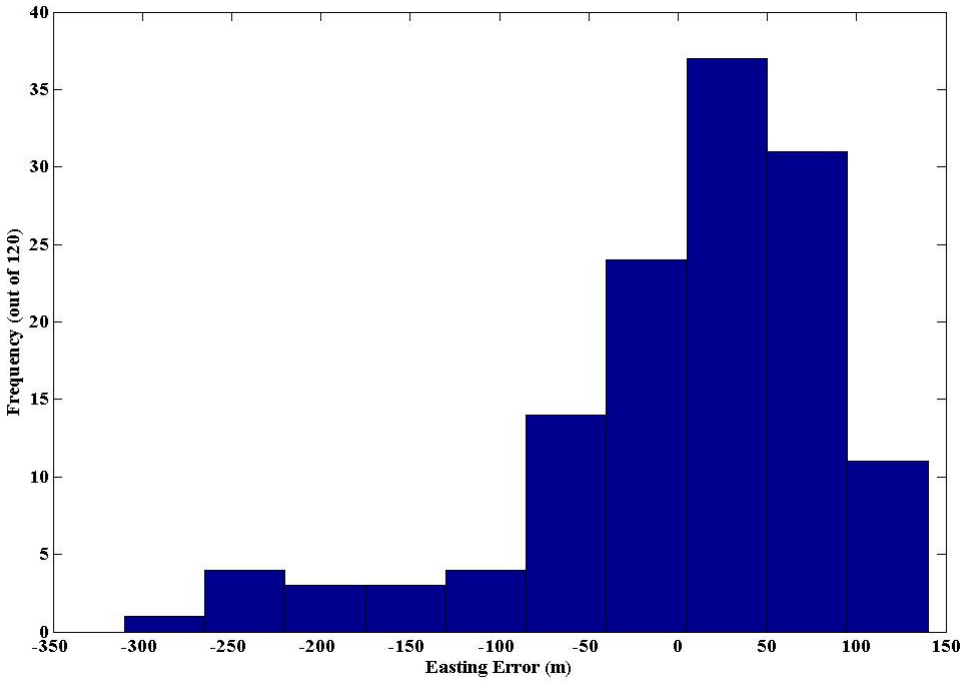

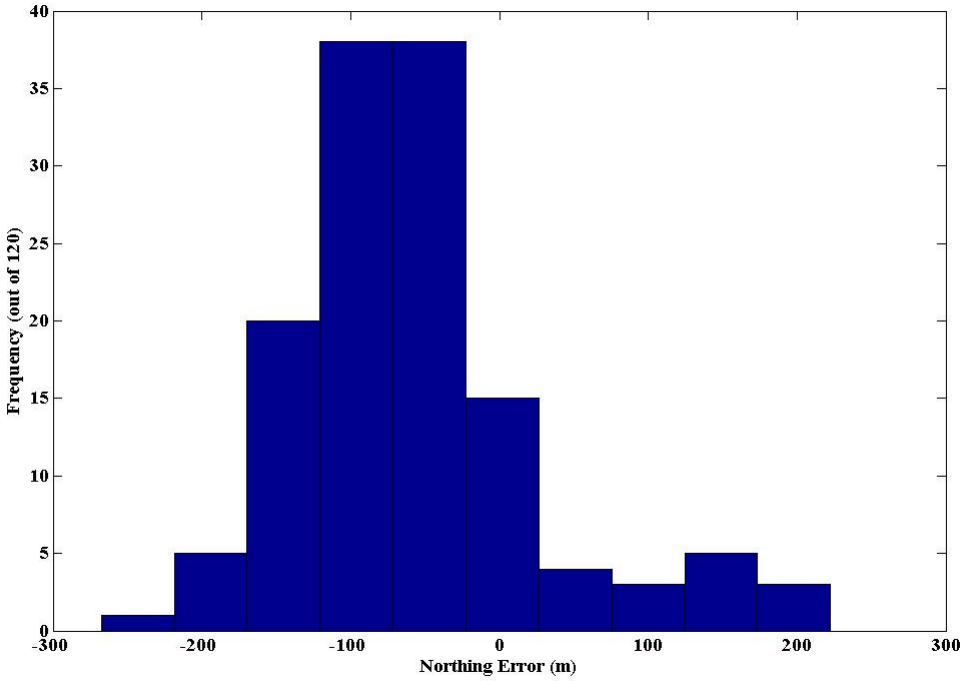

Figure 6.14: Easting and northing error distribution (MUSIC)

The histograms in Figure 6.14 may suggest a Gaussian distribution for easting and northing positioning errors for MUSIC. The central-limit-theorem (CLT) intuitively could predict these behaviours. However, due to the non-linearity in the MUSIC pseudospectrum expression, it may not be obvious and may require additional statistical work which is beyond the scope of this thesis.

6.4 Space-Time MUSIC

It was mentioned that MUSIC assumes independent signal components in its derivation in order to resolve them. Spatial smoothing and the FB method for covariance matrix estimation assist in achieving this goal because estimation of the correlation matrix using spatial smoothing and FB has an intrinsic decorrelation effect. The decorrelation effects in the forward and forward-backward correlation matrices were analyzed in Xinrong and Pahlavan (2004). It can be proved (Reddy, et al., 1987) that in the forward correlation matrix estimation method (spatial smoothing), given a two-source model, the correlation coefficient between $\alpha_i^{'}$ and $\alpha_j^{'}$ (i.e., the *i*th and *j*th element of $\boldsymbol{a}$ in Equation (6.5)) can be derived as:

$$\rho_{ij}^{(FCM)} = \frac{A_{ij}}{\sqrt{A_{ii}A_{jj}}} = Ke^{-j\phi} \tag{6.24}$$

where, A_{ij} is the *(i,j)*th element of the parameter correlation matrix, *A*:

$$A_{ij} = E\left\{\alpha_i^{'}\alpha_j^{'*}\right\} = \alpha_i\alpha_j^{*}e^{-j2\pi f_0\left(\tau_i-\tau_j\right)}e^{-j\pi(M-1)\Delta f\left(\tau_i-\tau_j\right)} \times \frac{\sin\left(M\pi\Delta f\left(\tau_i-\tau_j\right)\right)}{M\sin\left(\pi\Delta f\left(\tau_i-\tau_j\right)\right)} \tag{6.25}$$

and also $A_{ii} = \left|\alpha_i\right|^2$. Hence;

$$K = \frac{\sin\left(M\pi\Delta f\left(\tau_i-\tau_j\right)\right)}{M\sin\left(\pi\Delta f\left(\tau_i-\tau_j\right)\right)} \tag{6.26}$$

$$\phi = -\left(\theta_i-\theta_j\right) + 2\pi f_0\left(\tau_i-\tau_j\right) + \pi(M-1)\Delta f\left(\tau_i-\tau_j\right)$$

Similarly, the correlation coefficient of the forward-backward estimation method can be derived as:

$$\rho_{ij}^{(FBCM)} = K\cos\left(\phi+\frac{\psi}{2}\right)e^{j\psi/2} \tag{6.27}$$

where

$$\psi = 2\pi(L-1)\Delta f\left(\tau_i-\tau_j\right) \tag{6.28}$$

6.4.1 Space-Time MUSIC Derivation

It is inferred that the decorrelation effects of the forward estimation method are a function of the number of segments *M*, the frequency sampling interval *Δf,* and time-delay

difference $(\tau_i - \tau_j)$ between components. Figure 6.15 shows the correlation coefficient for a nominal case, $\Delta f = 1MHz$ and $\tau_i - \tau_j = 15ns$.

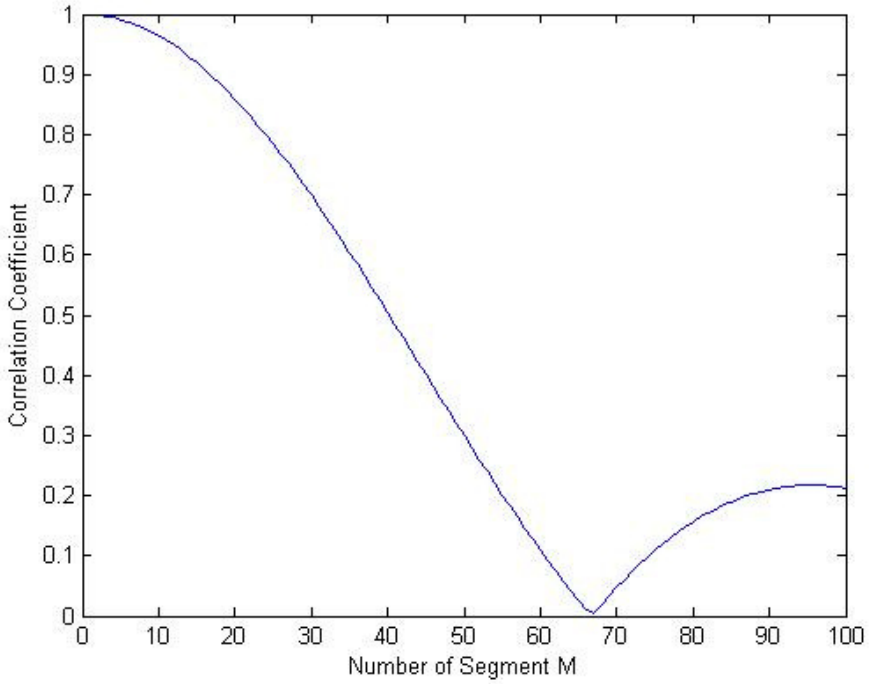

Figure 6.15: Correlation coefficient of FCM

For the forward-backward estimation method, in addition to the aforementioned parameters, the length of the segments *L*, phase difference of parameters $(\theta_i - \theta_j)$, and the lowest frequency of the spectrum, f_0, also affect the correlation coefficient behaviour. It can be shown that:

$$\left|\rho_{ij}^{(FBCM)}\right| = \left|\rho_{ij}^{(FCM)}\right| \times \left|\cos\left(\phi + \frac{\psi}{2}\right)\right| \tag{6.29}$$

Equation (6.29) implies that FBCM has better decorrelation effects than FCM because the *cos* term attenuates the $\rho_{ij}^{(FCM)}$ counterpart. Fundamentally, the correlation coefficients in correlation matrix *A* determine the characteristics of the MUSIC pseudospectrum and corresponding eigenvector values. These characteristics have direct impact on resolvability of the components. Because MUSIC assumes independence among different components, any attempt (in coherent scenarios) to make this assumption more valid can eventually increase the performance and applicability of the MUSIC in resolving multipath with a lower amount of bias. More succinctly, the more diagonalized *A* is, the less correlation in the subspace domain, the better resolvability of the components, and also the less smearing of the resolved components by each other. The space-time paradigm can help to achieve the independence assumption by introducing observations with independent parameters. The fundamental reason for *why* space-time MUSIC works, and *how* it must be implemented to work is explained here.

Equation (6.24) stresses that in addition to the aforementioned parameters used in determining the amplitude of the correlation coefficient (e.g., *M*, *Δf,* and $\tau_i - \tau_j$ in the forward method), there is a phase term, $e^{-j\phi}$, which depends on phase difference $(\theta_i - \theta_j)$ and also the fundamental frequency, f_0. These parameters implicitly bring some degrees of freedom which can be diversified using diversity techniques (i.e., frequency, space and time). The diversities take advantage of the random nature of a radio propagation channel by finding and combining independent signal paths. Combining the covariance matrices corresponding to each finger of diversity can asymptotically lead to a diagonal covariance matrix which is favourable in MUSIC.

The underlying assumption concerning the radio propagation channel is that the time delay for each path and the number of signal paths are the same from the transmitter to all diversity fingers of the receiver. This restricts the diversity technique to only quasistationary scenarios, where the channel remains unchanged during data collection in different fingers.

If $A_{ij}^{d}, d = 1,2,...,D$ is the *(i,j)*th element of the correlation matrix for the *d*th branch of diversity fingers, averaging correlation matrixes among different fingers can make off-diagonal elements of the resultant correlation matrix asymptotically approach zero. This occurs regardless of the coherence among different components and regardless of the scheme for estimating the covariance matrix (i.e., forward or forward-backward) in each individual finger. For example, if A^{d} is the correlation matrix corresponding to the *d*th branch of diversity, its *(i,j)*th element, A_{ij}^{d}, can be estimated from the forward method as:

(6.30)

$$A_{ij}^{d} = E\left\{\alpha_i'^{d}\alpha_j'^{d*}\right\} = \alpha_i^{d}\alpha_j^{d*}e^{-j2\pi f_0^{d}\left(\tau_i-\tau_j\right)}e^{-j\pi(M-1)\Delta f\left(\tau_i-\tau_j\right)}\times\frac{\sin\left(M\pi\Delta f\left(\tau_i-\tau_j\right)\right)}{M\sin\left(\pi\Delta f\left(\tau_i-\tau_j\right)\right)}$$

Given coherent combining of covariance matrices corresponding to all different branches, the smoothed-enhanced covariance matrix has the following property:

$$A_{ij} = \frac{1}{D}\sum_{d=1}^{D}A_{ij}^{d} = e^{-j\pi(M-1)\Delta f\left(\tau_i-\tau_j\right)}\times\frac{\sin\left(M\pi\Delta f\left(\tau_i-\tau_j\right)\right)}{M\sin\left(\pi\Delta f\left(\tau_i-\tau_j\right)\right)}\sum_{d=1}^{D}\alpha_i^{d}\alpha_j^{d*}e^{-j2\pi f_0^{d}\left(\tau_i-\tau_j\right)} \qquad (6.31)$$

where,

$$\alpha_i^d = \left|\alpha_i^d\right| e^{j\theta_i^d} \quad i = 0,1,...,L_p - 1 \;;\; d = 1,2,...,D \tag{6.32}$$

Equation (6.31) can be expressed as Equation (6.33) by:

$$A_{ij} = F\left(M, \Delta f, \tau_i - \tau_j\right) U\left(\overline{\alpha}_i, \overline{\alpha}_j, \bar{f}_0, \tau_i - \tau_j\right) \tag{6.33}$$

where

$$\begin{aligned} \overline{\alpha}_i &= \left[\alpha_i^1 \alpha_i^2 ... \alpha_i^D\right] \\ \bar{f}_0 &= \left[f_0^1 f_0^2 ... f_0^D\right] \end{aligned} \tag{6.34}$$

If the time delay for each path and the number of signal paths are the same from the transmitter to all diversity fingers of the receiver, then given a large diversity order (i.e., $D >> 1$), the diversity gain, *U,* is asymptotically expressed as Equation (6.35).

$$U\left(\overline{\alpha}_i, \overline{\alpha}_j, \bar{f}_0, \tau_i - \tau_j\right) = \frac{1}{D}\sum_{d=1}^{D} \alpha_i^d \alpha_j^{d*} e^{-j2\pi f_0^d (\tau_i - \tau_j)} \approx E\{\alpha_i\} \times E\left\{\alpha_j^*\right\} \times E\left\{e^{-j2\pi f_0 (\tau_i - \tau_j)}\right\} \tag{6.35}$$

It should be emphasized that the equality in Equation (6.35) needs an extra assumption for frequency diversity, i.e., independence of amplitude attenuation, α_i^d, from frequency, f_0^d. This assumption is not necessary when a receiver uses the space-time diversity exploiting signal phase (i.e., θ_i^d) in different fingers.

Equation (6.35) suggests that if different diversity fingers represent realizations of a zero mean process for θ_i or f_o, off-diagonal elements of the covariance matrix tend to approach zero which is favourable.

$$A_{ij} = F(.).U(.) \approx F(.).0 \approx 0 \tag{6.36}$$

6.4.2 Spatial Diversity Realization

Using different antenna elements in the receiver, given the same number of signal paths (i.e., $L_p^d \; d = 1,2,...,D$) and given the same time delay for each path (i.e., $\tau_i^d = 1,2,...,L_p ; d = 1,2,...,D$) in all antenna elements, an observer who watches a given signal path among different antenna elements experiences a signal with random phase. In other words, α_i^d can be conceived as a complex random variable, α_i , with PDFs associated with its amplitude, $|\alpha_i|$, and phase, θ_i , respectively. A uniform PDF for θ_i is reasonable.

$$\theta_i \sim u(0,2\pi) \tag{6.37}$$

Space diversity exploits the phase randomness along different fingers which equivalently makes Equation (6.38) realizable.

$$E\{\alpha_i\} = E\{|\alpha_i|\}E\{e^{j\theta_i}\} = 0 \tag{6.38}$$

Equation (6.38) says that $A_{ij} = 0, \; i \neq j$, which has a desirable impact on the characteristic of the covariance matrix used in the MUSIC.

6.4.3 Temporal Diversity Realization

Using different epochs of a pseudostationary receiver (e.g., a pedestrian walk), given the same number of signal paths and given the same time delay for each path among different epochs, an observer who watches a given signal path during different time epochs, experiences a signal with random phase. In this scenario, the number of diversity fingers increases linearly in time; hence, the assumption $D >> 1$ in Equation (6.35) is satisfied asymptotically as time goes by. It is worthwhile to reemphasize that the number of diversity fingers in a spatial diversity realization is the number of antenna elements. However, in the temporal diversity realization, only one antenna suffices to build the diversity fingers in a pseudostationary scenario. A simultaneous spatial-temporal diversity is also realizable using antenna arrays and a pseudostationary receiver which increases the achievable diversity order. The required assumptions (i.e., the same number of signal paths and the same time delay for each path among different epochs) seem stringent for a high dynamic receiver; however, if the dynamic is not too much and if the receiver is located far afield from the transmitters, the assumption is justifiable.

A mathematical manipulation can be similarly performed for the spatial-diversity scenario which eventually leads to the favourable characteristic: $A_{ij} = 0,\ i \neq j$.

6.4.4 Frequency Diversity Realization

Equation (6.35) implies that the frequency diversity is also realizable to improve the covariance matrix characteristic. Two approaches for frequency diversity realization are: 1) segmenting the frequency response, and 2) using a multi-frequency transceiver.

In the first approach (i.e., segmentation), given the wideband transmitted signal, the estimated frequency response is split into overlapping and non-overlapping segments as different diversity branches, and then the covariance matrix corresponding to each segment is estimated. By combining all estimated covariance matrixes, the $E\left\{e^{-j2\pi f_0(\tau_i-\tau_j)}\right\}$ in Equation (6.35) is invoked with f_0 as a random zero mean process. Again, an observer who watches a given signal path among different segments of the frequency response experiences a signal with random phase. In this scenario, the number of diversity fingers is equal to the number of segments. Imposing a uniform PDF for f_0 of $f_0 \sim u(-F_{Max}, F_{Max})$. It can easily be seen that:

$$E\left\{e^{-j2\pi f_0(\tau_i-\tau_j)}\right\}=0 \tag{6.39}$$

which again leads to $A_{ij}=0,\ i\neq j$.

The second approach in frequency diversity (i.e., using a multi-frequency architecture) requires that the transmitter use multiple carriers in its air interface, and also requires that the receiver use a multiple carrier structure in its front end and demodulator. This is realizable whenever the BTSs transmit CDMA pilot code on different carriers or use frequency diversity oriented modulation (e.g., orthogonal-frequency-division-

multiplexing) for transmitting the pilot code. The frequency diversity in these schemes, again, has the same effect as $A_{ij} = 0,\ i \neq j$ asymptotically.

6.4.5 Field Measurement Results

The following section reports some field data results for positioning using the space-time MUSIC paradigm in the IS-95 CDMA cellular network. The data collection set up (i.e., PLAN prototype hardware as front end and GAGE card as digitizer) was explained in Chapter 4. Space diversity performance is analyzed using four antenna elements and time diversity performance is analyzed using a low dynamic for a single antenna. As the PLAN front end cannot simultaneously demodulate dual carrier content of the IS-95 CDMA signal, and as the signal itself is not of wide enough bandwidth to use the segmentation method, frequency diversity is not investigated in this thesis; although it is worth examining in future work.

Figures 6.16 compares delay profiles of 1) conventional despreading process, 2-) conventional MUSIC, and 3) temporal diversity MUSIC (space diversity is not used arbitrarily), corresponding to different BTSs with the same data set as Subsections 6.3.1 and 6.3.2 of this chapter.

In all delay profiles obtained by space-time MUSIC, the local peaks are more resolvable than conventional correlation techniques and epoch by epoch MUSIC, although there is a possibility for the peaks to be spurious. To verify the authenticity of the peaks, or at least the authenticity of the leading edge as our component of interest, positions are estimated

and then stochastical parameters are compared to the results presented in Subsections 6.3.1 and 6.3.2.

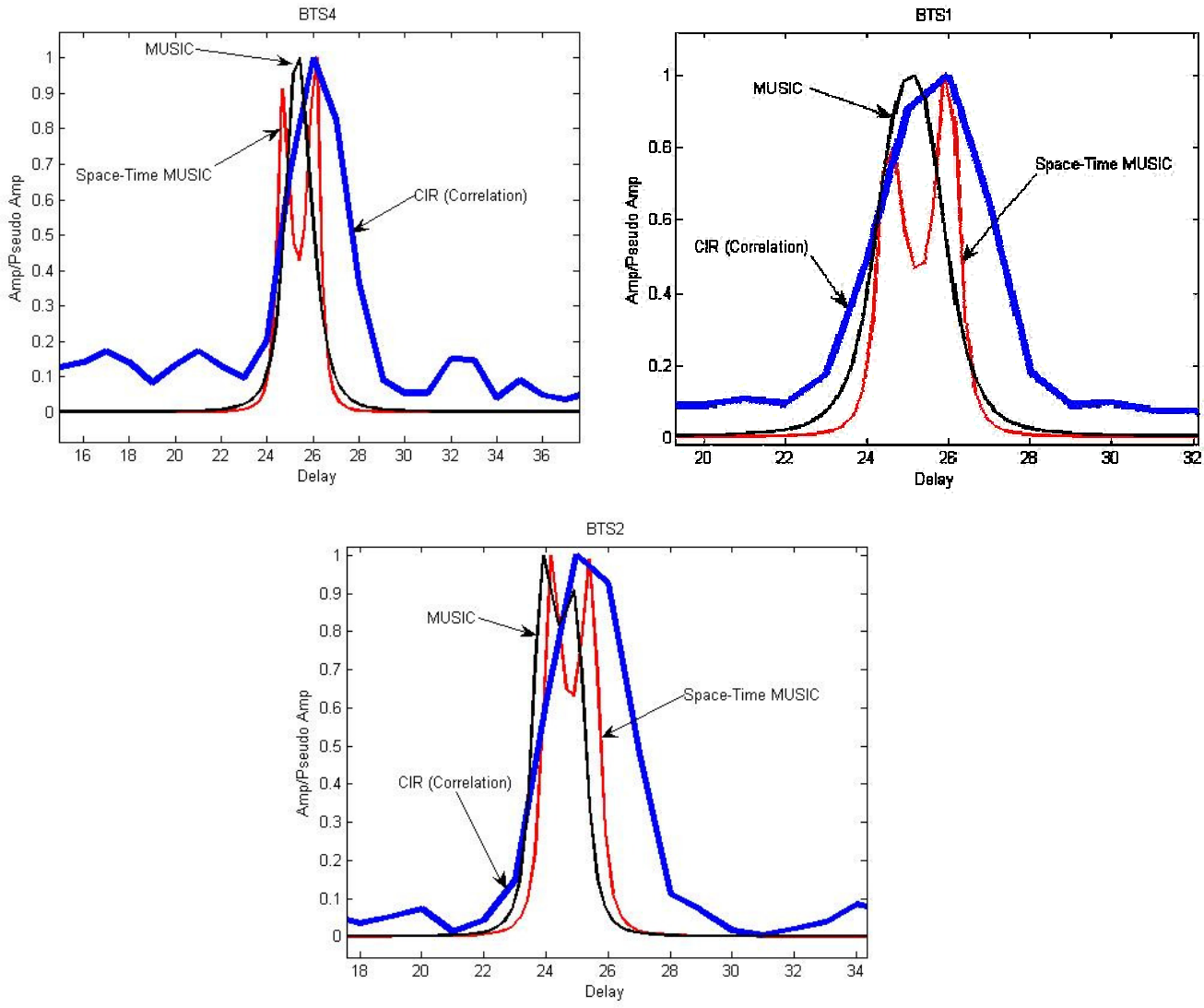

Figure 6.16: Delay profiles by different methods

Figure 6.17 shows the scatter plot corresponding to the same set of IS-95 CMDA field measurements on a roof top (CCIT roof top) for a low dynamic antenna with the speed of

a pedestrian as used in Figure 6.5. Here, the range corresponding to each BTS was derived based on applying a hard threshold to the estimated space-time MUSIC pseudospectrum delay profile and then choosing the first local maximum index having a pseudospectrum value greater than the threshold as the LOS component. It should be emphasized that in this test case, only time diversity was exploited because data corresponding to only one antenna was processed. However, we still call the scenario here by the more general term of space-time MUSIC.

The subarray size, number of subarrays, number of multipath components, and the zero padding factor applied to the original CIR window with size 51 are all similar to Subsection 6.3.2 and have values of 30, 124, 4 and 2, respectively.

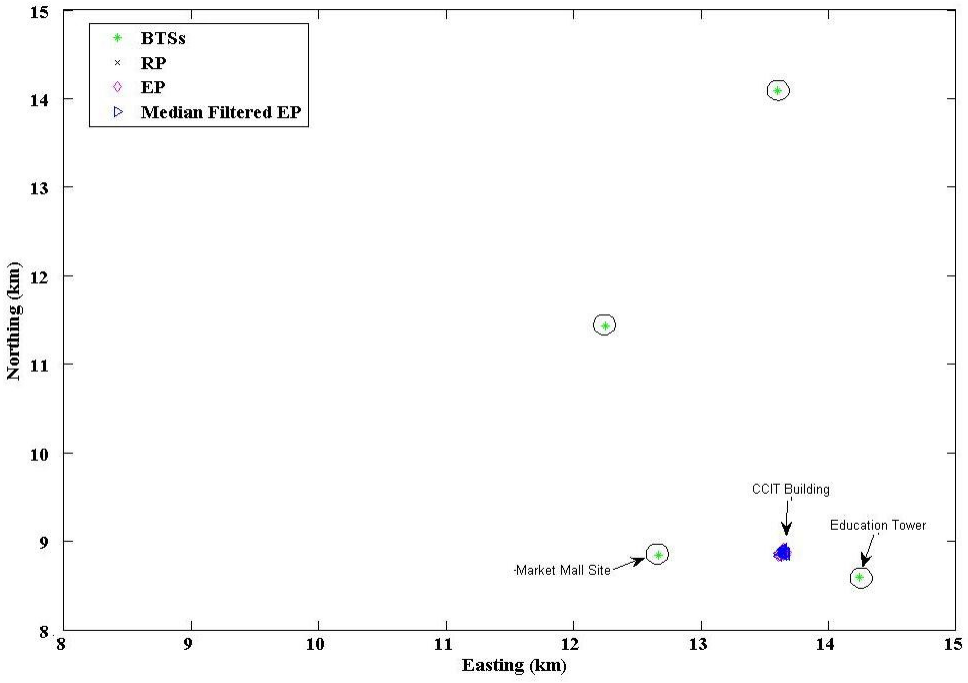

Figure 6.17: Scatter plot – Pseudoranges obtained by space-time MUSIC pseudospectrum

Performance improvement is apparent, as the estimated points are more clustered than Figure 6.5 and 6.10. Figure 6.18 illustrates the space-time MUSIC easting and northing positioning errors for different epochs.

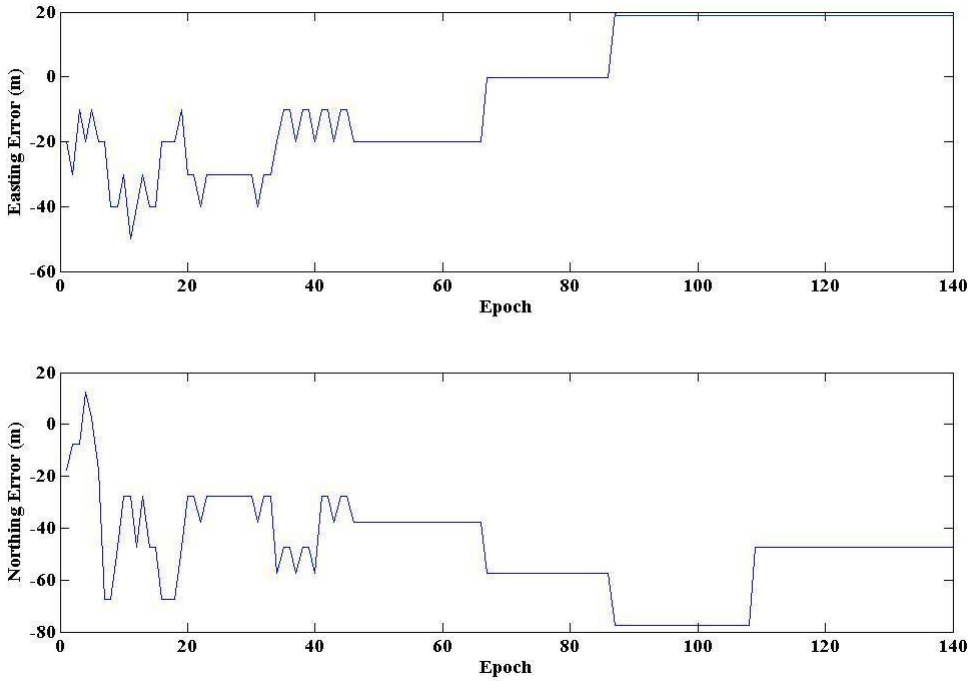

Figure 6.18: Easting-northing errors (space-time MUSIC)

It can be observed from Figure 6.18 that there is no substantial outlier in the ensemble. This implies that the space-time MUSIC pseudospectrum is more robust (i.e., has fewer false alarms) than the conventional MUSIC results shown in Figure 6.11 and the conventional despreading process. Figure 6.19 demonstrates estimated ranges using space-time MUSIC for different BTSs.

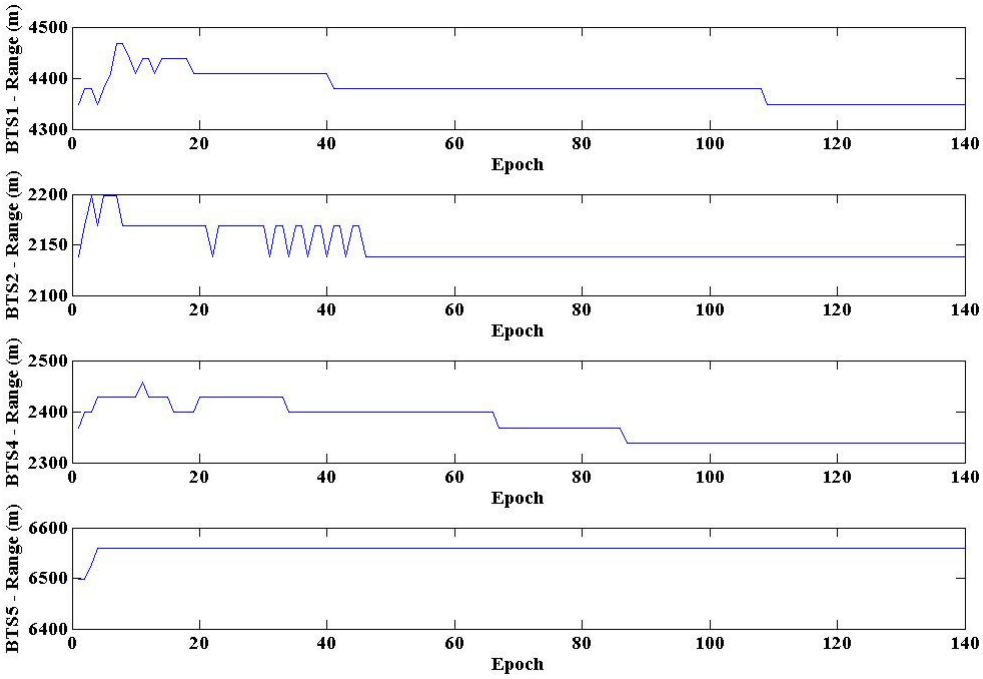

Figure 6.19: Estimated ranges for different BTSs (space-time MUSIC)

In Figure 6.19, it can be seen that the false alarm corresponding to BTS1 in Figure 6.12 does not exist in the space-time MUSIC delay profiles.

The easting-error mean and STD are -6 m and 18 m, respectively, and northing-error mean and STD are -46 m and 15 m, respectively. Although there is no necessity to use a median filter here, for the sake of fairness in terms of numbers of data sets used in Subsections 6.3.1 and 6.3.2, a median filter is applied to the ensemble .

Apparently, in this test case, there is a significant improvement in terms of estimation consistency (i.e., variance) compared to the traditional despreading technique and the

traditional MUSIC. In terms of estimation fidelity (i.e., bias), there is no substantial improvement compared to conventional MUSIC. Nevertheless, there is substantial improvement in terms of reliability of the detection, as there is no outlier in the estimation. Table 6.1 compares easting and northing error mean and STD for the conventional despreading technique, conventional MUSIC technique, and the space-time MUSIC technique.

Table 6.1: Easting-Northing Error Statistics

		Mean (m)	STD (m)
Conventional Despreading	Easting	55	56
	Northing	-114	79
MUSIC	Easting	6	86
	Northing	-59	88
Space-Time MUSIC	Easting	-6	18
	Northing	-45	15

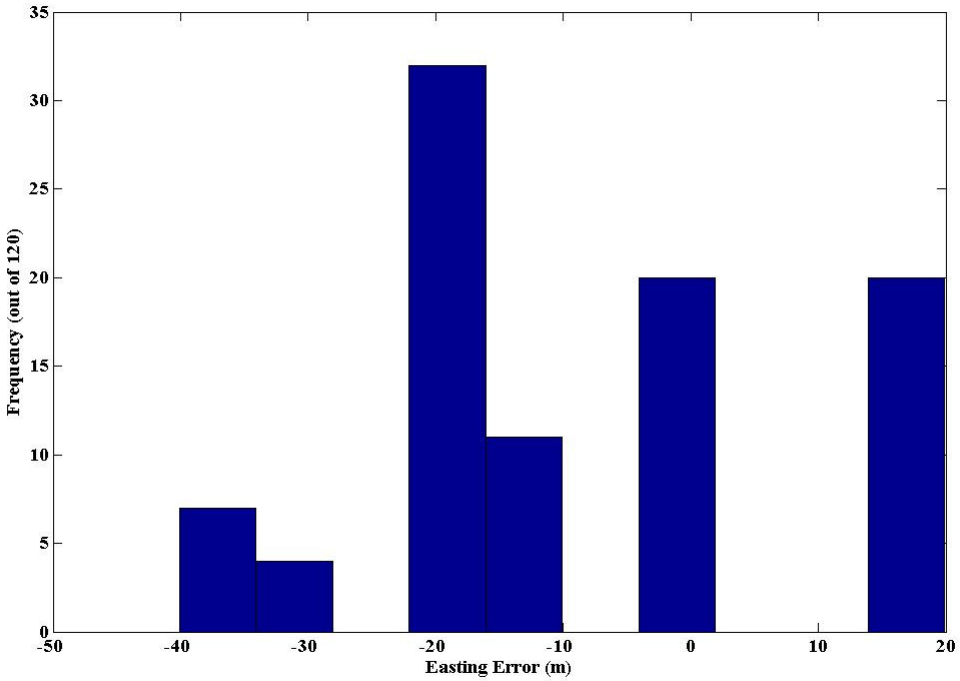

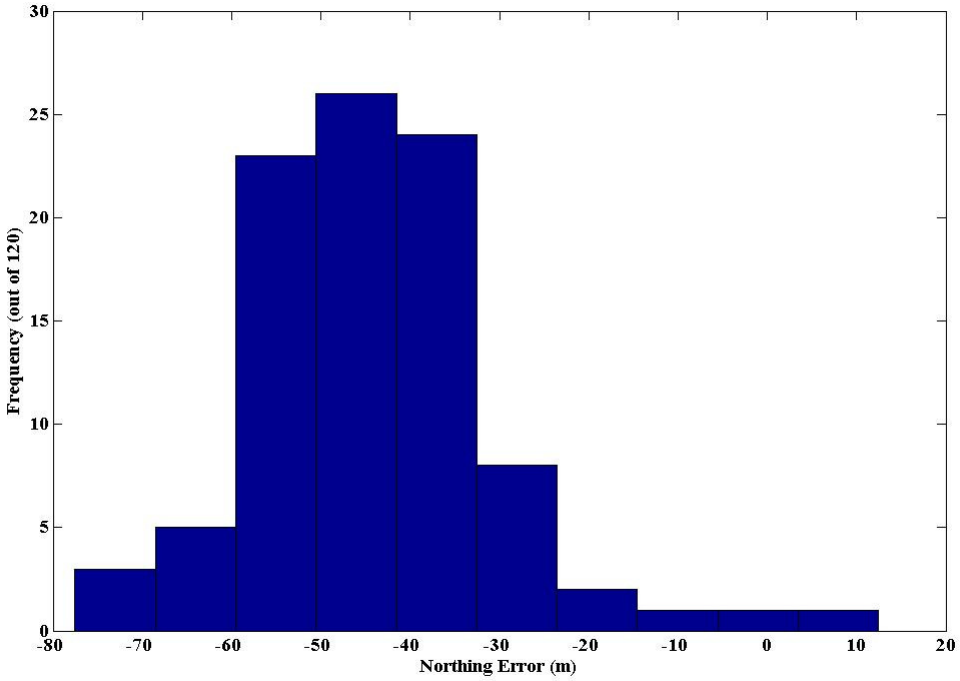

Figure 6.20: Easting-northing error distribution (space-time MUSIC)

Figure 6.20 depicts a histogram of easting and northing errors. Contrary to the easting, the histogram for northing suggests a Gaussian distribution for positioning error. This is likely due to multipath, which favours the easting component in this specific test case. In the following, another IS-95 CDMA field data set is analyzed and compared thoroughly for different scenarios.

6.5 Performance Comparison

Figure 6.21 shows the BTSs constellation and measurement point for an outdoor field data set. Since the data collection was set up on a parking lot on the University of Calgary campus with foliage surrounding it, some base stations were possibly compromised by detrimental multipath effects due to the NLOS channel. Received signals included IS-95 pilot signals corresponding to five different sites with dual reception from two different sectors of the "University of Calgary Education Tower" site. Therefore, six independent measurements were extractable from the received signal.

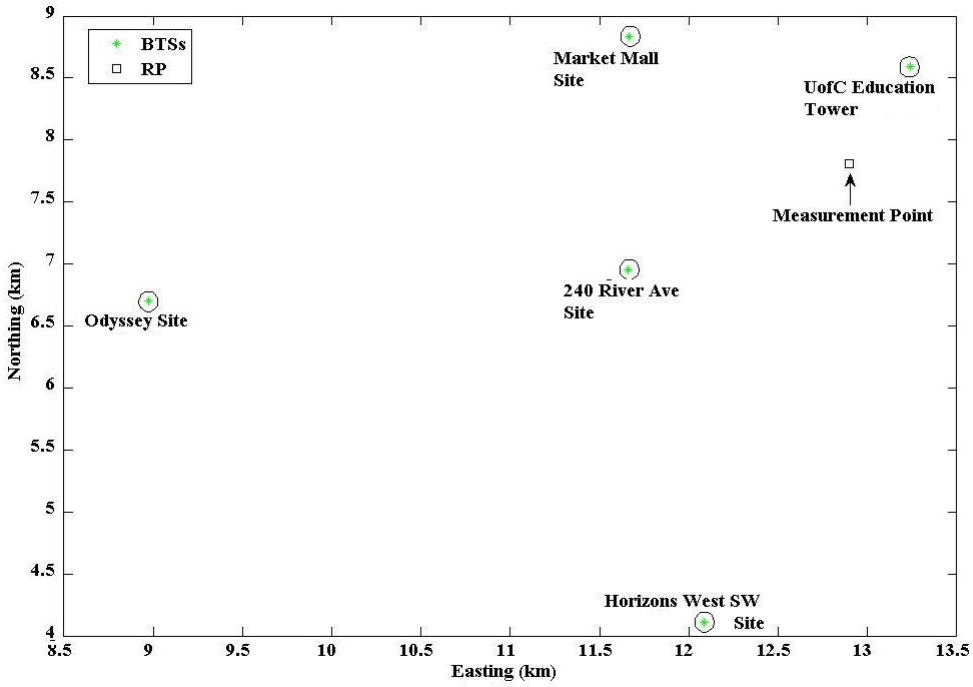

Figure 6.21: Measurement configuration

Two different raw data sets were collected corresponding to spatial and temporal analyses. In one data set, four antenna elements captured space diversity measurements during 3.25 seconds in static mode. In the second data set, a single antenna captured time diversity measurements in a very low dynamic (antenna arrays were placed on a Van's roof with a speed of less than 5 m/s) around the same point as the static case. Figure 6.22 shows the data collection set up during measurement.

Figure 6. 22: Data collection set up

The received signals in different antennas are despread with one full PRN period integration time (i.e., 26.7 ms) for estimating CIRs corresponding to different BTSs and antennas.

Figures 6.23, 6.24, 6.25, and 6.26 show the BTS availability status corresponding to six independent code offsets for different antenna elements in the static data set. Figure 6.27 shows the BTS availability status corresponding to six independent code offsets in the low dynamic data set. The measure for availability (i.e., value 1) is the signal strength of a given BTS. Signal amplitude corresponding to the first epoch for a given BTS is set as the reference level. If the amplitude is degraded by 50% relative to the reference level, a not available status (i.e., value 0) is broadcast.

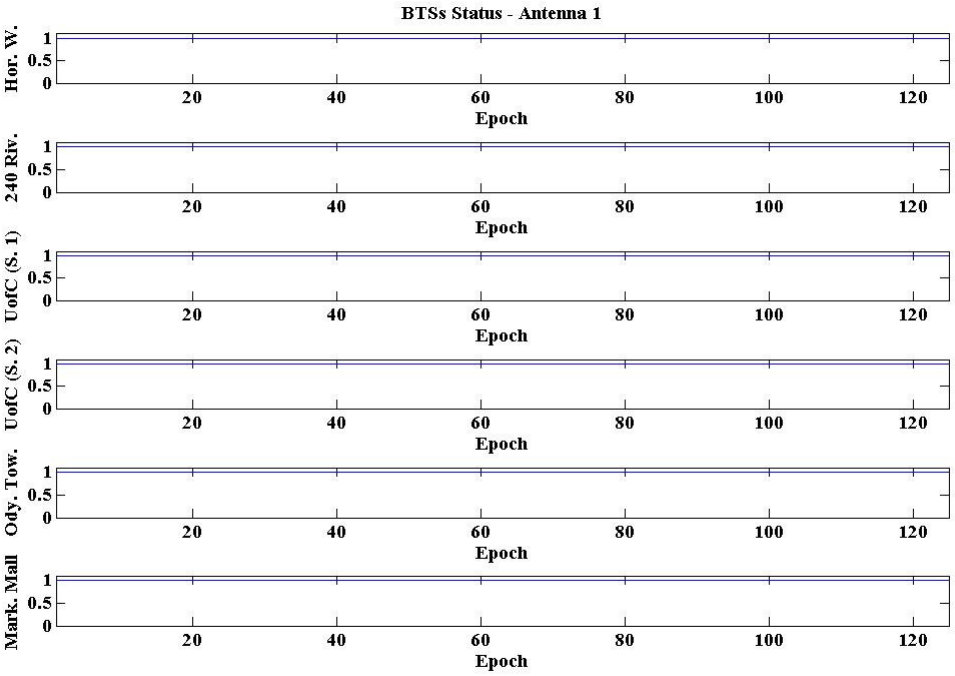

Figure 6.23: BTS availability – Antenna 1 (static)

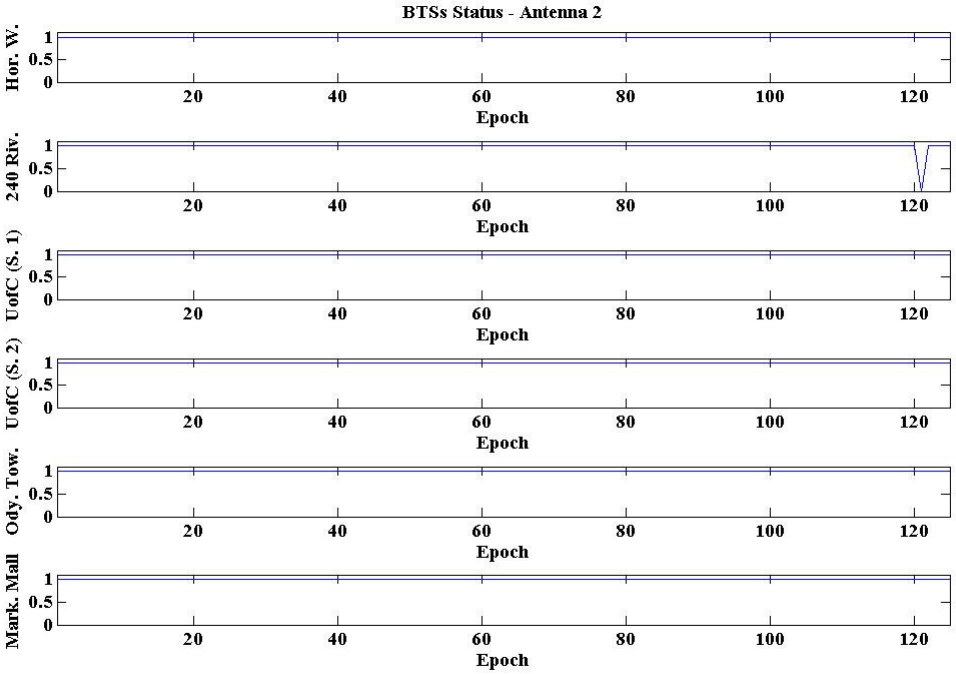

Figure 6.24: BTS availability – Antenna 2 (static)

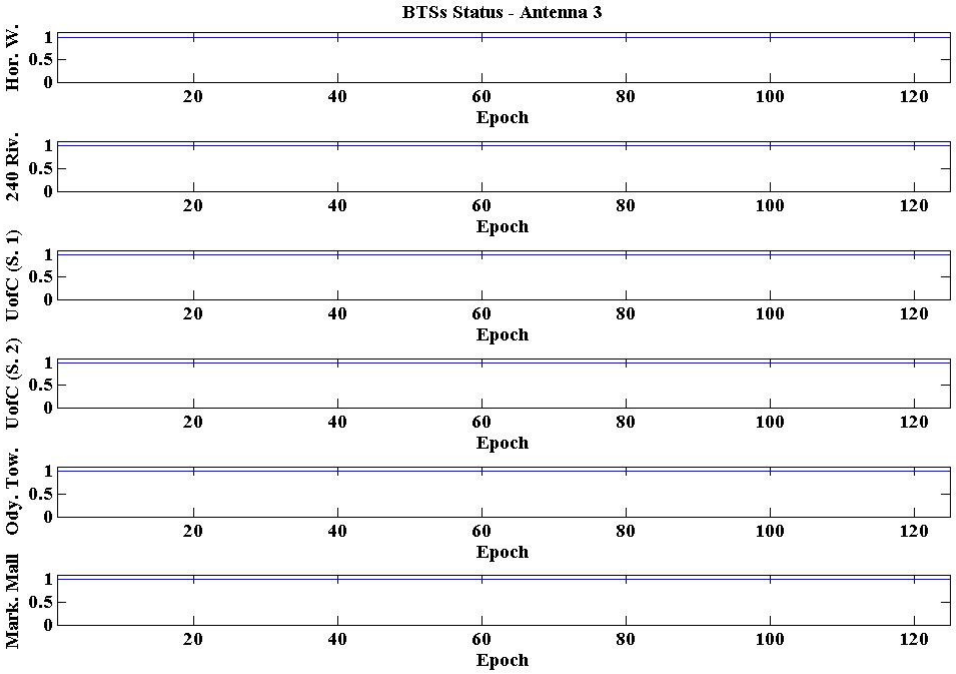

Figure 6.25: BTS availability – Antenna 3 (static)

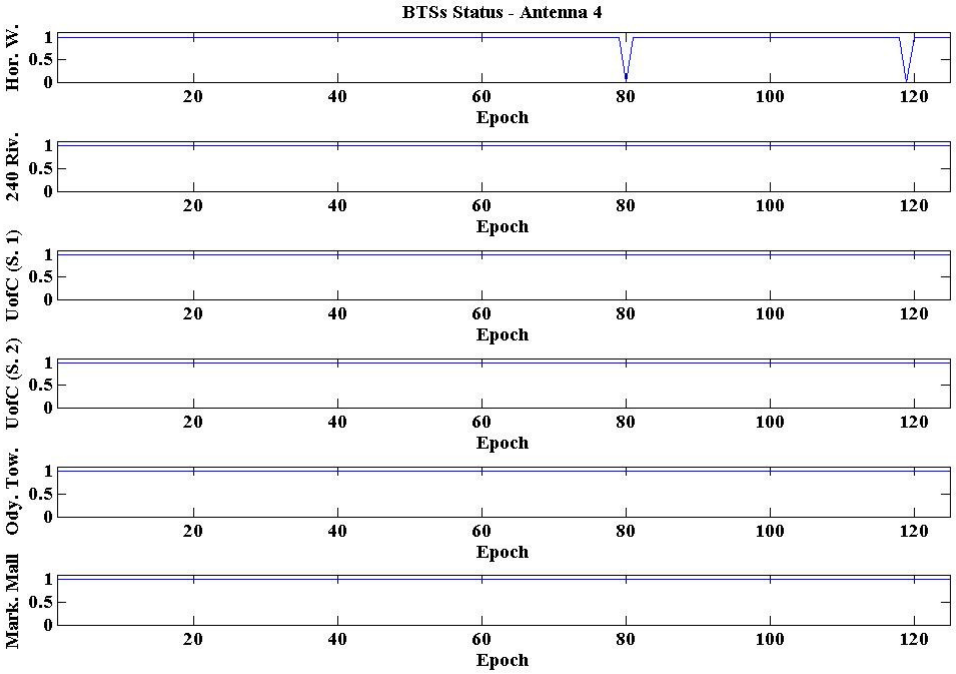

Figure 6.26: BTS availability – Antenna 4 (static)

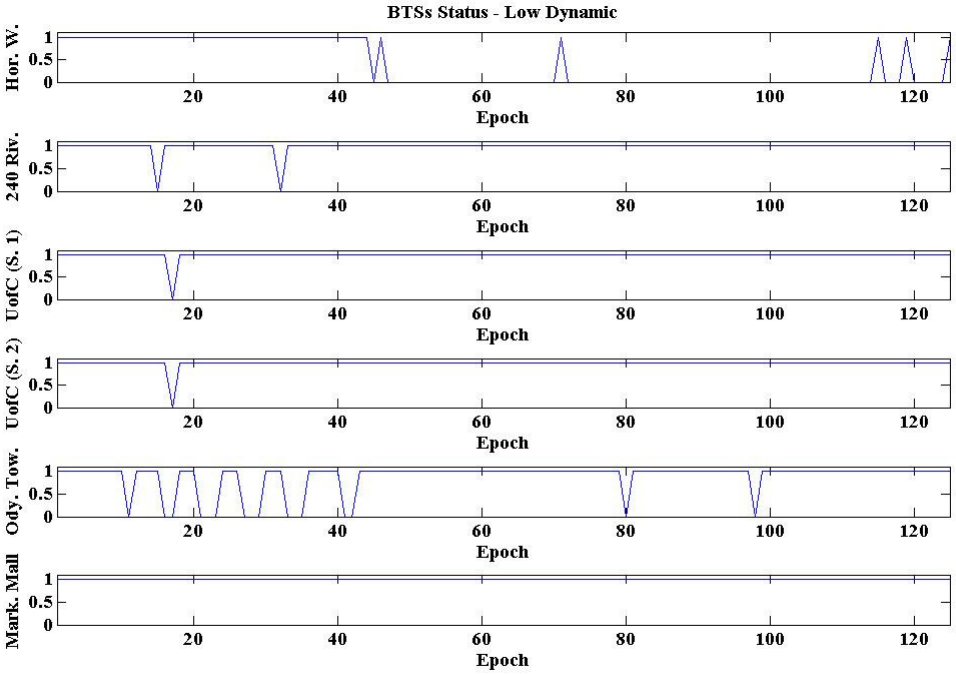

Figure 6.27: BTS availability – Antenna 1 (low dynamic)

The BTS status figures are useful for analyzing possible outliers caused by the false alarm condition in the estimation ensemble.

In the following, positioning statistics and performance curves for different scenarios are shown and analyzed. The pseudorange estimation technique and measurement mode is categorized by 12 scenarios:

1- Conventional despreading process applied to antenna 1 (static)
2- Conventional despreading process applied to antenna 2 (static)
3- Conventional despreading process applied to antenna 3 (static)
4- Conventional despreading process applied to antenna 4 (static)
5- Conventional MUSIC applied to antenna 1(static)
6- Conventional MUSIC applied to antenna 2 (static)
7- Conventional MUSIC applied to antenna 3 (static)
8- Conventional MUSIC applied to antenna 4 (static)
9- MUSIC with spatial diversity using antennas 1 and 2 (static)
10- MUSIC with spatial diversity using antennas 1, 2, and 3 (static)
11- MUSIC with spatial diversity using antennas 1, 2, 3, and 4 (static)
12- MUSIC with temporal diversity using antenna 1 (pseudostatic)

Figure 6.28 shows a histogram for easting and northing error after fixing position using conventional despreading for pseudorange estimation along different BTSs and antennas

individually (Scenarios 1, 2, 3, and 4). Figure 6.29 shows a histogram for easting and northing error after fixing position using the MUSIC pseudospectrum for pseudorange estimation along different BTSs and antennas individually (Scenarios 5, 6, 7, and 8).

Figure 6.30 shows a histogram for easting and northing error after fixing position using the space-time MUSIC pseudospectrum for pseudorange estimation along different BTSs and different combinations of antenna elements in static mode as well as a single antenna in low dynamic mode (Scenarios 9, 10, 11, and 12).

Consistently, the estimation variance for both MUSIC approaches is less than the conventional despreading process. Between space-time MUSIC and conventional MUSIC, the former also shows lower estimation variance. In general, the higher the diversity order, the lower the estimation variance.

In terms of estimation bias, the results are not fully consistent. Nevertheless, it seems that the bias in the MUSIC approaches tends to be lower in most cases. In order to make a firm conclusion in terms of estimation bias, a comprehensive campaign under different circumstances with more field data is needed. In the MUSIC technique, there is also an intrinsic bias issue explained in Subsection 6.2.4. The bias depends on SNR and number of multipath. As the system was not precisely calibrated for different antennas, the bias can potentially be different in different antennas. The number of multipath was also fixed for different BTSs, which is not optimal in terms of the MUSIC pseudospectrum.

Among the space-time MUSIC scenarios, the temporal MUSIC (Scenario 12) showed the best overall performance in terms of bias and variance.

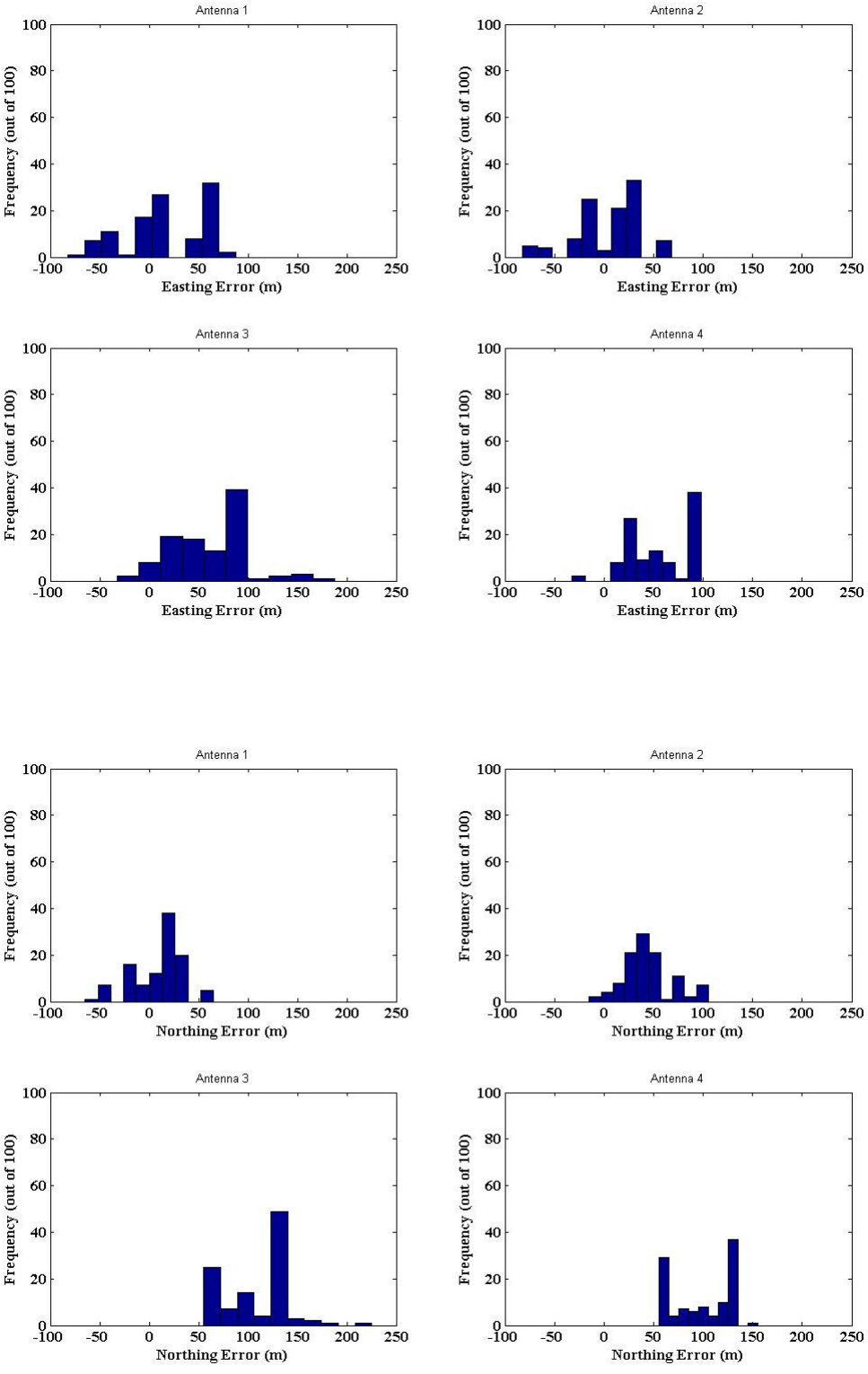

Figure 6.28: Easting-northing error distribution (conventional despreading)

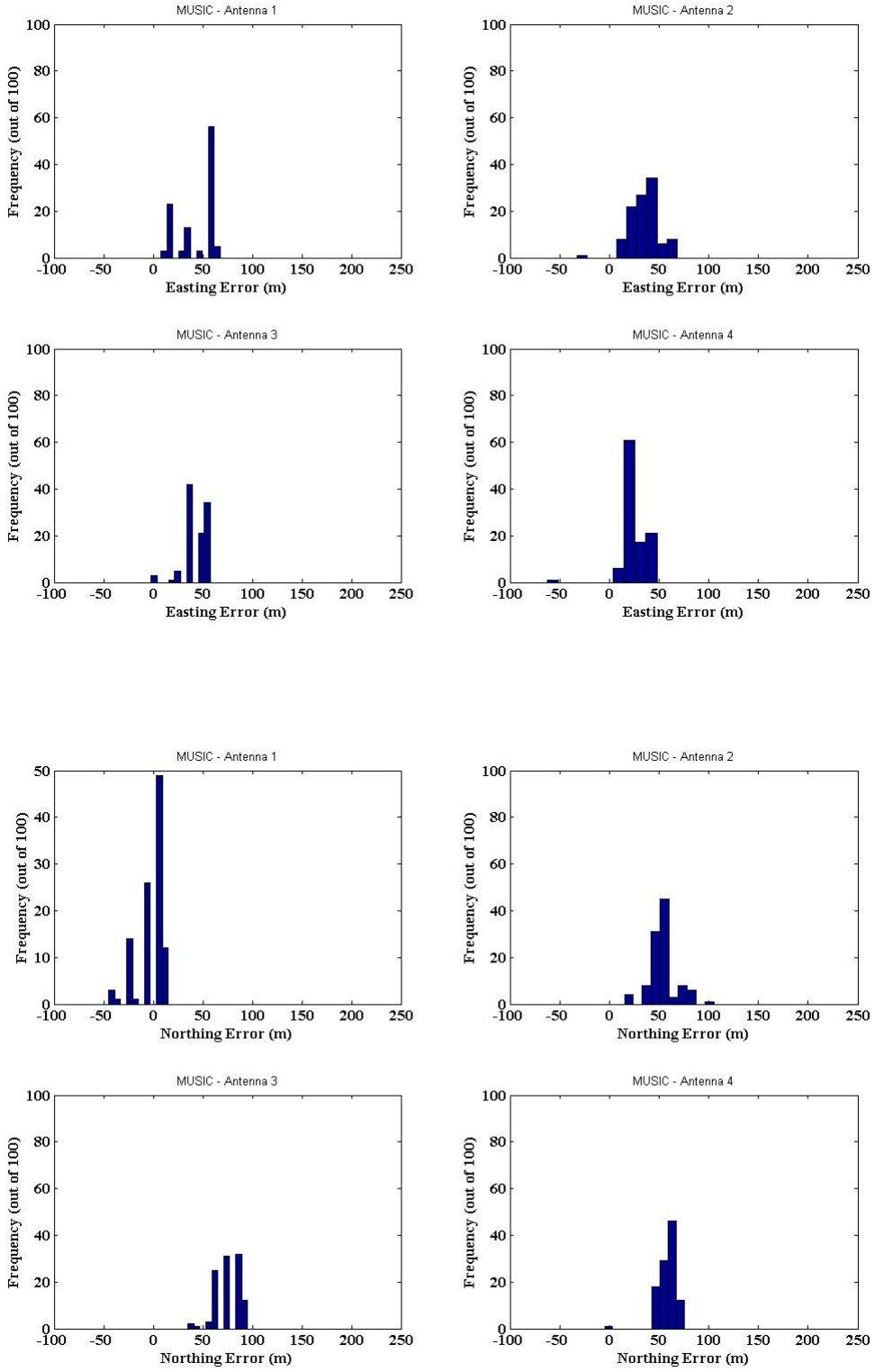

Figure 6.29: Easting-northing error distribution (conventional MUSIC)

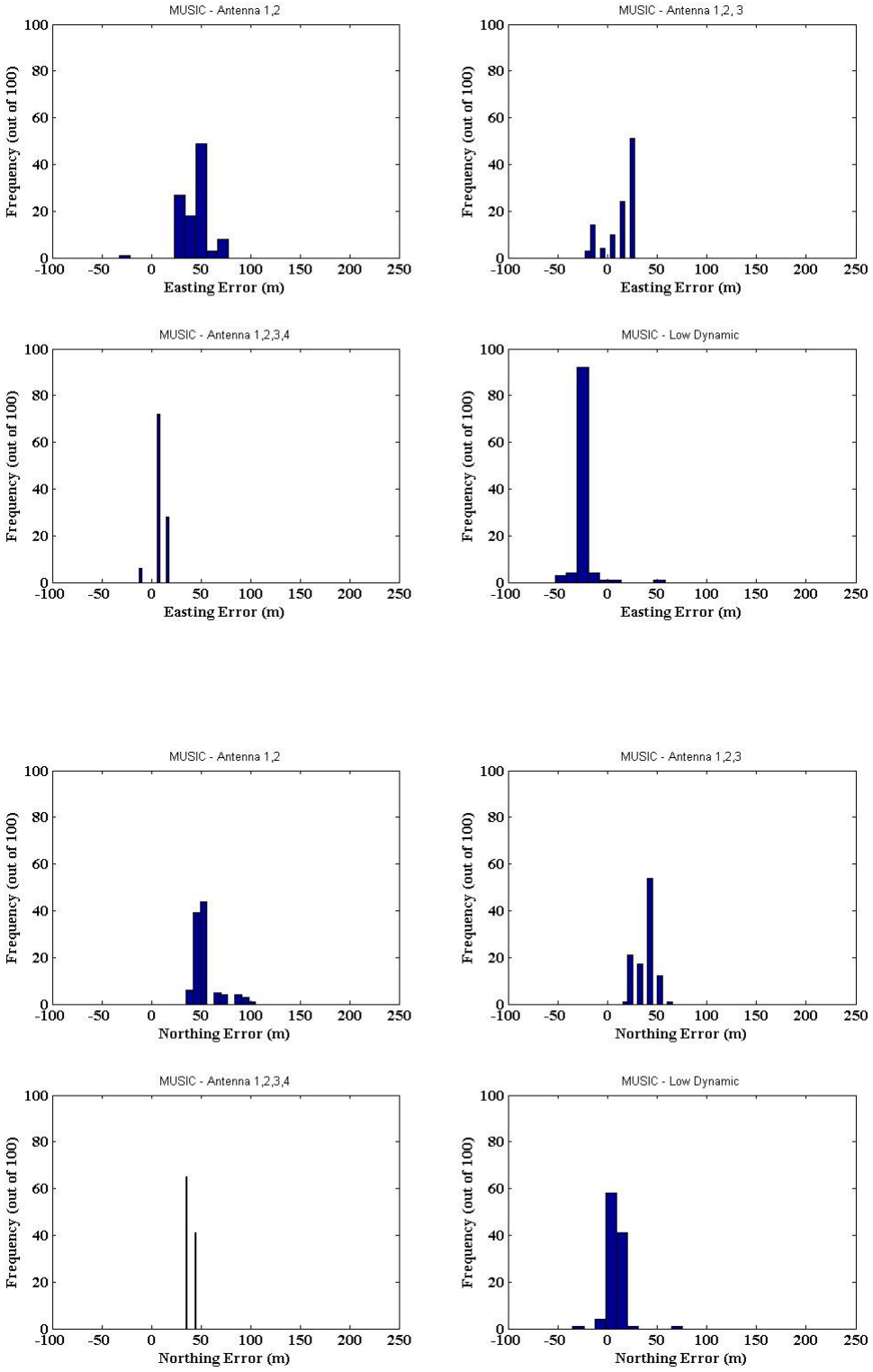

Figure 6.30: Easting-northing error distribution (space-time MUSIC)

Figures 6.31, 6.32 and 6.33 illustrate northing and easting positioning errors for different scenarios in different epochs. The plots are helpful in analyzing the intra-antenna error correlation and also the inter-antenna error correlation. In the figures, whenever the easting and northing error is greater than 150 m, an outlier is flagged and shown as a red bar. Results corresponding to MUSIC approaches demonstrate considerably robust estimation behaviour, as these include zero or negligible outliers for different antennas compared to the conventional despreading scenario. It can qualitatively be inferred from Figure 6.31 that the errors are uncorrelated in the conventional despreading technique between different channels which provides a diversity gain to the system.

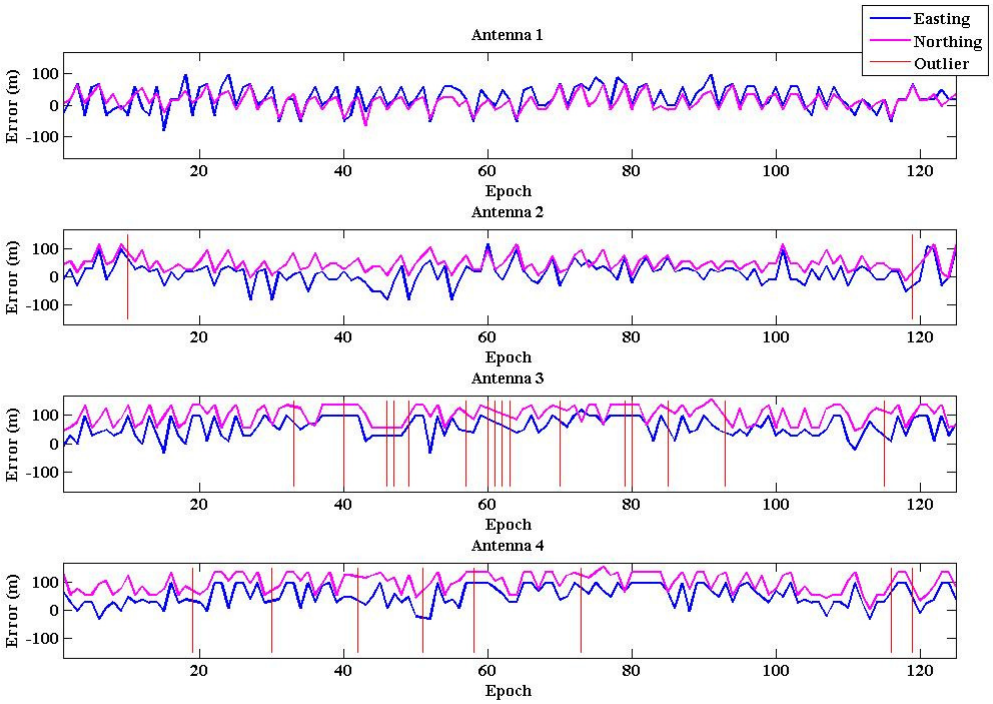

Figure 6.31: Easting-northing error for different epochs (conventional despreading)

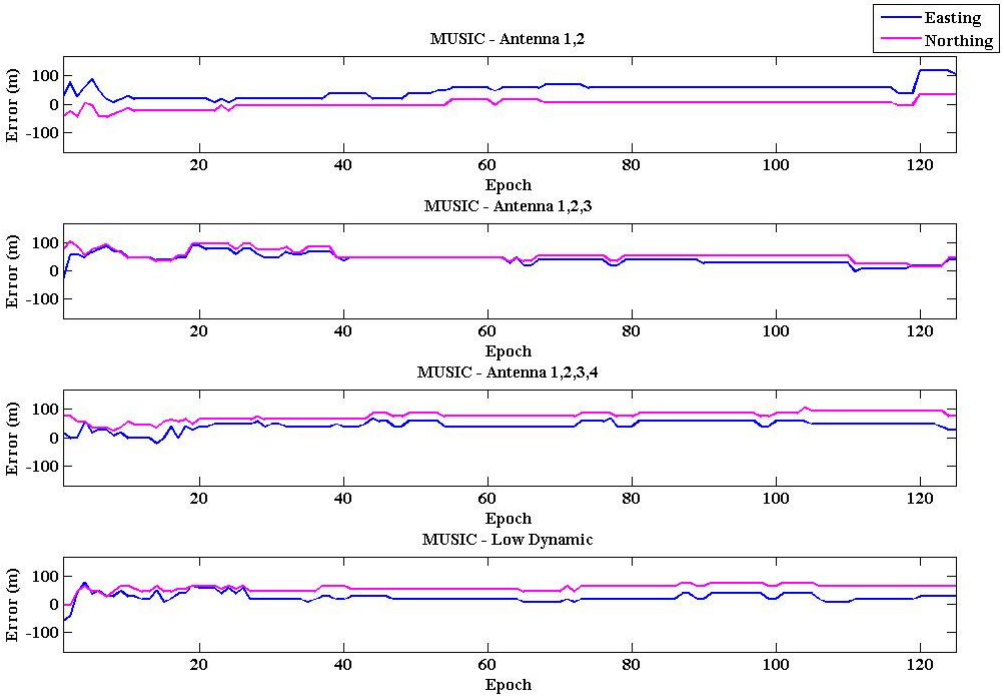

Figure 6.32: Easting-northing error for different epochs (conventional MUSIC)

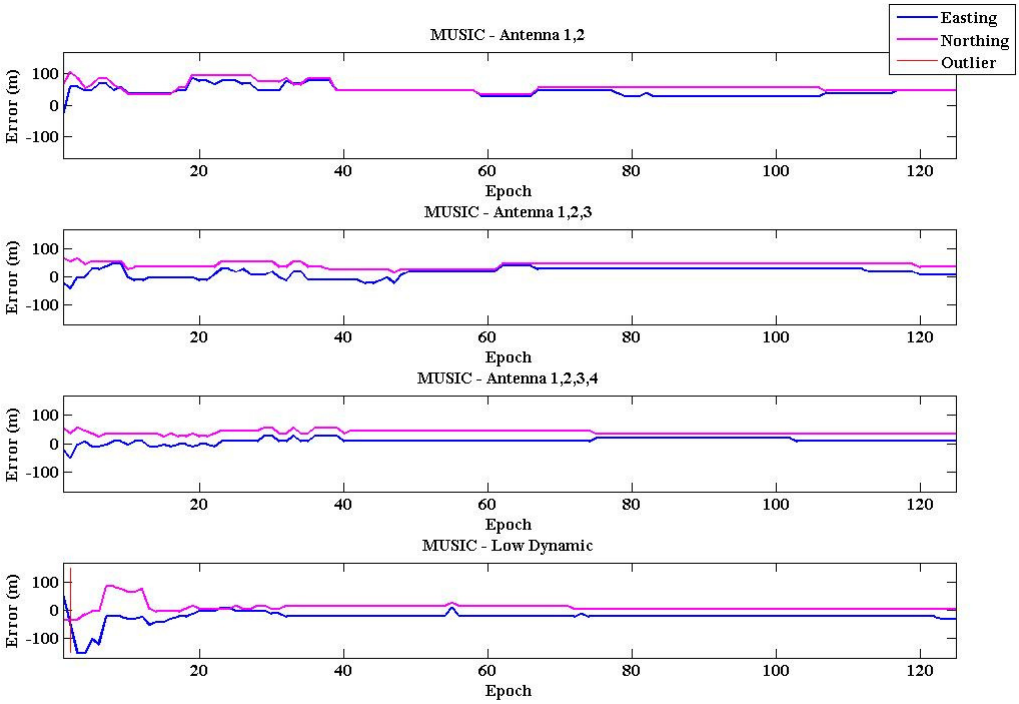

Figure 6.33: Easting-northing error for different epochs (space-time MUSIC)

Figures 6.31, 6.32 and 6.33 imply a noticeable correlation between easting and northing errors for a given antenna element. This correlation is due to both the geometry and the correlation of pseudoranges corresponding to two different sectors of the same site (UofC site) in the observations. For analyzing the source of correlation, the covariance matrix of the TDOAs corresponding to six site-sectors was estimated using 120 different epochs. The covariance matrix corresponding to TDOAs estimated by conventional despreading process for 120 epochs is shown below. A similar analysis can be accomplished for TDOAs derived by MUSIC or space-time MUSIC.

$$\hat{C}_{TDOA} = \begin{bmatrix} 2700 & 690 & 1350 & 1230 & 1080 \\ 690 & 999 & 537 & 369 & 576 \\ 1350 & 537 & 4071 & 2007 & 1488 \\ 1230 & 369 & 2007 & 3239 & 1456 \\ 1080 & 576 & 1488 & 1456 & 5504 \end{bmatrix} m^2 \tag{6.40}$$

where $i^{th}j^{th}$ element of $\hat{C}_{TDOA}$ is derived as $C_{TDOA}^{ij} = \dfrac{c^2 \sum_{m=1}^{120} \left(U_i^m - \overline{U}_i^m\right)\left(U_j^m - \overline{U}_j^m\right)}{120}$ on which U_i^m is the TDOA corresponding to *ith* BTS derived on m^{th} epoch, $\overline{U}_i^m = \dfrac{\sum_{n=1}^{120} U_i^n}{120}$ and c is speed of the light.

$\hat{C}_{TDOA}$ does not have the form of an identity matrix due to serial correlation, geometry and measurement error correlation. The common reference for TDOAs introduces the serial correlation. Since different BTSs incur different propagation losses (different

SNRs), the estimated standard deviations (diagonal values) of 32 m to 74 m are reasonable. Given $e = \begin{bmatrix} \Delta_x \\ \Delta_y \end{bmatrix}$ as the position error vector, where Δ_x and Δ_y are easting and northing error respectively, the covariance matrix of the error vector can be obtained as (Yarlagadda, et al, 2000):

$$C_e = E\{e.e^T\} = H^- C_{TDOA} H^{-T} \tag{6.41}$$

where,

$$H^- = \left(A^T A\right)^{-1} A^T \tag{6.42}$$

and the design matrix *A,* which accounts for the geometry, was defined as Equation 5.4. Given the geometry of the BTS-measurement point (Figure 6.21), the TDOA covariance matrix $\hat{C}_{TDOA}$ of Equation 6.40 is mapped into the following covariance matrix of 2-D position errors.

$$\hat{C}_e = \begin{bmatrix} 1616 & 745 \\ 745 & 692 \end{bmatrix} m^2 \tag{6.43}$$

The magnitude of the off-diagonal elements of $\hat{C}_e$ suggests a significant correlation as expected between the northing and easting errors, as can be deduced from Figure 6.31 and 6.32.

Figure 6.34(a) and (b) show the TDOA errors corresponding to different BTSs for antenna 2.in different epochs. In Figure 6.34 (a), the errors are derived between measurement TDOAs and actual TDOAs (based on surveyed measurement point coordinates), whereas, in Figure 6.34(b), the errors are derived between measured TDOAs and estimated TDOAs (based on estimated coordinates).

Figure 6.34(a) explicitly shows some biases (mostly due to the multipath) and outliers on estimated TDOAs corresponding to different BTSs. The residual errors can be analyzed and exploited to verify the correctness of the position fix process, to evaluate the long term behaviour of transmitter timing errors or to control the quality of measurements. For example, it is expected that given the redundancy in the number of visible BTSs (more than four BTSs in the TDOA scheme), removing a BTS that may have a significant TDOA bias would improve the positioning performance. However, it should be emphasized that removing a BTS may lead to a significant change in positioning geometry, which would manifest itself as change in GDOP. Hence, there is still a compromise between improving the quality of measurements and maintaining the GDOP to a reasonable value.

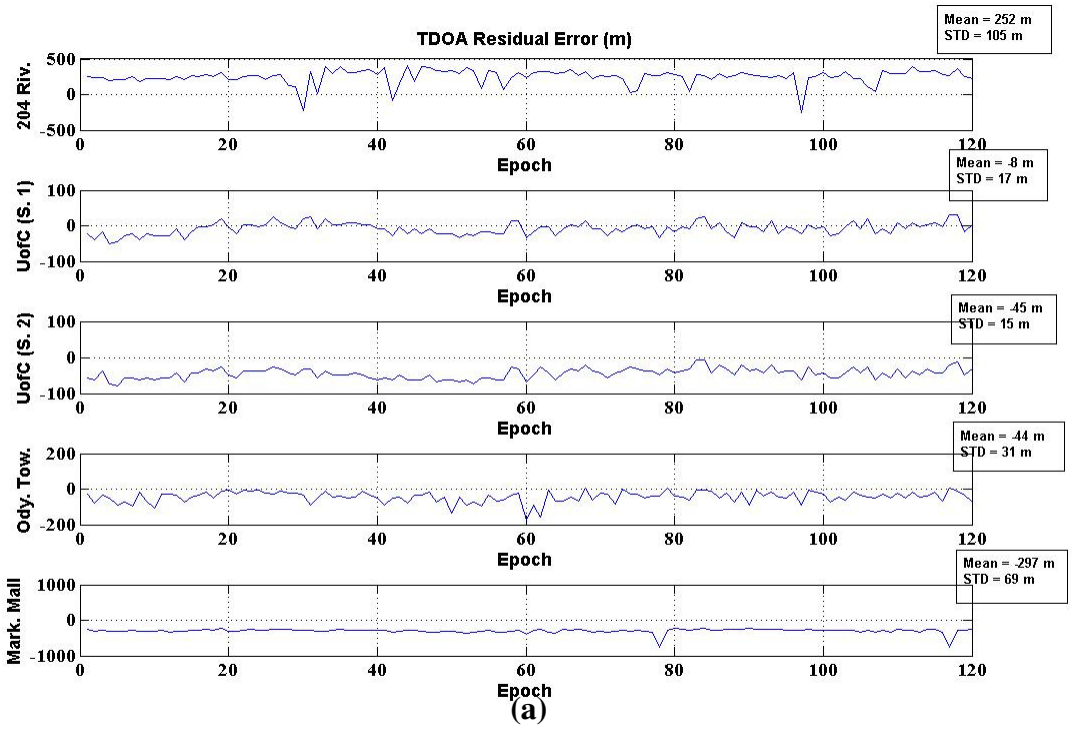

(a)

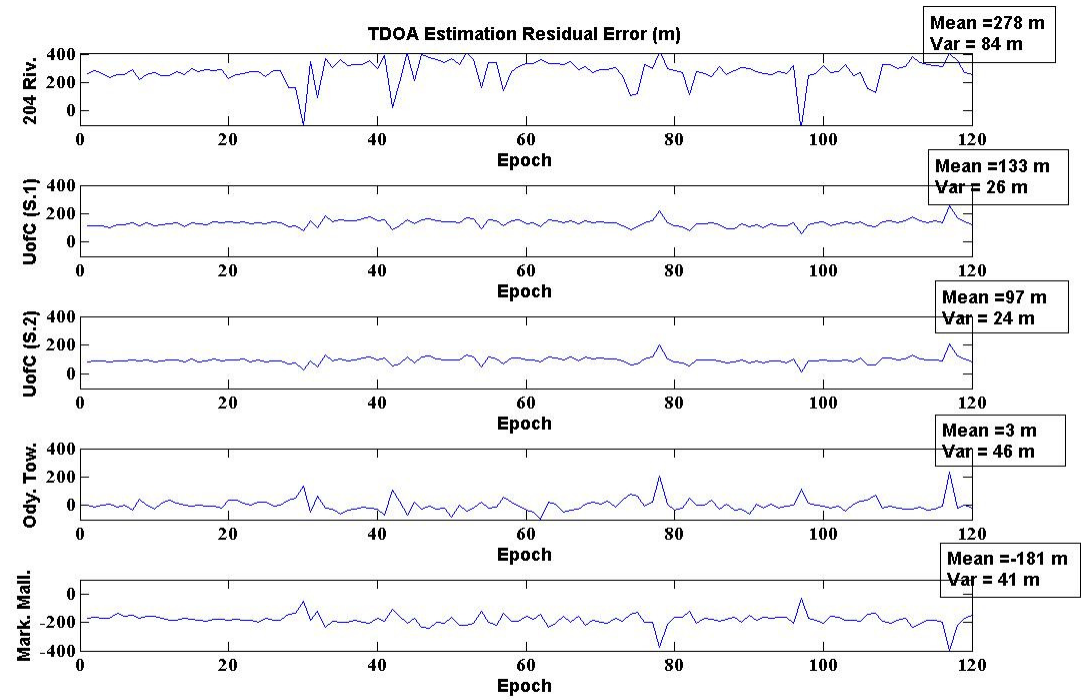

(b)

Figure 6.34: TDOA residual errors corresponding to different BTSs (a)-actual TDOA errors, (b) estimated TDOA errors

Redundant measurements in this test case provide the opportunity to investigate the impact of removing a biased measurement. Although there is a severely biased measurement set as Market Mall BTS with mean -297 m, there are two sectors corresponding to the same BTS (UofC site) that enable the GDOP to be preserved given the removal of one of them. The GDOP preservation makes a fair comparison between two cases on which only one sector is involved in the position fix process. Table 6.2 gives the easting and northing error means and standard deviations (STD) corresponding to the two cases.

Table 6.2: Positioning Error with Only One Sector Usage

		Mean (m)	STD (m)
Easting	With UofC (Sector 1)	1.7	29
	With UofC (Sector 2)	-18	28
Northing	With UofC (Sector 1)	58.5	10
	With UofC (Sector 2)	68	10

It can be inferred from Table 6.2 that the positioning bias is less with UofC Sector 1 than Sector 2. This improvement can be associated to a better quality (in terms of bias) of Sector 1 (TDOA residual mean of -8 m) as compared to that of Sector 2 (TDOA residual mean -45 m). Figure 6.35 shows the histogram of the TDOA residual errors for different BTSs. The histograms corresponding to UofC(S.1), UofC(S.2) and Odyssey sites may suggest a Gaussian distribution for TDOA errors, while for 204 River and Market Mall sites, the pattern suggests otherwise. This may be due to the limited amount of observation (120 epochs) or, more likely, multipath.

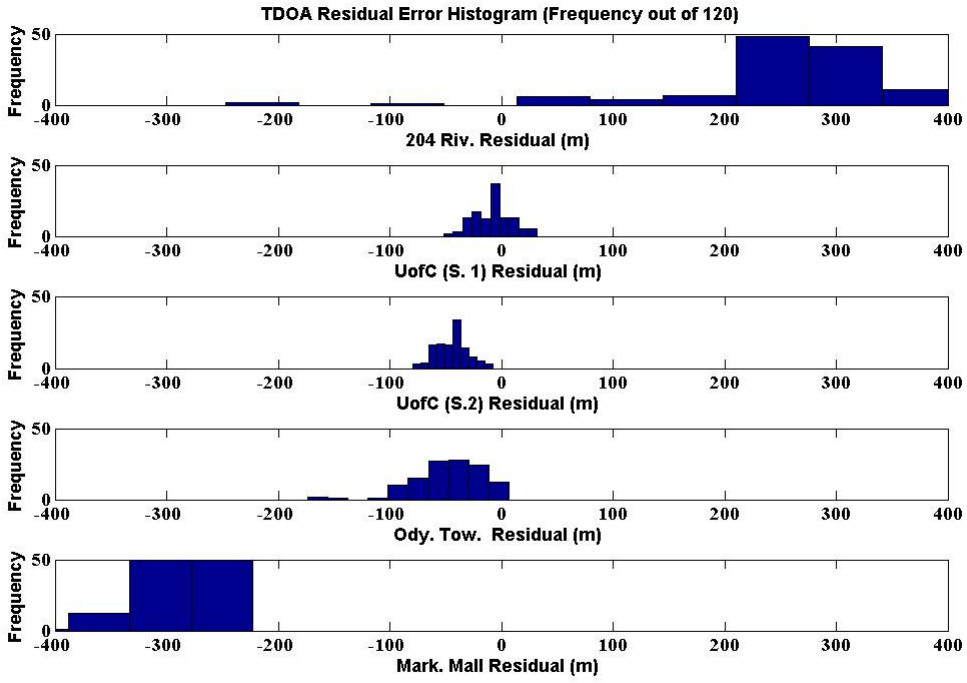

Figure 6.35: TDOA residual error histogram for different BTSs

Tables 6.3 and 6.4 give the summarized easting and northing error statistics for the different scenarios. These statistics include the mean and standard deviation of the estimation error. There is a notable difference in estimation error means (i.e., estimation offset) among different antennas in the conventional despreading process. The discrepancy can mostly be ascribed to the multipath effect because the TDOA approach in the position fix stage removes the common mode source of biases introduced by components and wires in different channels. Both estimation-error mean and STD decrease, if the diversity order in space-time MUSIC increases. Consistently, all estimation-error variances in the MUSIC approaches (both conventional and space-time) are less than those in the conventional despreading process. Given the BTS drop off which can be seen in Figure 6.27, in the dynamic scenario, temporal MUSIC shows superior performance compared to the other schemes.

Table 6.3: Position Errors (Mean)

Error Mean Unit (m)		Antenna #1	Antenna #2	Antenna #3	Antenna #4
Conventional Despreading	E.	9	4	45	36
	N.	4	38	93	85
Conventional MUSIC	E.	43	39	42	23
	N.	0	51	76	58
Spatial MUSIC Antenna 1,2	E.	40			
	N.	51			
Spatial MUSIC Antenna 1,2,3	E.	16			
	N.	41			
Spatial MUSIC Antenna 1,2,3,4	E.	11			
	N.	39			
Temporal MUSIC	E.	-21			
	N.	9			

Table 6.4: Position Errors (Standard Deviations)

Error STD Unit (m)		Antenna #1	Antenna #2	Antenna #3	Antenna #4
Conventional Despreading	E.	27	21	32	28
	N.	18	15	31	28
Conventional MUSIC	E.	19	9	10	14
	N.	12	8	10	8
Spatial MUSIC Antenna 1,2	E.	9			
	N.	8			
Spatial MUSIC Antenna 1,2,3	E.	14			
	N.	10			
Spatial MUSIC Antenna 1,2,3,4	E.	5			
	N.	5			
Temporal MUSIC	E.	4			
	N.	5			

Chapter Seven: Conclusions and Recommendations for Future Work

The presence of multipath can significantly distort the estimated arrival time of a given radio signal. This issue plagues those wireless based location systems requiring LOS path. The resulting loss in positioning accuracy was developed from theoretical and experimental perspectives in this thesis. This led to the development of two new methods for multipath mitigation.

The proposed techniques are based upon the use of space-time diversity methods. As shown, spatially sampled observations taken in a close proximity contain significant information regarding the LOS and NLOS components of the channel impulse response (CIR) and can be used to suppress the influence of the NLOS components. This enriched content, relative to conventional non-diversity methods, results in the possibility of significantly improving the achievable accuracy in the IS-95 cellular network position estimation system. Spatial and temporal diversity is implemented using a multi-channel receiver in stationary mode and a single or multi-channel receiver in low dynamic mode.

To mitigate the multipath impact on the received signal, two schemes which take advantage of multipath diversity across both spatial and temporal observations were suggested. The first approach attempts to alleviate the multipath components in the received signal directly, whereas the second approach improves the resolvability of the multipath components, which indirectly helps to reduce its effect.

In the first proposed scheme, it was shown that the complex CIRs corresponding to the spatial and temporal observations can be combined coherently to suppress the NLOS components of multipath. This coherent combination is based on the property that the

desired LOS component is spatially coherent while the NLOS components have random phase across the spatial extent. Practical considerations of coherent combination across spatial and temporal observations which required resolution were residual frequency (i.e., frequency offset between transmitter and local timing), inter-channel phase offset (only in the multichannel receiver scenario), clock drift and instability (i.e., Allan variance), inter-channel delays (due to non-identical hardware components), and inter-channel coupling (due to electromagnetic leakage). Static residual frequency can be estimated and then compensated for using the FFT method. Inter-channel phase offset can be estimated using a maximum-likelihood approach. Inter-channel delays and inter-channel coupling are properties of the receiver RF front end which can be compensated and quantified using calibration and experimental measurements. Also, careful construction and attention to interconnections between the various receiver channels reduced the level of inter-channel coupling and crosstalk. Having overcome these potential problem areas, it was demonstrated that the complex CIRs of the various channels could be coherently combined resulting in smaller estimation errors of the signal arrival times and consequently better position estimates as compared to the traditional single point method.

The second approach which was developed and experimentally tested is based on the MUSIC algorithm as a super-resolution technique for estimating the delays for different signal components. The proposed method is based on generalizing the MUSIC algorithm into its space-time form. It was demonstrated that the resulting space-time MUSIC outperformed the conventional MUSIC approach when applied to the signal arrival estimation problem. The improvement in the positioning error (especially in the error STD) is promising in terms of the improved positioning accuracy in the context of the IS-

95 CDMA cellular network. The theoretical investigation of the MUSIC algorithm shows that the signal components must be independent in order to be resolvable using the subspace-based decomposition method. Nevertheless, since the multipath components originate from the same transmitted source, the independence required for the conventional MUSIC algorithm is difficult to satisfy. Investigating the theoretical correlation coefficient expression in the frequency domain, this work suggests a generalized space-time form and corresponding deployment for the MUSIC algorithm. Space-time MUSIC suggests that the covariance matrices corresponding to the nearby spatial and temporal frequency domain CIRs, can be combined to give an effective covariance matrix with a more fitted property for the MUSIC to operate. Twelve different space-time scenarios and schemes were practically examined, based on the model, and results were then validated using the field IS-95 CDMA samples. Positioning results corresponding to the space-time MUSIC demonstrate considerably more robust estimation behaviours with lower amounts of position error mean and STD than the traditional despreading method and traditional MUSIC. It is concluded that the temporal only MUSIC outperforms the spatial only schemes, due to its potentially higher diversity order.

For instance, Table 6.3 and 6.4 showed standard deviations and measn for different schemes in a four element antenna array configuration. Using conventional correlation processing, the easting and northing coordinate means averaged over four antenna elements were 23.5 m and 55 m respectively. The use of temporal MUSIC as a high diversity order configuration yielded means of -21 m and 9 m, respectively. Using conventional correlation processing, easting and northing standard deviations averaged

over four antenna elements were 27 m and 23 m respectively. The corresponding values using temporal MUSIC were 4 m and 5 m, respectively. Table 6.3 and 6.4 suggest that both precision and accuracy tend to improve if diversity in space-time MUSIC increases.

In the space-time schemes introduced, there is a fundamental assumption that the leading component is correlated during the observations, whereas the multipath components are independent in terms of phase. Hence, the proposed schemes are mostly suitable for static or pseudo-static circumstances. This is a potential area of further research as a Kalman filter could potentially be used in conjunction with the space-time estimation schemes for dynamic scenarios.

Recommendations for Future Work

The research presented in this thesis can be extended in several ways. The analyses in Chapter 4 did not provide a general solution for determining the appropriate BTS site-sectors. A general BTS identification scheme can be implemented based on a maximum likelihood approach that scores all of the combinations of visible BTSs based on the received CIR observations. The BTS detectability issue was also neglected. Hence, the BTS identification algorithm must be sufficiently robust to accommodate the possibility that signals from certain BTSs may be completely blocked.

Further work also needs to be done on extending the detectability of very weak BTS signals that may be significantly attenuated due to shadowing or building penetration. Finally, MUSIC itself is not very robust due to the requirement of the dimension of the

received signal space. More research is required to estimate the dimensionality of the incoming signal space such that the parameters of MUSIC can be optimized. Another issue regarding MUSIC is that it has an bias that is a function of the SNR of the signal space component. Better understanding of this bias and perhaps compensation is an additional area of research in need of consideration.

References

Adusei, I.K., K. Kyamakya, & K. Jobmann (2002) Mobile Positioning Technologies in Cellular Networks: An Evaluation of their performance metrics. *MILCOM 2002. Proceedings*, 1239-1244.

Ash, N.J., & L.C. Potter (2004) Sensor Network Localization via Received Signal Strength Measurements with Directional Antennas. *Proc 2004 Allerton Conference Communication, Control and Computing*, pp. 18611870.

Blaunstein, N., & J. B. Andersen (2002) Multipath Phenomenon in Cellular Networks. Artech House, Boston London.

Borras, J., P. Hatrack, & N.B. Mandayam (1998) Decision Theoretic Framework for NLOS Identification. *IEEE VTC*, vol. 2, pp. 1583–1587.

Braasch, M.S. (2001) Performance Comparison of Multipath Mitigating Receiver Architectures. Aerospace Conference*, IEEE Proceedings*.

Caffery, J. (1998) Subscriber Location in CDMA Cellular Networks. *IEEE Transactions on Vehicular Technology*, Vol. 47, No.2.

Caffery, J.J. (2000) Wireless Location in CDMA Cellular Radio Systems. Kluwer Academic Publishers, Boston.

Chan,Y.T., & K.C. Ho (1994) A Simple and Efficient Estimator for Hyperbolic Location. *IEEE Transactions on Signal Processing*, vol. 42, pp. 1905-1915.

Chen, P.C. (1999) A Non Line of Sight Error mitigation Algorithm Location Estimation. *IEEE WCNC*, pp. 316-320, vol.1.

Chen., P.C. (1999) A Non-Line-of-Sight Error Mitigation Algorithm in Location Estimation. *IEEE Wireless Communications Networking Conference*, vol. 1, pp. 316–320.

Cheung, K.W., & R.D. Murch (1997) Improved Spatial Smoothing Technique. Electronics Letters, 9th, vol.33 no. 21.

Cong. L., & W. Zhuang (2001) Non-Line-of-Sight Error Mitigation in TDOA Mobile Location. Global Telecommunications Conference*, GLOBECOM* 01, Vol. 1, pp. 680 – 684.

Dumont, L., M. Fattouche, & G. Morrison (1994) Super-Resolution of Multipath Channels in a Spread Spectrum Location System*. Electronic Letter*. vol. 30, pp. 1583-1584.

Foy,W.H. (1976) Position-Location Solutions by Taylor Series Estimation. *IEEE Transactions on Aerospace Electron Systems*, vol. AES, pp.187-194.

Johnson, D., & S. Degraaf (1982) Improving the Resolution of Bearing in Passive Sonar Arrays by Eigenvalue Analysis*. IEEE Transactions on Acoustics, Speech, Signal Processing*, vol. ASSP-30, pp.638-647.

Kaveh, M., & A. J. Barabell (1986) The Statistical Performance of the MUSIC and Minimum-Norm Algorithms in Resolving Plane Waves in Noise. *IEEE Transactions on Acoustics, Speech, Signal Processing*, vol. ASSP. 34.

Kay, S.M. (1998) Fundamental of Statistical Signal Processing: Detection Theory. Vol II, Prentice Hall PTR, RI.

Klukas, R. W. (1997) A Super resolution Based Cellular Positioning System Using GPS Time Synchronization. *PhD's Thesis*, Department of Geomatics Engineering, University of Calgary, Canada.

Koorapaty, H. (2004) Cramer-Rao Bounds for Time of Arrival Estimation in Cellular Systems. *IEEE Vehicular Technology Conference* , VTC 2004.

Lachapelle, G. (1999) Hydrography, *ENGO 545 Lecture Notes*, Department of Geomatics Engineering, University of Calgary, Canada.

Landa, L., D. Munoz, & H. Maturino (2000) Performance Analysis of Power Up Function in Position Location Systems. *IEEE Transactions on Vehicular Technology*, Vol. 54, No. 1.

Le, B.L., K. Ahmed, & H. Tsuji (2003) Mobile Location Estimator with NLOS Mitigation Using Kalman Filtering. *Wireless Communications and Networking, WCNC* 2003.

Li, X., & K. Pahlavan (2004) Super-Resolution TOA Estimation with Diversity for Indoor Geolocation. *IEEE Transactions on Wireless Communications*, vol. 3, no.1.

Liao, J.F., & B.S. Chen (2006) Robust Mobile Location Estimator with NLOS Mitigation using interacting multiple Model Algorithm. *IEEE Transactions on Wireless Communications*, 11, 3002-3006.

Liberti, J.C., JR., T.S. Rappaport (1999) Smart Antennas for Wireless Communications IS-95 and Third Generation CDMA Applications. Prentice Hall PTR.

Lo, T., J. Litva, & H. Leung (1994) A New Approach for Estimating Indoor Radio Propagation Characteristics. *IEEE Transaction on Antennas Propagation*, vol. 42, pp 1369-1379.

Lopez, A. (2006) Design and Implementation of a 5-CDMA Receiver for Mobile Position Location. *MSc Thesis*, Department of Electrical Engineering, University of Calgary, Canada.

Lu, D. (2007) Multipath Mitigation in TOA Estimation Based on AOA. *PhD's Thesis*, Department of Electrical and Computer Engineering, University of Calgary, Canada.

Ludden, B., &, L. Lopes (2000) Cellular Based Location Technologies for UMTS: a Comparison Between IPDL and TA-IPDL. *IEEE 51st Vehicular Technology Conference*, vol. 2, pp. 1348-1353.

Ma, C. (2003) Techniques to Improve a Ground-Based Wireless Location Performance using a Cellular Telephone Network. *PhD's Thesis*, Department of Geomatics Engineering, University of Calgary, Canada.

Morrison, G., & M. Fattouche (1998) Super-Resolution Modeling of the Indoor Radio Propagation Channel. *IEEE Transactions on Vehicular Technology*, vol. 47, pp. 649-657.

Pallas, M., & G. Jourdain (1991) Active High Resolution Time Delay Estimation for Large BT Signals. *IEEE Transaction on Signal Processing*, vol. 39, pp. 781-788.

Parsons, J.D. (2000) The Mobile Radio propagation Channel. Second Edition, John Wiley & SONS LTS.

Patwari, N., J.N. Ash, S. Kyperounats, A.O. Hero, R.L. Moses, & N.S. Correal (2005) Locating the Nodes Cooperative localization in Wireless Sensor Networks. *IEEE Signal Processing Magazine*.

Proakis, J.G. (2000) Digital Communications. Fourth Edition. Mc Graw Hill.

Qi, Y. (2003) Wireless Geolocation in a Non Line of Sight Environment. *PhD's Thesis*, November 2003, Electrical Engineering Department Princeton University.

Qi, Y., H. Suda, & H. Kobayashi (2004) On Time of Arrival Positioning in Multipath Environment. *IEEE Vehicular Technology Conference*, VTC 2004.

Reddy, V., A. Apulraj, & T. Kailath (1987) Performance Analysis of the Optimum Beam Former in the Presence of Correlated Source and its Behavior under Spatial Smoothing. *IEEE Transactions on Acoustics, Speech, Signal Processing*, vol. ASSP-35, pp. 927-936.

Saarnisaari, H. (1997) TLS-ESPRIT in a Time Delay Estimation. *IEEE 47th VTC*, pp. 1619-1623.

Selva, J. (1999) Subspace Methods Applied to Multipath Mitigation in a Navigation Receiver. *IEEE VTC*, vol. 4, pp. 2077-2081.

Silventoinen, M. I., & T. Rantalainen (1996) Mobile Station Emergency Location in GSM. *IEEE International Conference on Personal Wireless Communication*, India.

Tarighat, A., N. Khajehnouri, & Ali H. Sayed (2003) Improved Wireless Location Accuracy Using Antenna Arrays and Interference Cancellation. *International Conference on Acoustics, Speech, and Signal Processing, Proceedings*. (ICASSP).

Trevisani, E., & A. Vitaletti (2004) Cell-ID Location Technique, Limits and Benefits: and Experimental Study. Mobile Computing Systems and Applications, WMCSA 2004.

Vossiek, M., L. Wiebking, P. Gulden, J. Wieghardt, & C. Hoffmann (2003) Wireless Local Positioning Concepts, Solution, Applications. *Radio and Wireless Conference, RAWCON* 03.

Wang, S., & M. Green (2000) Mobile Location Method for Non-Line-of-Sight Situation. *IEEE VTC*, vol. 2, pp. 608–612.

Wax, M., & T. Kailath (1985) Detection of Signals by Information Theoretic Criteria. *IEEE Transactions on Acoustics, Speech, Signal Processing*, Vol. ASSP-33, pp. 387-392.

Woo, S.S., H. R. You, Tae, & G. Kim (2000) The position Location System Using IS-95 CDMA Networks. Eurocomm 2000, *Information Systems for Enhanced Public Safety and Security. IEEE/AFCEA*, 20-24.

Woo, S.S., H.R. You, & J.S. Koh (2000) The NLOS Mitigation Technique for Position Location using IS-95 CDMA Networks. IEEE VTC, vol. 4, pp. 2556-2562.

Wylie, M.P., & J. Holtzman (1996) The Non-line of Sight Problem in Mobile Location Estimation. *IEEE International Conference on Universal Personal Communications*, vol. 2, pp. 827–831.

Xu, X.L. (1992) Bias Analysis of the MUSIC Location Estimator. *IEEE Transaction on Signal Processing,* vol. 40, no. 10.

Yarlagadda, R., I. Ali, N.Al-Dhahir & J. Hershey (2000) GPS GDOP metric. *IEE Proc.-Radar, Sonar Navig.*, vol. 147, No. 5.

Yu, X.J., W. Wei, & Z.Z Liang (2003) A New TDOA Location Technique based on Taylor Series Expansion in Cellular Networks. *IEEE PDCAT'2003*.